Filipe Rodrigues Medina de Sousa

Degree in Biochemistry

Structural and functional investigation of type II NADH:quinone oxidoreductase from the pathogenic bacteria *Vibrio cholerae* and *Staphylococcus aureus*

Dissertation to obtain the Master degree in Biochemistry for Health

Orientador: Dra. Manuela M. Pereira
Co-orientador: Dra. Ana Paula Batista

October, 2015

Filipe Rodrigues Medina de Sousa

Degree in Biochemistry

Structural and functional investigation of type II NADH:quinone oxidoreductase from the pathogenic bacteria *Vibrio cholerae* and *Staphylococcus aureus*

Dissertation to obtain the Master degree in Biochemistry for Health

Orientador: Dra. Manuela M. Pereira
Co-orientador: Dra. Ana Paula Batista

Juri:

Presidente: Prof. Doutor(a)
Arguente(s): Prof. Doutor(a)
Vogal(ais): Prof. Doutor(a)

Instituto de Tecnologia Química e Biológica, António Xavier

October, 2015

Structural and functional investigation of type II NADH:quinone oxidoreductase from the pathogenic bacteria *Vibrio cholerae* and *Staphylococcus aureus*

Agradecimentos

Em primeiro lugar quero agradecer às minhas orientadoras Dra. Manuela M. Pereira e Dra. Ana Paula Batista por me aconselharem, apoiarem e guiarem neste projecto e nesta aventura pessoal que foi escrever esta tese de mestrado. Espero não vos ter desiludido e ter correspondido da melhor forma que sei à oportunidade que me deram. Obrigado por me darem o espaço e o ambiente para errar e aprender. Por me permitirem perceber que o sentimento de curiosidade e espirito critico que sempre tive é algo de que me devo orgulhar.

Quero agradecer ao Professor Miguel Teixeira, como responsável da *Metalloproteins and Bioenergetics Unit*, me ter dado a oportunidade única de desenvolver a minha tese de mestrado no seu laboratório.

Quero agradecer ao Afonso, à Patricia, à Sandra, ao Bruno, ao Paulo, à Filipa Calisto, à Filipa Sena, à Andreia, à Dalila e ao Zé por facilitarem a minha adaptação a esta nova fase da minha vida e por todo o apoio cientifico e pessoal que deram ao longo deste ano. Em especial à Patricia por ter sido a minha segunda consciência em alguns momentos importantes, por todos os esclarecimentos cientificos e por toda a motivação e apoio nos momentos de dúvida. Ao Bruno por me espicaçar a curiosidade todos os dias, pelas horas a ouvir-me quando todos os outros já tinham desistido, pela amizade e ajuda a me integrar no grupo, mas principalmente por servir como exemplo de entrega, profissionalismo, competência e boa disposição . À Filipa Sena por me obrigar a exigir o máximo de mim, por toda a disponibilidade cientifica e pessoal, pela paciência e companhia, por ter partilhado a sua bancada, mas acima de tudo pelo apoio que me deu nos dias mais dificeis.

Ao ITQB, à FCT e à FCM por terem criado as condições necessárias para que eu pudesse desenvolver a minha tese de mestrado.

À professor Smilja Todorovic e à Dra. Célia Silveira do grupo *Raman Spectroscopy of Metalloproteins* pela disponibilidade e ajuda nas experiências de Voltametria ciclica.

À professora Teresa Catarino pela boa disposição, pela incansável disponibilidade e por todo o debate e ajuda prestada na recolha e análise dos resultados de Fast e Steady state Kinetics.

A todos os meus amigos que me dão a alegria, a motivação e a força para continuar a lutar. Em especial ao André, Nuno e Rafa por simplesmente serem o que são todos os dias mesmo quando o trabalho e a distância tenta atrapalhar.

À Joana pela amizade e apoio de sempre, nos bons e nos maus momentos. Por ao longo deste ano ter sido aquela presença amiga nesta nova fase.

À Márcia por ao longo destes dois anos ter sido tudo. Por me ter dado a força que sempre me faltou, por me fazer rir quando mais ninguem conseguia, por me aturar mesmo nas

minhas birras mais parvas, por me dar a confiança que nunca tive, por me dar o seu carinho e a sua amizade incondicional que espero que durem para além das circunstâncias que hão de vir. Não estaria onde estou e não seria quem sou se não fosse pelo que me deste. É só deixar rolar.

Ao André, ao Ricardo e ao Hugo por serem aqueles irmãos de sempre e para sempre. Não é assim tão dificil pôr o nome dos amigos nos agradecimentos.

A toda a minha familia por me apoiar desde sempre em todos os erros que cometi. Por se interessarem e preocuparem com o que faço e com quem sou, por me educarem e moldarem na pessoa que hoje sou. Em especial à minha avó Manuela por me ter apoiado e motivado durante este ano complicado com toda a sua preocupação e dedicação.

Ao Afonso por ser o irmão de que me orgulho, e que me motiva a ser mais e melhor todos os dias para tentar acompanhar o seu ritmo. Porque há de ser sempre o meu mano mais novo.

Por fim, agradeço aos meus pais. Pela forma como me educaram, pelo exemplo, pelo amor e amizade que nunca me faltou, por todos os sacrificios para me dar tudo, pelo apoio incondicional nas minhas decisões ou na falta delas. Por serem a base de estabilidade, confiança, formação e carinho que acima de tudo me faz ser quem sou. Obrigado.

Aims and motivations

Type II NADH:quinone oxidoreductases (NDH-2), are proteins which catalyze the transfer of two electrons from NADH to the quinone. Their study has received a new impetuous with the determination of its crystallographic structure, which made this project timely.

NDH-2 is considered a functional replacement of the respiratory Complex I, since it performs the same catalytic reaction as this protein complex and has been shown to restore the NADH dehydrogenase activity in Complex I deficient cells. NDH-2 is also the only protein with NADH:quinone oxidoreductase activity in some pathogenic organisms, like *Vibrio cholerae* and *Staphylococcus aureus* for example, having been proposed as possible new targets for rational drug design. For those two reasons the study of NDH-2 may have implications in human health and quality of life.

We aimed at investigating the catalytic mechanism of NDH-2 and the structural determinants for substrate specificity, considering that NDH-2 is capable of interacting with different quinones. Specifically our objectives were:

- expressing, purifying and biochemically characterizing the NDH-2 from *Vibrio cholerae* for the very first time;
- investigating the role of Glutamate 172 in the catalytic mechanism of NDH-2, by constructing site specific mutants of the NDH-2 from *Staphylococcus aureus*.

Resumo

Staphylococcus aureus e *Vibrio cholerae* são duas bactérias patogénicas que sozinhas são responsáveis pela morte de mais de 150.000 humanos por ano (afectando quase 5.000.000 de pessoas). Os antibióticos e as vacinas, em conjunto, já erradicaram algumas doenças infecciosas e surgem como as únicas hipóteses viáveis para o tratamento de algumas das doenças mais comuns de origem bacteriana.

NADH: quinona oxidoredutases do tipo II (NDH-2) são os únicos enzimas expressos na cadeia respiratória de organismos patogénicos com actividade de NADH desidrogenase e, por isso, foram propostos como novos alvos terapêuticos para o design racional de novos antibióticos. Este objectivo final, só é passível de ser atingido graças à investigação fundamental realizada ao nível funcional e estrutural nestes enzimas. Neste trabalho expressámos e purificámos, parcialmente, pela primeira vez, a NDH-2 de *Vibrio cholerae,* abrindo novas perspectivas para futuros estudos relacionados com este enzima. Também, investigámos o papel do Glutamato 172 no mecanismo enzimático da NDH-2 de *Staphylococcus aureus*, recorrendo a mutantes desse mesmo resíduo. Foi feita uma caracterização bioquímica dos mutantes E172A, E172S, E172Q e E172D. Estudos de cinéticas rápidas e em estado estacionário mostraram uma diminuição clara na velocidade da reacção e estudos de interacção com o substrato por medições do “quenching” de fluorescência, sugerem que a ligação da quinona também foi afectada pela mutação. Em conjunto, os resultados aqui apresentados sugerem que o Glutamato 172 tem uma importância central no mecanismo do enzima, que a sua importância é transversal a ambas as semi-reacções (oxidação e redução) e que a sua cadeia lateral parece orientar (directa ou indirectamente) a ligação do NADH e da quinona. Com este trabalho esperamos contribuir para o conhecimento ao nível funcional das NDH-2, tornando possível o desenvolvimento de novos antibióticos para o tratamento de algumas das principais pandemias de origem bacteriana.

Abstract

Staphylococcus aureus and *Vibrio cholerae* are two pathogenic bacteria that, on their own, are responsible for more than 150,000 human deaths per year (affecting almost 5,000,000 people worldwide). Antibiotics and vaccines have been proved to work as a viable strategy to treat bacterial related epidemics such as cholera and MRSA associated infections. Nevertheless, new drugs are increasingly necessary due to the appearance of resistant strains.

Type-II NADH:quinone oxidoreductase (NDH-2) are the only enzymes with NADH:quinone oxidoreductase activity expressed in many pathogenic organisms and for that, they have been proposed as possible new drug targets for the rational design of antibiotics. This final objective may only be possible after a thorough functional and structural investigation of NDH-2. In this work we expressed and partially purified for the first time the NDH-2 from *Vibrio cholerae* opening new perspectives to further studies of this protein. We also performed a thorough investigation of the role of the strictly conserved Glutamate 172 (E172) residue on the enzymatic mechanism of NDH-2 from *Staphylococcus aureus*. For this we performed a complete biochemical characterization of the mutants E172A, E172S, E172Q and E172D. Our steady state kinetic measurements show a clear reduction in the overall reaction rate; and our substrate interaction studies by fluorescence quenching analysis show that the binding of the quinone to the protein was also affected by the mutations. Together our results suggest that E172 is of central importance in the catalytic mechanism of the enzyme, having an important role on both half reactions, and that the properties of its side chain are indirectly important for the orientation of both substrates. In the long term this work aims at contributing to the functional knowledge on the NDH-2 family, and inspire the development of new drugs, targeting some of the main bacterial related infections causative agents.

Index

Index of figures

Index of tables

List of abbreviations

[X] - concentration of "X"

$\Delta\mu_{H+}$ - proton electrochemical potential

ΔF_{max} - maximum quenching

2Fe-2S - 2 iron - 2 sulfur center

Abs - absorbance

ATP - adenosine triphosphate

cAMP - cyclic adenosine monophosphate

CD - circular dichroism

Cl^- - chloride anion

CpI/NDH-1 – complex I

CpII – complex II

CpIII – complex III

CpIV – complex IV

CT – charge transfer

CV - Cyclic Voltammetry

cyt *c* – cytochrome *c*

DBDF - two dinucleotide binding domains flavoprotein

DDB - 2,3-Dimethoxy-5,6-dimethyl-p-benzoquinone

DDM - n-Dodecyl-β-D-maltopyranoside

DLS - dynamic light scattering

DMN - 2,3-Dimethyl-1,4-naphthoquinone

e^- - electron

E. coli - *Escherichia coli*

E172 - glutamate 172

E172A – type II NADH:quinone oxidoreductase from *S. aureus*, with Glutamate 172 mutated into an Alanine

E172D - type II NADH:quinone oxidoreductase from *S. aureus*, with Glutamate 172 mutated into an Aspartate

E172Q - type II NADH:quinone oxidoreductase from *S. aureus*, with Glutamate 172 mutated into a Glutamine

E172S - type II NADH:quinone oxidoreductase from *S. aureus*, with Glutamate 172 mutated into a Serine

EA - electron acceptor

EC - electron carrier

ED - electron donor

FAD - flavin adenine dinucleotide

FMN - flavin mononucleotide

H^+ - proton

HMW - high molecular weight

HQNO - 2-n-Heptyl-4-hydroxyquinoline N-oxide

IP - isoelectric point

IPTG - isopropyl-β-D-thiogalactosidase

K - constant

K_D - dissociation constant

K_I - inhibition constant

K_M - Michaelis-Menten constant

LMW - low molecular weight

MRSA - meticillin-resistant *Staphylococcus aureus*

MSA - multiple sequence alignment

MT - melting temperature

MW - molecular weight

MWC - Monod-Wyman-Changeux

Na^+ - sodium cation

Na^+-NQR - sodium-translocating NADH:quinone oxidoreductase

NAD^+ - oxidized nicotinamide adenine dinucleotide

NADH **-** nicotinamide adenine dinucleotide

NADPH **-** nicotinamide adenine dinucleotide phosphate

NDH-2_Sa – type II NADH:quinone oxidoreductase from *Staphylococcus aureus*

NDH-2_Vc – type II NADH:quinone oxidoreductase from *Vibrio cholerae*

OD_{600} – cell density at 600 nm

PPM - parts per milion

PVL - Panton–Valentine leukocidin

Q - quinone

QH_2 - quinol

$R^{280}/_{450}$ - ratio between absorbancies at 280 and 450 nm

rpm - rotations per minute

S. aureus - *Staphylococcus aureus*

S. cereviseae – *Sacharomyces cereviseae*

S200 - Superdex 200

SAXS - Small-angle X-ray scattering

SDS-PAGE - sodium dodecyl sulphate – polyacrilamide gel electrophoresis

SEC – size exclusion chromatography

SHE - standard hydrogen electrode

Trp - Tryptophan

UV-Vis - ultra violet-visible

V. cholerae - *Vibrio cholerae*

V_0 - initial rate

V_{max} - maximum rate

WT - wild type

ε - extinction coefficients

1. Introduction

1.1 Energetic Metabolism

1.1.1 Cell Energy

The transformation and utilization of energy are common to all biochemical reactions needed to regulate and maintain the electrochemical disequilibria which we call life. Bioenergetics is a vast scientific domain, studying the mechanisms which allow the cell to harvest and store energy in the form of reduced substrates or electrochemical potentials.

Cellular metabolism can be divided in catabolic reactions (degrading reactions) and in anabolic reactions (synthesis reactions). In the catabolic phase, complex molecules with high energetic value (proteins, carbon hydrates and fats) are degraded into structurally simpler precursors (lactate, CO_2, NH_3) in a thermodynamic favorable process. In the anabolism reactions (biosynthesis) the same precursors are combined and transformed, with energy consumption, in biomolecules capable of playing all the functions that are characteristic of a living organism.

The energy contained in the catabolism thermodynamically favorable reactions may be harvested and conserved by the differential accumulation of chemical or electrical molecules between the two sides of the membrane. This electrochemical disequilibrium creates a ready to use potential which allows the cell to perform biochemical work needed to the perpetuation of its life such as solute transport, flagellar rotation or adenosine triphosphate (ATP) synthesis. The proton (H^+) electrochemical potential is one of the main chemical gradients in the cell and is directly responsible for the synthesis of ATP (*1*).

The proton electrochemical potential ($\Delta\mu_{H+}$, measured in kilojoules per mole) consists of two distinct components: an electrical potential resulting from the charge separation across the membrane ($\Delta\Psi$); and a chemical potential originated by the asymmetrical proton distribution through the membrane (ΔpH).

$$\Delta\mu H^+ = -F \times \Delta\Psi + 2.3 \times RT \times \Delta pH$$

eq. 1 – Equation relating the electrical potential ($\Delta\Psi$) and chemical potential (ΔpH) of the protons across the membrane used to calculate the proton electrochemical potential ($\Delta\mu H^+$). F is the Faraday's constant, R is the "ideal gas" constant and T is the temperature (*2*).

The differential accumulation of H^+ in one of the membrane sides is only possible thanks to the impermeability of the membrane to ions; and to the work of a small number of protein complexes composing the respiratory chain. These have the unique ability to couple the electron transport to proton translocation against its electrochemical gradient. Those proteins make possible this thermodynamically unfavorable process by using the energy that is released

from electron transfers from highly negative reductive potential substrates (NADH or NADPH for example) to a final acceptor with a positive reduction potential (O_2 in the case of aerobic organisms) (*2*).

In prokaryotes the respiratory chain proteins are expressed in the cellular membrane and they translocate protons from the cytoplasm into the periplasmic space. In eukaryotic organisms, in order to make the expression and regulation of these proteins as tight as possible, some subunits are coded in the mitochondrial genome and expressed in the inner membrane of this same organelle, while the rest is coded in the nucleus with signal peptides that orient those proteins into mitochondria (*3*). In the case of mitochondria, the proton electrochemical potential is created by translocating protons from the mitochondrial matrix to the inter membrane space.

Respiratory chains are as diverse as life on earth. Depending on the general metabolic needs of the organism, respiratory chains have changed and adapted to be able to act as slightly different transport systems (*4*). For the sake of comprehending the general constitution, mechanisms and function of respiratory chains, and despite not being fully representative, the mammalian mitochondrial respiratory chain was used as a model in this introduction.

1.1.2 Respiratory chains

In general, respiratory chains are composed of membrane associated protein complexes with three different enzymatic activities: 1 - electron donor (ED): quinone (Q) oxidoreductase (Fig.1A); 2 - quinol (QH_2): electron carrier (EC) oxidoreductase (Fig.1B) and 3 - electron carrier: final electron acceptor (EA) oxidoreductase (Fig.1C).

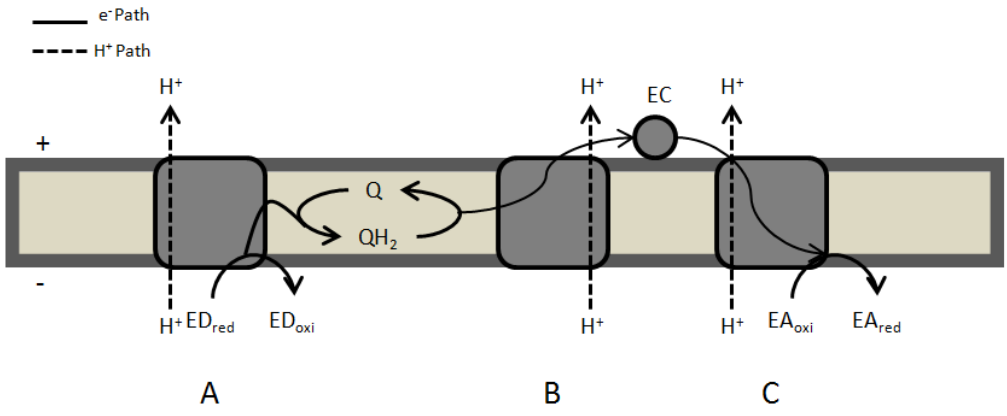

Figure 1. 1 - Schematic representation of respiratory chain components indicating their respective enzymatic activities. A – ED:quinone oxidoreductase; B – quinol:EC oxidoreductase; C – EC:EA oxidoreductase. Adapted from (*5*).

Electron transfer between respiratory complexes is guaranteed by the lipid soluble quinones/quinols (Q/QH_2) and in some cases by a soluble electron carrier (EC) (like cytochrome *c* for example). In the mammalian respiratory chain, the best characterized electron transfer

chain, there are four different complexes (complex I to IV) that catalyze the electron transfer from the NADH or succinate to O_2 through a redox potential span of 1,1V (in the case of NADH being the electron donor) (*1, 6*).

Complex I (EC:1.6.5.3), the largest of the four respiratory complexes, is composed of ~44 polypeptides, having a molecular mass of as much as 1 MDa, and as cofactors one Flavin Mononucleotide (FMN) and eight iron-sulfur clusters. This "L" shaped complex is the main entry point of electrons to the respiratory chain, feeding the quinone pool with electrons from NADH (NADH:quinone oxidoreductase). Complex I (CpI) catalyses the transfer of two electrons, reducing quinone to quinol, coupling this redox transfer with the translocation of H^+ across the membrane (*7-8*).

From the quinol the electrons are transferred to cytochrome *c* in a reaction catalyzed by Complex III (quinol:cytochrome *c* oxidoreductase). Complex III (EC:1.10.2.2), or Cytochrome bc_1 complex, is a transmembrane protein complex composed by a cytochrome c_1, a cytochrome *b* and a Rieske iron-sulfur subunit as its three catalytic subunits. This respiratory enzyme can have up to eleven subunits, but only cytochrome *b* and the Rieske subunit are conserved throughout this protein family (*6, 9*). Translocation of protons occurs through a Q-cycle mechanism first proposed by Peter Mitchell, in which there is an asymmetric consumption and release of protons in each side of the membrane. For every two electrons passing from quinol to cytochrome *c*, CpIII releases four protons at the positive side but takes only two from the negative side (*10*).

After being reduced, cytochrome *c* reduces Complex IV (CpIV). CpIV (EC:1.9.3.1), or cytochrome *c* oxidase, catalyses the final step in the electron transfer chain of mitochondria, the oxidation of cytochrome *c,* and the respective O_2 reduction (cytochrome *c*:O_2 oxidoreductase). Mitochondrial Complex IV has 13 subunits of which only two are considered to have catalytic activity (subunits I and II). During the reduction of molecular oxygen to two molecules of water, four protons are pumped to the positive side for every four electrons that are given to the system by cytochrome *c* (*6, 11*).

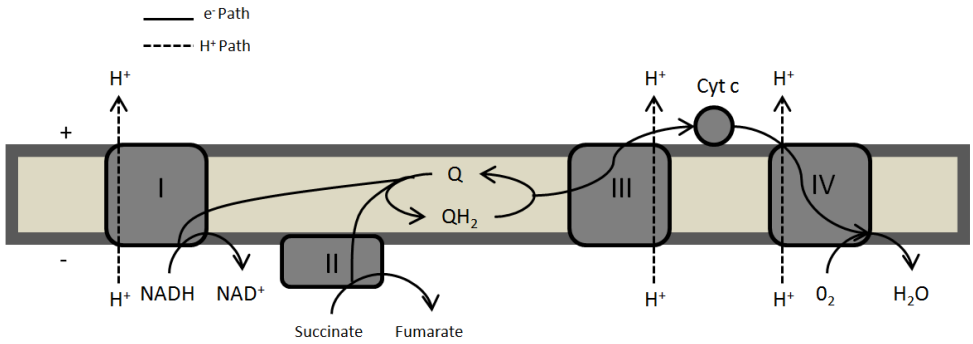

Figure 1. 2 - Schematic representation of the mammalian mitochondrial respiratory chain sequence. Complex I, III and IV transport electrons sequentially from NADH to O_2, while translocating protons across the membrane. The electron carrier in the case of the mammalian respiratory chain is cytochrome *c,* and the expressed quinone is Ubiquinone. Complex II also feeds the quinone pool with electrons from succinate oxidation.

Although mammalian mitochondria present a relatively straight forward respiratory chain, some diversity is observed with the presence of secondary donor:quinone oxidoreductases. Besides CpI, a succinate dehydrogenase (Complex II – figure 1.2), an α-glycero-phosphate dehydrogenase and an electron transfer flavoprotein:ubiquinone oxidoreductase are responsible for supplying electrons into the quinone pool (*12*).

This diversity is even more obvious outside of the mammalian class, probably because of the multiplicity of different environments and consequent need to have more robust and adaptable respiratory systems. Depending on the growth conditions, the same organism can express different electron carriers (including quinones) and different respiratory proteins.

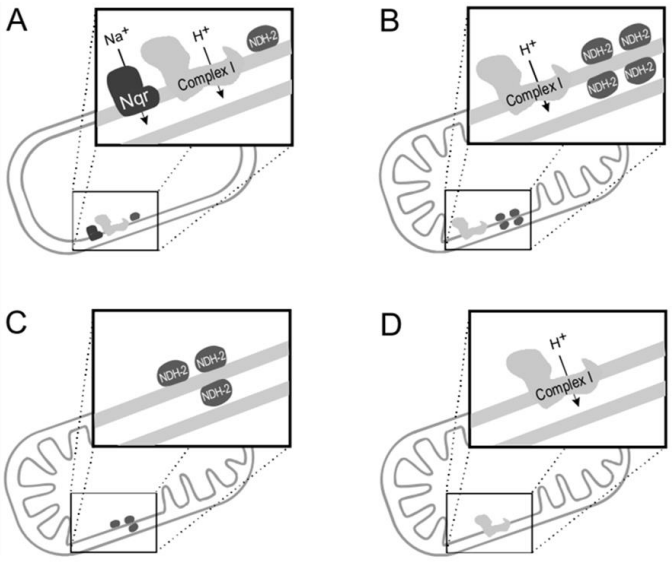

Figure 1. 3 - Schematic representation of the occurrence and localization of the three families of respiratory NADH dehydrogenases. A - Prokaryotes may have all three types of NADH dehydrogenases. B - Mitochondria from fungi and strictly aerobic yeast may contain CpI and up to four different NDH-2. C Mitochondria from fermentative yeasts do not contain CpI, but up to three NDH-2. D - Mitochondria from higher eukaryotes only contain CpI, adapted from *(13)*.

In prokaryotes the respiratory proteins are, in general, analogous to the mitochondrial ones but with less polypeptide chains (corresponding to the minimal functional units). In some cases the original protein may have been substituted by another one with similar function but different structure, and in other cases genes coding for the different enzymes performing the same enzymatic reaction may co-exist. In the specific case of the NADH dehydrogenases, CpI (or NDH-I) may be replaced by type-II NADH:quinone oxidoreductase (NDH-2) or even sodium-translocating NADH:quinone oxidoreductase (Na^+-NQR). It is also possible to observe the presence of two or three of these NADH dehydrogenases in the respiratory chain of the same organism, being their expression dependent on the growth conditions. The presence of different types of NADH dehydrogenases in the same organism allows for adjustments of the overall redox state of the cell by regulating the flow of electrons/protons by oxidative phosphorylation (*13*).

1.1.3 Type II NADH:quinone oxidoreductases

Type II NADH:quinone oxidoreductase (NDH-2) is a respiratory enzyme that catalyses the transfer of two electrons from NADH to the quinone (ubiquinone or menaquinone – see Supplementary figure 6.2) contributing indirectly to the overall electrochemical potential, meaning it does not translocate protons across the membrane. This protein is distributed through the three domains of life. In eukaryotes, its presence has been described in plants (*14*), fungi (*15*) and protozoa (*16*). NDH-2 has also been confirmed in bacteria (*17-19*) and in archaea (*5, 20*). Depending on the organism, there can be several isoforms distributed through different organelles or at different sides of the same organelle, allowing the oxidation of NADH from different cell compartments (Figure 1.3).

NDH-2 is a membrane associated homodimeric enzyme, localized at the surface of the lipid bilayer through electrostatic interactions. Each monomer has approximately 45 KDa and has a non covalently bound FAD (Flavin adenine dinucleotide) as the only redox prostetic group (*13, 21*). NDH-2 belongs to the "Two Dinucleotide Binding Domains Flavoprotein" (DBDF) super family, which as the name indicates, are characterized by their two domains for the binding of FAD and a pyridine nucleotide. The DBDF super family includes other protein families such as glutathione reductases, dihydrolipoamide dehydrogenases, NADH:ferredoxin oxidoreductases, 2,4-dienoyl-CoA reductases and sulfide dehydrogenases (*22-23*).

Roughly the structure of NDH-2 can be divided in three domains: 1 - Flavin binding domain, 2 - NADH binding domain; 3 - C-terminal domain (membrane interaction) (Figure 1.4).

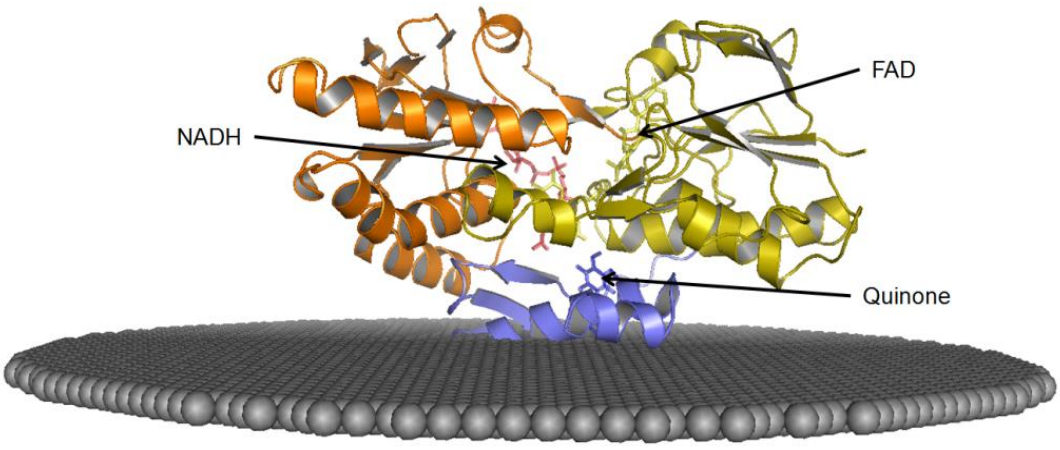

Figure 1. 4 - Cartoon representative of the crystallographic structure of NDH-2 from *S. aureus*, highlighting the three different domains. *Staphylococcus aureus* NDH-2's protomer structure model divided by its domains: Orange – NADH binding domain; Yellow – FAD binding domain; Blue – C-terminal domain. Phospholipidic membrane is represented as gray spheres. The figure was constructed using Pymol .

The presence of FAD attributes the characteristic yellow colour to the protein. The colour corresponds to a maximum absorption at 450 nm in the absorption spectrum (Supplementary figure 6.1). FAD, as well as NADH, binds to the protein by one of its two Rossman-fold domains, the dinucleotide binding domains, consisting of β-strand-α-helix-β-strand structures with GlyXGlyXXGly motives (*21-22*).

The C-terminal domain is thought to be responsible for the quinone binding and membrane anchoring. *In vitro*, a broad range of quinone substrates was proved to be accepted by the protein. Depending on the structure of the hydrophobic ring or in the size of their isoprenoid side chain, the enzyme performs different catalytic rates. Studies show that partial truncation of the bacterial C-terminal domain, specifically the terminal amphipathic helices, results in a soluble cytoplasmatic form of NDH-2, with no changes in its dimerization state, proving the membrane anchoring role of this structural feature (*17*).

Despite the recent advances in the structural knowledge of NDH-2, there is some debate about the binding site of the substrates hence the reaction mechanism associated with the redox turnover of the protein. Two different types of mechanism have been proposed for NDH-2 enzymatic activity: ping-pong or ternary complex. According to Iwata *et al* (*24*) NDH-2 has two overlapping binding sites for NADH and the quinone suggesting a single site ping-pong mechanism. In contrast Yang *et al* (*25*) proposes a ternary complex mechanism, with donor and acceptor both bound to the protein simultaneously in distinct binding sites. This ambiguity observed even at the very basic structural/mechanistic level illustrates how little is known about this protein family and the need of further exploring the molecular basis of its enzymatic functioning.

Inhibitors for type-II NADH:quinone oxidoreductases are rare and mostly unspecific. Mainly two classes of NDH-2 inhibitors are known: quinolones, in which HQNO (2-n-Heptyl-4-hydroxyquinoline N-oxide) is included, and phenothiazines**.** Besides these family of compounds, just a few other molecules have been proposed to have inhibitor activity, but they are either hard to manipulate or have weak inhibiting activity (*21, 26-29*).

The presence of NDH-2 has not been reported in mammalian mitochondria, and has been proved to have an essential role in the bioenergetics of some human pathogens, sometimes being the only NADH dehydrogenase present. These observations led to the proposal of this enzyme as a new drug target to deal with pathogenic related diseases (*28, 30-32*).

Although type-II NADH:quinone oxidoreductase has been given new attention, and so, a lot of new knowledge has been gathered in the recent years, many questions are still open to debate. These include the way how these enzymes associate with biological membranes, their interaction with hydrophobic quinones, their redox reaction mechanism and their function/regulation in metabolism. With the ascension of the genomic era, new genomes were

sequenced and genes encoding type-II NADH:quinone oxidoreductases have become available for experimentation, opening new opportunities to study NDH-2.

1.2 *Staphylococcus aureus*

1.2.1 General characteristics

The organism *Staphylococcus aureus* (*S. aureus*) is a facultative anaerobic, Gram-positive, non motile, asporogenous, coccal bacterium belonging to the Firmicuttes phylum. These bacteria can be frequently found in the human respiratory tract and in the skin. Although *S. aureus* is not always pathogenic, infection can be caused by entering of the bacteria to usually sterile sites due to trauma or abrasion in skin or mucosa (*33*).

S. aureus is a frequent cause of skin infections, respiratory diseases (sinusitis), food poisoning and one of the five most common causes of hospital-acquired infections. Each year, as much as 500,000 patients in United States' hospitals contract a staphylococcal related infection (*34*).

The treatment of choice for *S. aureus* infection was penicillin, but since the introduction of this antibiotic in 1943 the percentage of penincilin-resistant isolates has been growing, and by 1960 it had reached 80 %. Treatment of *S. aureus* became a therapeutic challenge, even with combination therapies with gentamycin and meticillin, after the rise of antibiotic-resistant strains in the 1960s and 1970s, particularly meticillin-resistant *S. aureus* (MRSA) (*35*).

MRSA represents between 5 and 54 % of clinical isolates in Western Europe (*36*) and over 50 % in the United States (*37*). Besides being more challenging to treat, MRSA has a significantly higher mortality than the susceptible isolates (*38*) and leads to longer hospital stays, therefore higher health care associated costs (*39*). It is the increasingly higher hospital associated costs that has alerted the industrialized countries to one of the biggest threats to human health into the second decade of the 21st century.

S. aureus produces and secretes enzymes, toxins, adhesions and immunomodulators that allow the pathogen to colonize and interact with the host cells, inducing cell destruction. The most studied *S. aureus* virulence factor is Panton–Valentine leukocidin (PVL), a toxin associated with abscess formation and severe necrotizing pneumonia (*38*).

1.2.2 Respiratory chain

As facultative anaerobic bacteria *S. aureus* are able to perform both aerobic and anaerobic respiration, and also change into fermentative metabolism. Not much is known about *S.aureus* respiratory chain. Similarly to other Staphylococci species, it has genes coding to two A-type O_2 reductases (*40*).

Based on genome analyses, there is no gene cluster that suggests the presence of Complex I nor of sodium-translocating NADH:quinone oxidoreductase (Na^+-NQR) (http://www.sanger.ac.uk/resources/downloads/bacteria/staphylococcus-aureus.html), meaning that NADH oxidation, with its correspondent electron transport into respiratory chain, has to be performed by an alternative respiratory enzyme.

1.2.3 Type II NADH:menaquinone oxidoreductase

Type II NADH:menaquinone oxidoreductase (EC:1.6.99.3) from *S. aureus* (NDH-2_Sa), is a respiratory enzyme that catalyzes the transfer of two electrons from NADH to menaquinone (Staphylococci's physiological quinone (*41*)). This 88 KDa dimeric membrane protein (44 KDa per monomer) has already been purified and characterized (*42-43*) and is one of the very few to have a crystallographic structure determined (*44*). As all NDH-2, this protein has two Rossman-fold domains for the binding of NADH and its cofactor FAD, and contains a C-terminal domain associated to the membrane docking. The protein is a dimer in solution as showed by the performed SAXS studies. It was also shown that binding of NADH to NDH-2 leads to the formation of a stable charge transfer complex characterized by the appearance of a band around 670 nm in the protein UV-Visible absorption spectrum. Fast kinetics studies showed that the limiting step of the reaction was the oxidation of FAD (and concomitant quinone reduction). HQNO was shown to inhibit the reaction and to affect the binding of the quinone and NADH differently (*43*).

At the moment of my arrival to the hosting laboratory, studies related with NADH:quinone oxidoreductase from *S. aureus* (NDH-2_Sa) wild type (WT) were already in progress. Besides contributing to the NDH-2_Sa WT studies, I started the expression, purification and biochemical characterization of NDH-2_Sa mutants (E172A, E172Q, E172S and E172D), to further investigate the structural/functional relationship in this protein.

1.3 *Vibrio cholerae*

1.3.1 General characteristics

Vibrio cholerae (*V. cholerae*), the etiological agent of cholera disease, is a facultative anaerobic, asporogenous, motile, curved, Gram-negative bacterium. There are over 130 different serougroups of *V. cholerae* but only O1 and O139 strains are associated with human disease (*33*).

Both O1 and O139 *V. cholerae* strains secrete an exotoxin known as cholera toxin which binds to a specific receptor (GM1 ganglioside) in the intestinal mucosa cells. The A subunit of this toxin is then released into the cell activating adenylate cyclase, leading to the increase of the cyclic adenosine monophosphate (cAMP) which inhibits the Na^+ absorption by the cell. To compensate this ion gradient, cells are forced to pump Cl^- to the intestine lumen, followed by water.

The pathogenesis of *V. cholerae* depends on the synergistic action of a number of other different factors which allow the cell to reach and colonize the human intestine, but the cholera toxin is the direct responsible for the most common symptoms associated with this disease, diarrheas and vomits. In acute cholera cases, the amount of water lost in the small intestine is greater than the possible reabsorption in the large intestine, eventually leading to death by dehydration.

These pathogenic bacteria are commonly found in places with poor sanitation and it spreads through contaminated food and water, colonizing the human small intestine. This association with non treated waters explains the higher cholera incidence in places like south Asia, Latin America and Africa (*33, 45-46*).

The worldwide incidence of cholera has increased approximately 25 % throughout the first decade of the 21^{rst} century. In 2013 there were 129064 reported cases of cholera that are considered to be underestimated due to “the fear of negative impact on travel and trade” (*46-47*).

1.3.2 Respiratory chain

V. cholerae are facultative anaerobes, and so, they are able to perform both aerobic and anaerobic respiration, depending on the oxygen availability. Its respiratory adaptability is further enhanced by the fact that they can also change its metabolism into the fermentative state if needed. This pathogen is extremely adaptable, constantly changing its transcriptome according to its needs (*48-49*). Based on genome databases and sequence analysis, it is accepted that *V. cholerae*’s respiratory chain has no Complex I

(http://gcid.jcvi.org/projects/msc/vibrio/ - March 2015), therefore the oxidation of NADH has to be performed by other respiratory enzymes.

The *Vibrio cholerae*'s Na^+-NQR is a redox-driven pump that couples de sodium transport across the membrane with the electron transfer from NADH to quinone. This 210KDa respiratory enzyme is composed of six different subunits and contains a non covalently bound FAD, two covalently bound FMNs, a 2Fe-2S center, a non covalently bound riboflavin and an iron center (*50-51*).

1.3.3 Type II NADH:ubiquinone oxidoreductase

In addition we have identified another hypothetical NADH dehydrogenase, based in amino acid sequence analyses. This hypothetical enzyme is coded by the chromosome's I VC1890 gene located between positions 2038194 and 2039498, and little or nothing is known about it. After blasting (*52*) the amino acid sequence coding already characterized NDH-2 from different organisms against the genome from *Vibrio cholerae*, the best scoring hit was identified as a NADH:quinone oxidoreductase. This hypothetical classification was further supported by the presence of the characteristic signature for Rossman-Fold domains (GlyXGlyXXGly) in the coding sequence.

We propose that this protein belongs to the NDH-2 family catalyzing the transfer of electrons from NADH to the ubiquinone (*Vibrio's* physiological quinone), serving as another electron entry point to the Vibrio's respiratory chain, having an estimated molecular mass of 47.5 KDa per monomer.

Together, both NQR and NDH-2 from *Vibrio cholerae* seem to serve as the only membrane NADH dehydrogenases, regulating the entry of electrons to the respiratory chain and therefore controlling the respiration rate of this organism. Studies on this protein have not been published to date, so if confirmed, this will be the first step in the identification and characterization of this unknown protein.

2. Materials and Methods

2.1 NDH-2 Structural Models

NDH-2_Sa WT, E172A, E172S, E172Q, E172D and NDH-2_Vc structural models were generated using the Protein Homology/analogy Recognition Engine V 2.0 (Phyre^2) web tool (*53*), using bacterial *Staphylococcus aureus* NDH-2 structure (PDB code 4XDB) as the crystallographic protein template.

Generated models were analyzed and used to create illustrational figures supporting theoretical discussions using PyMOL (*54*).

2.2 Protein Expression and Purification

Escherichia coli (*E. coli*) Rosetta 2 (DE3)pLysS cells (Novagen) were transformed with the plasmid pET-28a(+) containing the coding sequence of each of the studied NDH-2 (NDH-2_Sa WT, E172A, E172S, E172Q, E172D and NDH-2_Vc). Plasmid construction was made previous to my arrival to the lab. Transformation was achieved using a heat shock protocol (*55*).

Cells were grown in 2YT rich medium with 100 μg/mL kanamycin (Roth) and 34 μg/mL chloramphenicol (Roth) at 37 ºC and 180 rpm. Protein expression was induced with the addition of 1 mM IPTG (isopropyl-β-D-thiogalactosidase) (Apollo Scientific) to the media when cells reached an optic density (OD_{600}) of 0.6. After 4 hours of induction, cells were harvested by centrifugation at 8.000 rpm, 10 minutes and stored at -20 ºC.

Thawed cells were suspended in 100 mM phosphate buffer pH 7.0, 250 mM NaCl, containing a tablet of protease inhibitors (Roche), before being disrupted in a French Press at 6,000 psi. Disrupted cells were separated from non disrupted ones by centrifugation at 10,000 rpm, 10 min. The resulting supernatant was ultra-centrifuged at 42,000 rpm for 2 hours. The resulting pellet (membrane fraction) was resuspended in 100 mM phosphate buffer pH 7.0, 2 M NaCl, using a Potter homogenizer, and incubated at 4 ºC over night (under agitation). The membrane fraction was ultra-centrifuged again at 42,000 rpm for 1 h. The ionic strength of the resulting supernatant (soluble fraction), containing NDH-2, was lowered to 50 mM NaCl, with successive additions of 100 mM phosphate buffer pH 7.0, to a Amicon filtration system, at 4 ºC.

The resulting sample was injected in an ionic exchange chromatography column, Q-Sepharose High Performance (GE Healthcare), and eluted with a NaCl concentration gradient ranging from 0 to 1 M in 100 mM phosphate buffer pH 7.0. The eluted fraction containing NDH-2 was then injected into a size exclusion chromatography column, Gel filtration Superdex 200 (S-200) (GE Healthcare), and eluted with 100 mM phosphate buffer pH 7.0, 250 mM NaCl. Both chromatography columns were connected to an AKTA Prime Plus system (GE Healthcare)

allowing following the absorbance of the eluted fractions at 280 and 450 nm. The purified proteins were stored at -80 ºC.

The described protocol was applied to all the studied NDH-2. For NDH-2_Vc specifically three different buffer´s pHs (6, 7 and 8) were tested during purification protocol optimization (see discussion).

2.3 Biochemical characterization

The biochemical characterization aimed first, to evaluate the quality of the protein samples, by determining its concentration, flavin content and purity; second, to make a preliminary spectroscopic characterization of the samples (allowing simultaneously to access its enzymatic redox reversibility, hence its correct functioning, and to obtain the protein UV-Visible spectra); and third to determine/confirm some more specific physical/chemical parameters such as molecular mass, oligomerization state, stability and secondary structure content.

2.3.1 Protein purity

Protein purity was evaluated by sodium dodecyl sulphate – polyacrilamide gel electrophoresis (SDS-PAGE) using a Mini-PROTEAN® Electrophoresis System (BIORAD). Samples, containing 15 μM NDH-2 in 5 μL of loading buffer (Tris-HCl 50 mM, pH8; SDS; Bromophenol Blue; Glycerol; β-mercaptethanol and Urea), were subjected sequentially for 15 minutes to 150 V, 400 mA, 200 W and 45 minutes to 180 V, 400 mA, 200 W in 4 % and 12.5 % acrilamide stacking and resolving gel respectively. Low molecular weight (LMW) standards (GE Healthcare) were used ranging from 14 to 97 KDa. Protein bands were revealed using Blue Coomassie Stainer (0.1 %).

2.3.2 UV-Visible spectroscopy

These spectroscopic studies had as main objectives the acquisition of both oxidized and reduced NDH-2 spectra, confirm the appearance of a charge transfer complex, assess protein quantification, as well as showing the reversibility of the system, hence its functionality, before proceeding into more advanced techniques.

UV-Visible absorption spectroscopy was performed on a Shimadzu UV-1800 spectrophotometer. Spectra were collected on an anaerobic chamber where O_2 level was kept bellow 1 ppm. To further guarantee the absence of O_2 in the assays all the solutions were

prepared inside the anaerobic chamber with degassed water, and a Scavenging System, composed of 5 mM glucose (Roth), 4 U/mL glucose oxidase (Sigma Aldrich) and 130 U/mL catalase (Sigma Aldrich), was used.

Reduction of 6 μM NDH-2 was achieved by addition of NADH (12 μM for E172A, E172S and E172Q; and 30 μM for E172D and NDH-2_Vc) (Sigma Aldrich) or sodium dithionite (Sigma Aldrich) (same concentrations of NADH) and for its oxidation 2,3-Dimethoxy-5,6-dimethyl-p-benzoquinone (DDB) (Sequoia Research Products) (in the case of NDH-2_Vc) or 2,3-Dimethyl-1,4-naphtoquinone (DMN) (synthesized from menadione from Sigma Aldrich (*56*)) (for NDH-2_Sa mutants) respectively was added. The added quinone concentration was the same as NADH, to maintain a 1:1 ratio of substrates. Spectra were collected at wavelengths ranging from 250 to 900 nm, at 35 ºC and using 100 mM phosphate buffer pH 7.0, 250 mM NaCl.

2.3.3 Protein and flavin quantification

After purification, protein was quantified spectroscopically in a Shimadzu UV-1603 spectrophotometer, using the obtained spectra and extinction coefficients at 280 nm (ε280) of 50.364 and 35.534 $mM^{-1}cm^{-1}$ for NDH-2_Sa and NDH-2_Vc respectively. The ε280 were calculated using the following equation and considering the ε280 for the free oxidized flavin:

$$\varepsilon 280_{(\text{protein})} = \varepsilon 280_{(\text{FAD})} + (\#\text{Trp} \times 5500 \; + \; \#\text{Tyr} \times 1490 \; + \; \#\text{Cys} \times 120) \;\; M^{-1}cm^{-1}$$

eq. 2 - Extinction coefficients at 280 nm (ε280) calculation formula based in the number of tryptophan, tyrosine and cysteine reisudues in the coding sequence.

Flavin content was determined by comparing the results from protein and FAD concentration. FAD concentration was calculated by quantification of its absorbance at 450 nm using the extinction coefficient of 11.3 $mM^{-1}cm^{-1}$ for the free oxidized flavin.

2.3.4 Oligomerization state

To investigate the oligomerization state of the purified proteins size exclusion chromatography was performed using a Superdex 200 10/300 GL column, 25 mL (GE-Healthcare) on a AKTA Prime Plus system (GE Healthcare) pre-equilibrated with 100 mM potassium phosphate buffer pH 7.0, 250 mM NaCl; at 12 ºC. A calibration curve was obtained by plotting the mass of known standards vs the respective elution time (elution time was determined by following the absorbance at 280 nm). Cytochrome *c* (12 KDa), Mioglobin (17 KDa), BSA (67 KDa), Conalbomin (77 KDa), Glucose oxidase (160 KDa) and Ferritin (440 KDa) were injected separately in the column and their elution volumes were determined to be used as standards (Dextran blue (2000 KDa) elution determined the “dead volume” of the column).

To further confirm the oligomeric state of the purified proteins Native-PAGE was performed. The protein samples, containing 15 μM NDH-2 in 2.5 μL of loading buffer, 1 μL Coomassie blue G-250 sample additive and 10 μL of water, were loaded on a 1 mm thick, 3-12 % polyacrylamide gradient gel, containing 50 mM BisTris and 500 mM aminocaproic acid, and were subjected 1 hour to 150 V and followed by 40 min at 250 V, always at 4 ºC. High molecular weight markers (GE Healthcare) were used ranging from 67 to 669 KDa. The anode buffer was 50 mM BisTris pH 6.8. The initial cathode buffer was 50 mM Tricine, 15 mM BisTris pH 6.8, and 0.5 % Brilliant Blue G-250 (used during the first hour) and the second cathode buffer was 50 mM Tricine, 15 mM BisTris pH 6.8, and 0.05 % Brilliant Blue G-250 (used during the last 40 minutes). At the end of the electrophoretic process, the gel was stained with Coomassie Blue to further guarantee an homogeneous staining (0.1 %).

2.3.5 Circular Dichroism

Circular Dichroism (CD) makes use of an optical characteristic of some materials, or structural features, in which light rays having different polarizations are absorbed in different proportions. In CD the quantification of the differential absorption of circularly polarized light may provide a set of different structural information about very different optically active molecules. The most common use of CD is in the study of secondary structure of proteins. Different secondary structure features, affect the CD spectrum of a protein differently, hence, it may be used to identify and calculate the relative percentage of α-helix/β-sheet/Turn/Unordered structure (*57*).

In this case the CD spectra of the different purified NDH-2_Sa mutants (E172A, E172Q, E172S and E172D) were acquired to investigate, in a non quantitative analysis, if the secondary structure was maintained when comparing with the wild type.

CD experiments were performed in a Spectropolarimeter J-815 at 25 ºC with 50 sequential acquisitions at 100 nm/sec. Spectra ranged from 260 to 200 nm. Proteins were studied at 5 μM concentration in 1 mM potassium phosphate buffer pH 7.0.

2.3.6 Thermal denaturation

The thermal denaturation assays had as objective the determination of the temperature from where the studied proteins started to denaturate, allowing to conclude about their thermal stability and insure that the protein is stable under all working conditions. Thermal denaturation assays were performed using a Peltier temperature controller with a rate of 0.5 ºC/min between 25 and 90 ºC. Data was recorded in intervals of 1 ºC with an acquisition time of 0.1 min. Denaturation was monitored by fluorescence spectroscopy using excitation at 450 nm and

emission at 530 nm. The assays were performed using 2 µM of protein in 100 mM phosphate buffer pH 7.0, 250 mM NaCl.

The Melting Temperature was calculated using the OriginPro8 software, fitting a Boltzman function (sigmoidal curve) to the data.

2.3.7 Cyclic Voltammetry

Cyclic Voltammetry (CV) is a technique that allows the study of electrochemical reactions. In a CV experiment a voltage is applied in a "working" electrode. Starting in a preselected value (E_i), the potential is scanned linearly, increasing until a determined limit (Switching potential), and then decreasing, returning to the starting value, thus completing the voltage cycle. During the scanning of the potential (measured against a reference electrode), the generated electrical current is recorded as a function of the applied potential originating a Voltammogram (Figure 2.1) (*58*). During the first half of the cycle, the potential has to reach a value that allows the studied sample to have been reduced originating a peak in the Voltammogram (E_{pc} – Figure 2.1). In the second half of the cycle, starting in the switching potential, the sample is reoxidized giving rise to a second peak (E_{pa} – Figure 2.1). The number of cycles, as well as the scan rate, can be varied to generate more robust data (*59*).

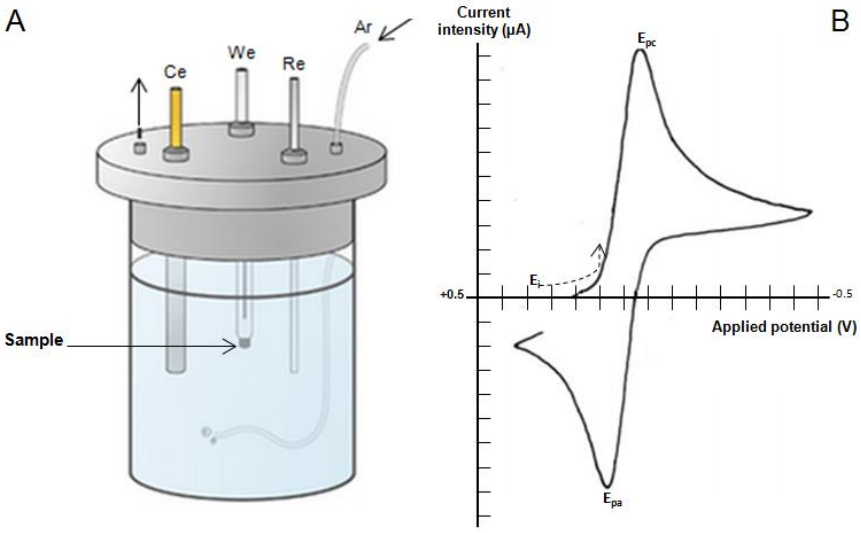

Figure 2. 1 - Cyclic Voltammetry setup and representative Voltammogram with current intensity (µA) plotted vs Applied potential. (A) – Cyclic Voltammety instrument setup: We – working electrode; Re – reference electrode; Ce – Counter electrode; Ar - Argon entry point. (B) - E_{pc} - Cathodic peack potencial; E_{pa} - Anodic peack potential; E_i - Initial potential. The arrow represents the direction of the potential during the scan. Adapted from *(58)*.

CV can be used to study the presence of intermediates in redox reactions, electron stoichiometry of a system, formal reduction potentials, determine diffusion coefficient of an analyte and concentration of an unknown solution (since concentration is proportional to current in a reversible Nernstian system) (*58*).

In this case, Cyclic Voltammetry assays were meant to determine the formal reduction potential of the FAD in the studied NDH-2. The reduction potential (mV) was determined using a silver chloride electrode (Ag/AgCl) as the reference, graphite (Pg) as the working electrode and platinum (Pt) as the counter electrode. The electrolyte solution used was 100 mM potassium phosphate buffer pH 7.0, to ensure sufficient conductivity. The measurements were done with scan rates of 10, 20, 50, 75, 100, 150, 200, 300 and 500 mV/s and the recorded data were plotted as current (i) vs potential (E) to generate the cyclic Voltammogram trace. To ensure anaerobic conditions during the assays, a constant influx of Argon was maintained into the Voltammetry cell.

Reduction potentials were calculated by averaging the E_{pc} and E_{pa} values of each scan rate, and then reaveraging the values obtained from the nine tested scan rates. Final reduction potential was converted to have the reduction potential of the Standard Hydrogen Electrode (SHE) as reference.

2.4 Steady state kinetics

Enzyme kinetics is a general term that defines the study of chemical reactions catalyzed by enzymes. In these studies, reaction rates constants (k) are determined and the effect of different reaction conditions, such as substrate concentration, temperature or pH, are investigated. Briefly, steady state kinetics can be described as a specific approach in enzyme kinetics where the concentration of enzyme-substrate complex [ES] is considered to be constant during the time that the experimental reaction rates are measured (activity assays). This is achieved by maintaining the substrate concentrations [S] orders of magnitude above the enzyme concentration [E], meaning that virtually there is no free enzyme and that all of the protein is bound to its substrate (saturating conditions). As a biochemical model to enzymatic studies, the steady state kinetics model is an approach and does not fully represent all enzyme mechanistic behavior possibilities, but its ability to provide a working foundation that is both conceptually correct and easy to compare between different enzymatic systems, made it widely used.

Steady state activity assays were performed on a Shimadzu UV-1800 monitoring the change in the absorbance at 340 nm, corresponding to the wavelength at which the electron donor (NADH) absorbs the most. The reaction mixture (1000 µL) contained 20 nM of protein (final concentration) in the case of NDH-2_Sa WT and NDH-2_Vc; and 500 nM in the case of the studied NDH-2_Sa mutants; all diluted in 100 mM potassium phosphate buffer pH 7.0, 250 mM NaCl.

Both aerobic and anaerobic enzymatic activities were studied. Activity assays in anaerobic conditions were performed inside an anaerobic chamber at 35 ºC (all the solutions

were prepared inside the anaerobic chamber with degassed water), and meant to determine both the substrates' Michaelis-Menten constant (K_M) and the maximum rate (V_{max}) of the enzyme. To the NDH-2_Sa mutants, two independent curves were done. In the first titration DMN was used as electron acceptor at concentrations ranging from 5 to 150 μM (with NADH stable at 100 μM). In the second curve, NADH concentrations ranged from 5 to 100 μM (with the electron acceptor stable at 150 μM). In the case of NDH-2_Vc, single concentration measurements were performed (only the V_{max} was studied) at 100 μM for NADH and 150 μM for both DDB and DMN.

NADH extinction coefficient of 6.22 $mM^{-1}cm^{-1}$ was used to calculate NDH-2 specific activity (μmol/min/mg protein). Measured initial rate (V_0) was plotted vs substrate concentration. The Michaelis-Menten equation was used to create fitting curves to the experimental data, using a non-linear least-squares regression to determine K_M and V_{max} values.

Inhibition studies (still in anaerobic conditions) were performed in NDH-2_Sa mutants using HQNO. HQNO titrations were performed to calculate the inhibition coefficient (K_I) of this inhibitor to the different NDH-2_Sa mutants. Titrations were made ranging the concentration of the inhibitor from 0 to 100 μM, maintaining NADH and DMN concentrations stable at 100 and 150 μM respectively.

Aerobic activity assays were performed at atmospheric O_2 concentrations at 35 ºC, with 100 μM NADH and with both 0 and 150 μM of the quinones used in the anaerobic assays. All measurements were made in triplicates.

2.5 Fast kinetics

Fast kinetics experiments were performed in a Stopped-Flow system "SF-61DX2, TgK Scientific Ltd". The evolution of the system in the mixing chamber was followed spectroscopically with a photodiode array in a range of wavelengths from 350 to 700 nm. Stopped-flow is a technique that allows the study of fast reaction mechanisms in solution over timescales of about 1ms up to several minutes. In general, the content of two separated "driving syringes" is rapidly mixed together and then "stopped" in an observation cell called "mixing chamber". This chamber is then irradiated with light and as the reaction proceeds the change in the UV-Visible absorbance spectrum is recorded as a function of time. The small period of time from which the reaction can be followed and before the initial measure is called "dead time" and is physically limited by the quickness of the apparatus. Lesser efficacy/quickness means bigger "dead times" which can lead to the loss of important data. Analysis of the resulting kinetics can determine reaction rates, complexity of the reaction

mechanism, information on short-lived reaction intermediates for example. As in steady state kinetics, the effect of parameters such as temperature, pH and reagent concentration on the kinetics of the reaction can be determined with a series of experiments.

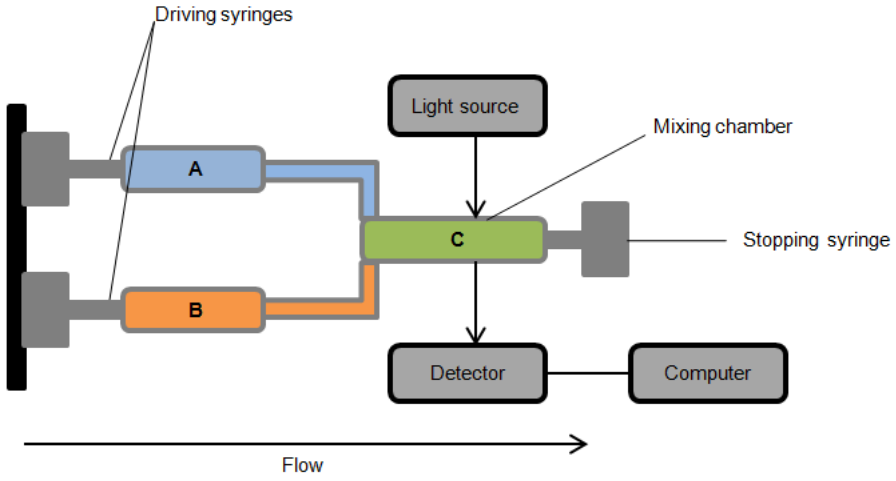

Figure 2. 2 - Schematic representation of the "Stopped Flow" apparatus. The arrow represents the direction of the flow. Chambers' A and B content is mixed in Chamber C and irradiated with light, which is then measured by the detector.

The main goal of the fast kinetics experiments performed in the frame work of this thesis was the study of both the reductive and oxidative half-reactions and the charge transfer complex formation from the different NDH-2 by the determination of their kinetic parameters. As the majority of the redox reactions, electron transfer between NADH, NDH-2 and quinone occurs in the ms timescale and is dependent of environmental conditions like pH and temperature. In order to maintain conditions as reproducible as possible during all fast kinetics experiments, the temperature of the entire apparatus was maintained at 15 ºC and pH was controlled with 100 mM phosphate buffer pH 7.0, 250 mM NaCl (conditions previously optimized in this lab while performing similar studies (*43*)). 15 ºC was a temperature that was previously tested in the lab, in order to guarantee that the reaction was slowed enough to occur outside of the "dead time" period. If the fast kinetics assays would have been performed at 30 ºC, the majority of the reaction would have ended by the time the readings started.

Since O_2 may interfere with the redox activity of the enzyme, generating misleading results, anaerobic conditions were guaranteed during all fast kinetics experiments by using the entire Stopped Flow apparatus inside an anaerobic chamber MBraun 130, where the oxygen level was kept bellow 1 ppm. To further ensure anaerobic conditions in the assays, all the solutions were prepared inside the anaerobic chamber with degassed water, and a Scavenging System (equal to the one described in the UV-Visible absorbance spectra assays) was used.

The rate constants were calculated from the fitting of the kinetic traces, obtained from the wavelengths at which the absorbance changes were most evident (reduction and oxidation were followed at 450 nm and charge transfer complex formation at 670 nm), to an exponential

curve using the tool *solver* from Microsoft Office Excel. The missing data corresponding to the dead time (~3 ms) was extrapolated considering the values of the absorbance at time zero obtained from control experiments with only NDH-2.

Reductive half-reaction

For the study of the reductive half-reaction (electron transfer from NADH to the flavin) 10 μM of oxidised NDH-2 (syringe A) was mixed with 10 μM of NADH (syringe B) (1:1 ratio). During the first 150 ms (dead time not included) 100 UV-Vis spectra were acquired. Reductive half-reaction studies were performed to NDH-2_Sa WT, E172A, E172S, E172Q and E172D.

Oxidative half-reaction

For the study of the oxidative half-reaction (electron transfer from the flavin to quinone) 10 μM of oxidised NDH-2 (syringe A) was mixed with 20 μM of NADH and 30 μM of DMN (syringe B). These conditions allowed the protein to complete two turnovers and the final oxidation was considered to the determination of the oxidation rate. During the first 750 ms (dead time not included) 100 UV-Vis spectra were acquired. Oxidative half-reaction studies were performed to NDH-2_Sa WT, E172A, E172S, E172Q and E172D.

2.6 Fluorescence Quenching Studies

Protein fluorescence studies are frequently used has they rely on relatively simple apparatus and can provide valuable information about the studied protein. The recorded data is related to changes in the fluorescence of specific protein features, most commonly the tryptophan residues, by the action of a quencher molecule which can be a substrate, an inhibitor or any other ligand (*60*).

In the specific case of enzyme-substrate interaction, fluorescence quenching studies can be used to obtain, for example, substrate-enzyme dissociation constants (K_D), substrate binding site relative positions or protein allosteric-induced conformational changes. Despite the easy handling with which the data is collected, a lot of variables have to be considered in order to allow a correct data analysis (*61*). The main goal of these Fluorescence quenching studies was the determination of the K_D from both NADH and quinone to the different NDH-2_Sa.

Fluorescence spectra were obtained using a Varian Cary Eclipse spectrofluorimeter. The effect of both NDH-2_Sa substrates, NADH and quinone, was tested with three independent titrations ranging from 0 to 100 μM. The reaction mixture (500 μL) contained 2 μM NDH-2, diluted in 100 mM potassium phosphate buffer pH 7.0, 250 mM NaCl, and the substrate being studied. The effect of HQNO (Alexis) in the protein quenching by both NADH and quinone

was tested by repeating the above described titrations but this time in the presence of 100 μM of this inhibitor.

Tryptophan and flavin fluorescence emission spectra were recorded at 25 ºC with excitation wavelengths of 280 nm and 450 nm respectively. The variation of the emission at 330 nm (ΔF) was normalized and represented as function of substrate concentration.

In order to determine the K_D, the obtained titration data was used to simulate curves using the Monod-Wyman-Changeux (MWC) model equation (for dimeric enzymes):

$$\Delta F = \Delta Fmax \times \frac{\frac{[S]}{Ks} \times \left(1 + \frac{[S]}{Ks}\right)}{L + \left(1 + \frac{[S]}{Ks}\right)^2} \text{ , with L } = \text{ 0 assuming no cooperativity.}$$

eq. 3 - Monod-Wyman-Changeux (MWC) model equation (for dimeric enzymes) (*62*). [S] – substrate concentration; ΔFmax – maximum fluorescence quenching; K_S – equilibrium constant (replaced by K_D); L – allosteric constant (considered as "0" for a non cooperative binding).

This was the model chosen before to describe the behavior of the tryptophan and flavin fluorescence emission spectra from the wild type NDH-2 (*43*).

3. Results and Discussion

3.1 Type II NADH:quinone oxidoreductase from *Staphylococcus aureus*

A thorough study of NDH-2_Sa wild type has already been performed at the hosting laboratory (*43*). In this study, the wild type protein was investigated in both structural and functional terms, and some of the drawn conclusions inspired the follow up of the project to further enlighten the catalytic mechanism.

The work reported in this thesis focused on the characterization of site specific mutants from NDH-2_Sa. The mutations were selected prior to the starting of this master thesis. In order to contextualize selection of the mutants, a brief description of the mutant selection related work is presented below.

A thorough multiple sequence alignment (MSA) of NDH-2, that lead to a robust definition of the NDH-2 family, was performed. This study involved 2566 sequences, selected from the KEGG database (*63*), which allowed to identify conserved amino acid residues. A set of 26 amino acid residues with conservation higher than 80 % was identified (with 80 % conservation meaning that the respective amino acid is present in 80 % of the proteins used in the MSA). Considering that, if a structural element is conserved (retained through evolution) it will probably be proved as important to the enzyme function (whether structurally or catalytically), the investigation of that amino acid residue, may be a powerful approach in studying the protein of interest. In addition we also took into account the localization of such amino acid residue in the structure. From those 26 conserved amino acid residues, 22 were Glycines (which are commonly found as a α-helix disruption feature due to their high conformational flexibility, making entropically expensive to adopt the α-helix conformation) or hydrophobic amino acid residues.

The four remaining highly conserved amino acid residues are Aspartate 302, Tryptophan 261, Glutamate 172 and Aspartate 103. Glutamate 172 (E172) is present on the NADH binding site in the interior of the protein close to the isoalloxazine ring of FAD. This was the elected amino acid residue to be investigated in this study (see Figure 3.1 below). By mutating this residue to other amino acids with different side chains, we aimed to study the overall mechanism of the protein, and more specifically the role that E172 has in this process.

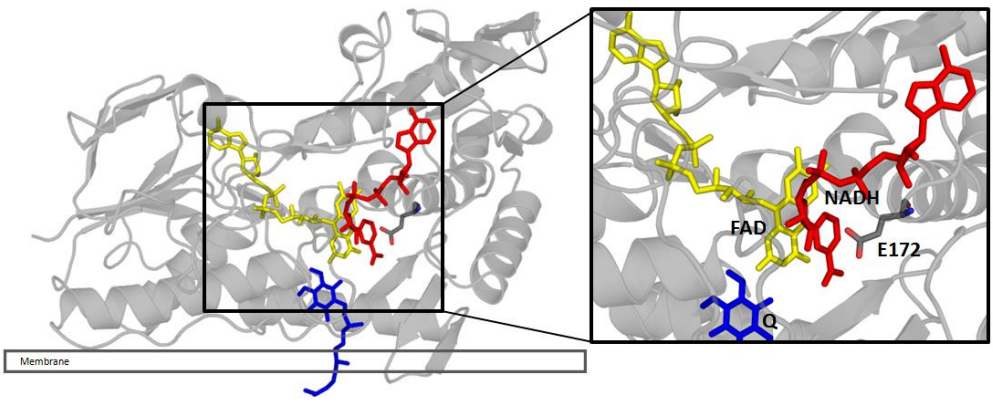

Figure 3. 1 - Cartoon representing NDH-2_Sa WT structure (PDB 4XDB) showing the localization of E172. E172 (gray), FAD (yellow), NADH (red) and quinone (blue) are highlighted in sticks. The position of the cofactors is proposed based on a superimposition of the *S. aureus* structure with the PDB from *S. cerevisiae* NDH-2 (PDB 4G6H).

Four different mutants were constructed to cover the different characteristics of the side chain of the Glutamate residue, trying to identify which of those were important to its role (see Figure 3.2 below). E172D – Figure 3.2 A (Glutamate residue replaced by an Aspartate residue) keeps the negative charge nature of the side chain (hence the ability to perform electrostatic interactions) but with a smaller range of action (due to the lack of a CH_2 group in the side chain); E172Q – Figure 3.2 B (Glutamate residue replaced by a Glutamine residue) keeps the length of the side chain and the ability to make hydrogen bonds, but looses the negatively charged nature; E172S – Figure 3.2 C (Glutamate replaced by a Serine) looses both the negative charge and the range of the side chain, maintaining only the ability to make hydrogen bonds; lastly E172A – Figure 3.2 D (Glutamate replaced by an Alanine) looses all three of these characteristics, since Alanine has a shorter side chain and is hydrophobic.

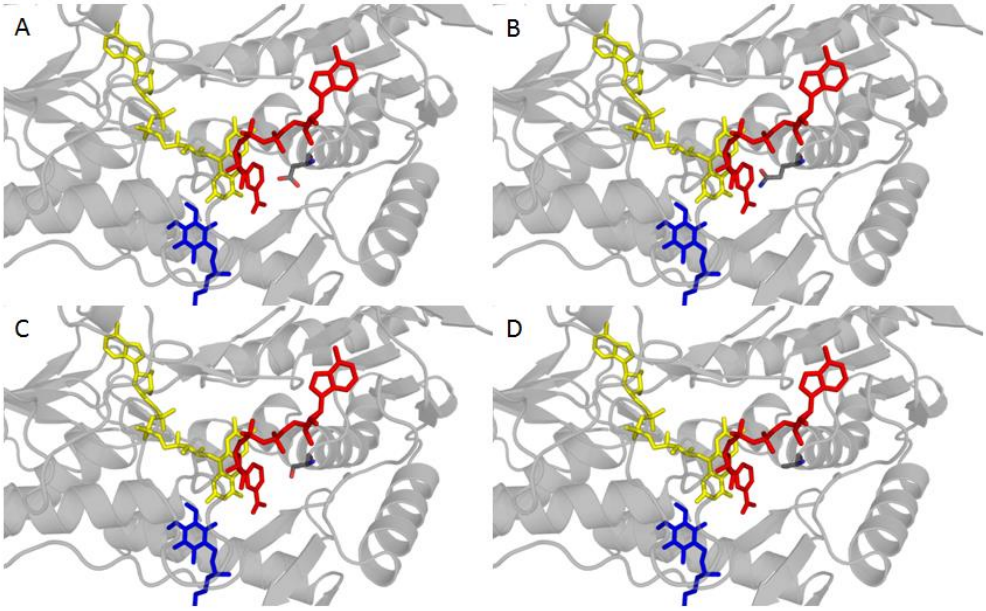

Figure 3. 2 - Cartoon representing NDH-2_Sa mutants' structure based in the WT structure (PDB 4XDB). A – E172D; B – E172Q; C – E172S; D – E172A. FAD is represented in yellow, NADH in red and quinone blue sticks. The position of the cofactors is proposed based with a superimposition of the *S. aureus* structure with the PDB from *S. cerevisiae* NDH-2 (PDB 4G6H).

3.1.1 Protein expression and purification

The expression conditions of the wild type NDH-2_Sa had already been optimized. Despite being different in only one amino acid residue, the mutated NDH-2 could have different expression patterns, so the first step in this work was to test different expression conditions of all the proteins being studied. This was achieved by doing small scale growths and monitoring the expression of the proteins by SDS-PAGE, always comparing the induced cells with no induced cell samples, as a control for basal expression.

The tested conditions varied in factors like: growth extent; cell density (OD_{600}) at the time of induction; type of expression cells; and temperature. What we observed was a similar expression pattern to all the studied NDH-2 from *S. aureus*. As described in *Sena et al* (*43*) the wild type protein could be expressed using in *E. coli* Rosetta cells, by adding 1 mM IPTG to the growing cells media (with 100 μg/mL kanamycin (Roth) and 34 μg/mL chloramphenicol (Roth)), at cell density corresponding to OD_{600} of 0.6. During the expression tests we observed that when increasing the growth extension before induction (as well as the cell density at the time of induction) the amount of expressed protein increased but so did the "background" expression of some contaminants. This meant that despite obtaining more protein per gram of cells, the amount of contaminants were also higher, possibly leading to more complex purification procedures. No other tested conditions seemed to influence positively the expression pattern of the studied proteins. Below in Figure 3.3 is shown a SDS-PAG that exemplifies one of the expression tests.

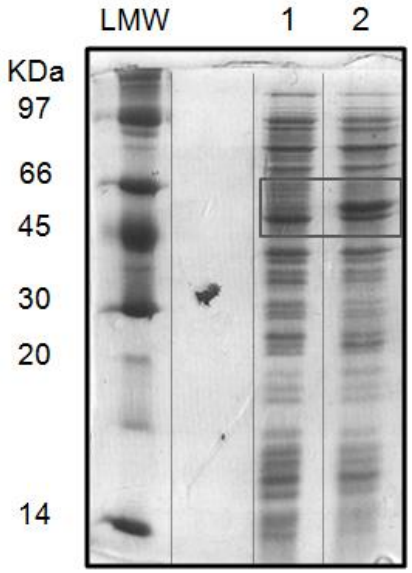

Figure 3. 3 - SDS-PAG exemplifying the NDH-2_Sa WT expression. SDS-PAGE: Stacking Gel – 4 % acrilamide; Resolving Gel – 15 % acrilamide; Molecular mass of NDH-2_Sa: ~ 44 KDa. 1 – Growth of *E. coli* Rosetta cells before IPTG addition (OD_{600} = 0.6); 2 – Growth of *E. coli* Rosetta cells after 4 hours of induction.

The gel shows the presence of a band in the 45 KDa region in lane 2 that is not observed in lane 1, confirming the expression of the protein. Based in the obtained results, that were similar to both wild type and mutants, we chose to maintain the expression conditions previously used here in the laboratory and advance to the medium scale growths: transformed *E. coli* Rosetta cells grown at 37 ºC and 180 rpm, in 2YT rich medium with 100 μg/mL kanamycin and 34 μg/mL chloramphenicol. 1 mM IPTG addition at an optic density of 0.6 to induce protein expression. 4 hours of induction (*43*).

In order to obtain sufficient cell mass as starting material to purify the proteins of interest, 4 L of cell growths were performed as described in the "Materials and Methods" section. With the exception of the volume, the conditions were the same as those used in the expression tests. Cells were harvested and stored at -20 ºC until further use.

The protocol used to purify the NDH-2_Sa mutants was the same optimized for the NDH-2_Sa wild type. Thawed cells (~100 g of cells, ~ 15 g per growth) were suspended in 100 mM phosphate buffer pH 7.0, 250 mM NaCl, before being disrupted using a French Press. Disrupted cells were separated from non disrupted ones by centrifugation at 10,000 rpm, and the membrane fraction (containing the protein) was separated from the soluble fraction by ultracentrifugation at 42,000 rpm. Protein membrane extraction was achieved by washing the membranes with high ionic strength (2 M NaCl) buffer. This procedure was possible to apply since the protein is attached to the membranes only by electrostatic interactions, and so, the addition of high salt concentrations allows the stabilization of the polar protein regions (that would be in contact with head of the phospholipids). The transfer of the protein from the membrane fraction to the soluble fraction was confirmed by the change in the colour of this last fraction to a "yellowish" tone. Soluble and membrane fractions were separated again by ultracentrifugation at 42,000 rpm. This method is advantageous when compared with the more commonly used detergent methods because not only it is environmentally friendly and economic; it also separates all the transmembrane proteins from the soluble/peripheral ones in a single step. In addition it leads to less detergent related interferences in further studies. The ionic strength of the resulting supernatant (soluble fraction), containing NDH-2, was lowered step wise in a Amicon concentrator/Diaflo to 50 mM NaCl in order to allow an ionic exchange chromatography step.

The soluble fraction was injected in a Q-Sepharose HP column and eluted with a NaCl gradient ranging from 0 to 1 M. An example of a chromatogram is showed below in Figure 3.4 for the purification of E172A (the other studied NDH-2_Sa had similar elution patterns). The fractions containing NDH-2 were identified by UV-Visible spectroscopy. In this case, the protein eluted at around 35 % B, corresponding to 350 mM NaCl, as shown below in Figure 3.4.

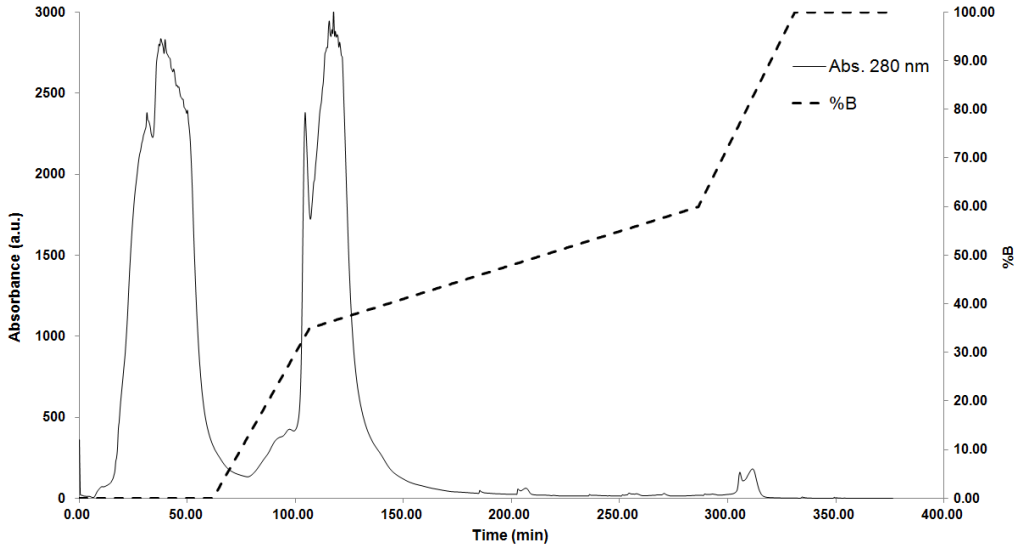

Figure 3. 4 - Example of a chromatogram obtained in the purification of the E172A NDH-2_Sa by a Q-Sepharose-HP column. In black filled line is represented the Abs_{280}, in green dashed line is represented the % of 1 M NaCl, 100 mM phosphate buffer pH 7.0 . All the purified proteins presented similar elution profiles.

The fractions containing NDH-2 were separated according to their ratio between the absorbance intensities at 280 and 450 nm (referred in this thesis as "$R^{280}/_{450}$"), concentrated and further purified in a size exclusion chromatography column. This type of chromatography separates the different compounds according to their size (higher molecular mass compounds have smaller elution volumes). The resulting chromatograms were again very similar for the different mutated NDH-2_Sa. An example S200 chromatogram is shown below in Figure 3.5. The fraction containing NDH-2 eluted at about 380 min. Again, the fractions containing NDH-2 were identified by UV-Visible spectroscopy, selected according to their $R^{280}/_{450}$ ratio, and until further analysis they were stored at -20 ºC.

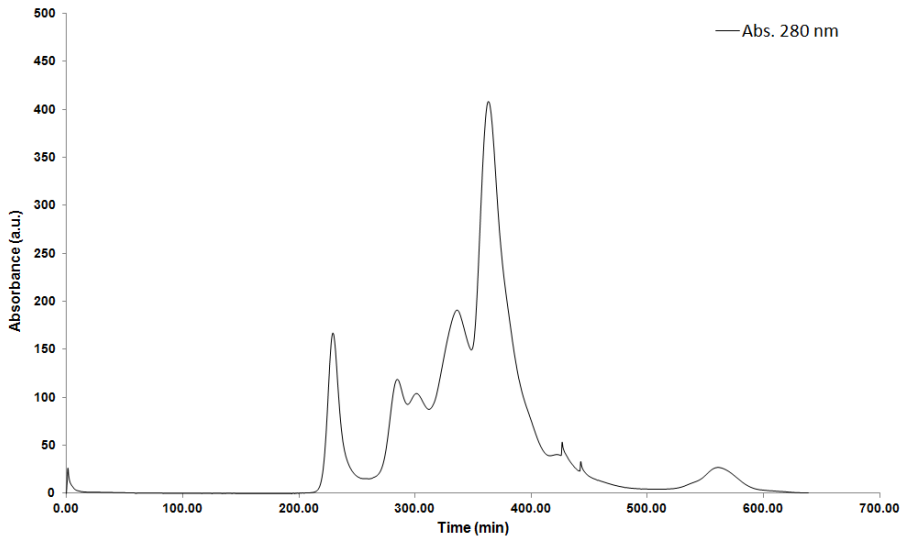

Figure 3. 5 - Example of a chromatogram obtained in the purification of E172A NDH-2_Sa by a S200 column. In black filled line is represented the Abs_{280}. This chromatogram serves as an example for all the size exclusion chromatographies performed during the purification of the studied proteins.

3.1.2 Protein purity

In order to assess the overall protein purity, two different approaches were followed: SDS-PAGE analysis and spectroscopic analysis. The different NDH-2_Sa samples were first analyzed using SDS-PAGE (Figure 3.6 below).

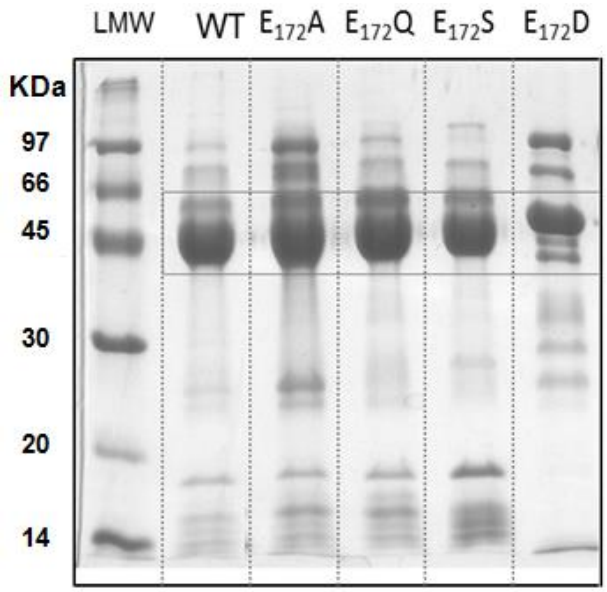

Figure 3. 6 - SDS-PAG with the purified NDH-2_Sa mutants and wild type at 15 µM. SDS-PAGE: Stacking Gel – 4 % acrilamide; Resolving Gel – 15 % acrilamide; Molecular mass of NDH-2_Sa: ~ 44 KDa. Wells: 1 – LMW markers; 2 – NDH-2_Sa WT; 3 – E172A; 4 – E172Q; 5 – E172S; 6 – E172D.

In the gel we can observe an intense band at around 45 KDa which probably corresponds to the protein of interest (molecular mass of 44 KDa) and a set of thinner and less intense bands which indicate that the protein is not completely pure. This means that there are vestigial amounts of contaminant proteins in all the NDH2_Sa samples, however they not interfere considerably in the type of studies that were performed. These results were further confirmed by the absorbance at 280 and 450 nm (Abs_{280} nm and Abs450 nm respectively).

Knowing the relative contributions of the different protein components (apoprotein and cofactor) to each of the absorbance picks, we can investigate the presence of other proteins in the sample simply by analyzing the $R^{280}/_{450}$ ratio (assuming they do not have any cofactor absorbing at 450 nm). The relative absorbance contribution analysis is possible knowing the extinction coefficients, ε, at 280 and 450 nm for the protein of interest.

The ε280 was calculated based on the number of Trp, Tyr and Cys residues in the protein sequence, also having into account the contribution of the FAD cofactor to the absorbance in this wavelength. The ε450 of the protein was considered, to be the same as that of the free oxidized FAD molecule, since the apoprotein does not absorb in this region. Considering both ε values (NDH-2_Sa WT, E172A, E172S, E172Q and E172D: ε280 = 50.364 $mM^{-1}cm^{-1}$; ε450 = 11.300 $mM^{-1}cm^{-1}$), and based in the experience obtained from previous purifications here in the lab, we can consider a $R^{280}/_{450}$ of about 5.5 to a completely pure NDH-2 with a 1:1 cofactor/apoprotein ratio. Based in this "thumb rule", and analyzing the data corresponding to the different NDH-2_Sa summarized in Table 3.1 (see below), which shows $R^{280}/_{450}$ between 6.1 and 7.0, we can consider the NDH-2_Sa wild type and mutants samples as relatively pure, thus confirming the results obtained in the SDS-PAG.

Table 3. 1 - NDH-2_Sa WT and mutants calculated $R^{280}/_{450}$ based on the absorbance intensities obtained from the UV-Visible spectroscopy.

	$R^{280}/_{450}$
WT	6.4
E172A	6.3
E172Q	6.1
E172S	6.1
E172D	7.0

3.1.3 Protein concentration and flavin content

Protein flavin content can be estimated based on the absorbencies at 280 and 450 nm. Table 3.2 summarizes the results obtained for the protein concentration using the extinction coefficients at 280 nm (ε280) of 50.364 $mM^{-1}cm^{-1}$ and at 450 nm (ε450) of 11.3 $mM^{-1}cm^{-1}$ for NDH-2_Sa wild type and mutants:

Table 3. 2 - Protein concentrations determined based in the absorbencies at 280 and 450 nm measured in the corresponding UV-Vis spectra. The ε280 and ε450 values used were 50.364 $mM^{-1}cm^{-1}$ and 11.3 $mM^{-1}cm^{-1}$ respectively.

	[Protein] $_{280\ nm}$ (μM)	**[Protein] $_{450\ nm}$** (μM)	**% Flavin**
WT	4.20	2.90	69.2
E172A	3.53	2.48	70.1
E172Q	5.48	3.98	72.7
E172S	4.82	3.54	73.4
E172D	4.33	2.74	63.4

As shown in Table 3.2, approximately 70 % of the proteins have their cofactor. The fact that there are traces of other proteins in the sample (as also suggested by the SDS-PAGE), means that the absorbance at 280 nm is not entirely from the protein of interest, and so the real value would be lower (hence a better/lower $R^{280}/_{450}$ value). A lower value in the 280 nm absorbance would also mean a different % Flavin. So we can safely say that the calculated value of ~70 % is underestimated, and without knowing the contribution of the "other proteins" in the sample (and based only in the data obtained in the scope of this thesis), it is not possible to conclude about the real % Flavin. Nevertheless, we can conclude that at least 70 % of the proteins have FAD, which is acceptable, considering that the quantification of the protein that is used to prepare the sample in the following studies, was performed based on the 450 nm absorbance (considering only the protein population with the FAD cofactor).

3.1.4 Structural analyses of NDH-2 from *Staphylococcus aureus*

Oligomerization state

Sena et al (*43*) showed that NDH-2_Sa wild type is a dimer in solution, and this two subunit supra organization may be important to maintain the protein in a specific structural position that promotes its correct functioning. To determine if the studied NDH-2_Sa mutants maintained this dimeric state, the oligomerization state of the proteins was determined.

The oligomerization state of the proteins was determined by analytical size exclusion chromatography, which was considered to be a good approach since NDH-2 has an approximate globular structure. Proteins with lower molecular mass have a higher retention time, which is reflected in a higher elution volume.

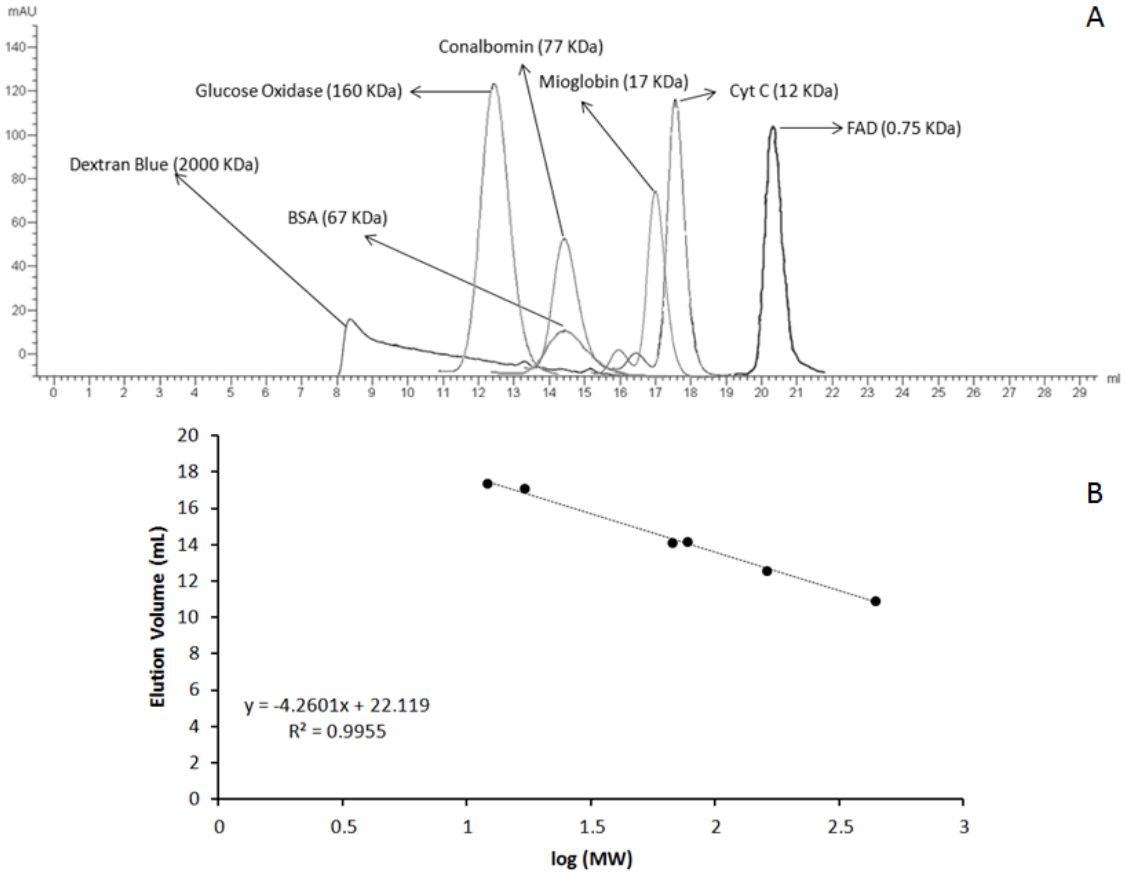

Figure 3. 7 – Chromatogram of the protein standards' size exclusion chromatography and corresponding calibration curve. The absorbance at 280 nm is represented as a function of the eluted volume. A - Superimposed chromatograms obtained from the independent injections of the standard commercial proteins; B – The calibration curve (dotted line) was calculated by a linear regression of the elution volumes from the injection of cytochrome *c* (12 KDa), Mioglobin (17 KDa), BSA (67 KDa), Conalbomin (77 KDa), Glucose oxidase (160 KDa) and Ferritin (440 KDa) (filled black circles).

In order to calculate the molecular mass of an injected sample a calibration curve must be determined. The calibration curve was constructed injecting standard commercial proteins (with known molecular mass), at pH 7, and registering their elution volume. In this case, six proteins, with masses ranging from 12 to 440 KDa, were used: Cytochrome *c* (12 KDa), Mioglobin (17 KDa), BSA (67 KDa), Conalbomin (77 KDa), Glucose oxidase (160 KDa) and Ferritin (440 KDa). The elution of the proteins was followed by measuring the absorbance at 280 nm. In Figure 3.7 above is represented the superimposition of the chromatograms of the individually injected standards (panel A) as well as the obtained calibration curve (panel B). The registered elution volumes of the studied proteins, and their calculated molecular masses are summarized in Table 3.3 below.

Table 3. 3 - Purified proteins' elution time in an analytical size exclusion chromatography column S200 (25 mL), and their corresponding calculated molecular mass.

	Elution Volume (mL)	Calculated Molecular mass (KDa)
WT	13.7	94
E172A	13.8	89
E172S	13.9	84
E172Q	14.2	72
E172D	12.8	154

Based in its amino acid residues sequence, the NDH-2_Sa molecular mass was estimated to be ~44,000 Da per monomer. The calculated molecular mass for the wild type, E172A and E172S are approximately 90 KDa, which corresponds to a dimer molecular mass, and is in agreement with the previously published data. E172Q presented an elution volume corresponding to 72 KDa, value between the dimer and monomer conformation. The calculated molecular mass to the E172Q protein does not translate into a "real" molecular mass (since in the SDS-PAG from Figure 3.6, we can observe the expected ~44 KDa band) and is probably caused by a different interaction with the resin (not a molecular mass difference), which might suggest a slight change in the protein's conformation. In the case of E172D the calculated value was ~ 150 KDa, corresponding approximately to a trimer conformation. The observed variation in this case may have happened because of two different reasons: in the first scenario the protein is in fact a trimer which can be explained by a change in the protein's structure caused by the introduction of this mutation, which favours a three subunit conformation; in the second scenario the protein is in a dimer conformation but it is aggregated with other proteins which we could not separate during the purification process (or a third monomer but with no cofactor), leading to a larger complex, explaining that unexpected value. We can consider the second hypothesis as the most probable (since the sample has a slightly higher $R^{280}/_{450}$ ratio), but we do not have sufficient data to correctly assume one of the two explanations as the actual cause of the ~150 KDa molecular mass.

A second approach was taken, where the proteins' quaternary structure was studied by Native-PAGE. The obtained results are summarized in Supplementary figure 6.4, and they corroborate the presence of a dimer conformation in the case of NDH-2_Sa wild type, E172A, E172S and E172Q (since a relatively more intense band can be observed around 90 KDa). This technique still does not answer if E172D is in a trimer or a dimer with a contaminant.

Tertiary and Secondary structure

To investigate if the mutation had any impact at the structural level of the protein, we performed studies at the tertiary and secondary structure level of the proteins.

Indirectly, we first studied the proteins' tertiary structure by analyzing their temperature stability. We followed the overall protein structural state, by measuring the fluorescence emission intensity at 530 nm (excitation at 450 nm), which corresponds to the flavin cofactor emission pick. An increase in the fluorescence emission can be interpreted as an increase in the exposure of the FAD cofactor to the environment, which is probably caused by exposition to the assay's buffer as the protein loses its conformation. We followed the protein's denaturation profile between 25 and 90 ºC, and the obtained results are shown in Figure 3.8 below.

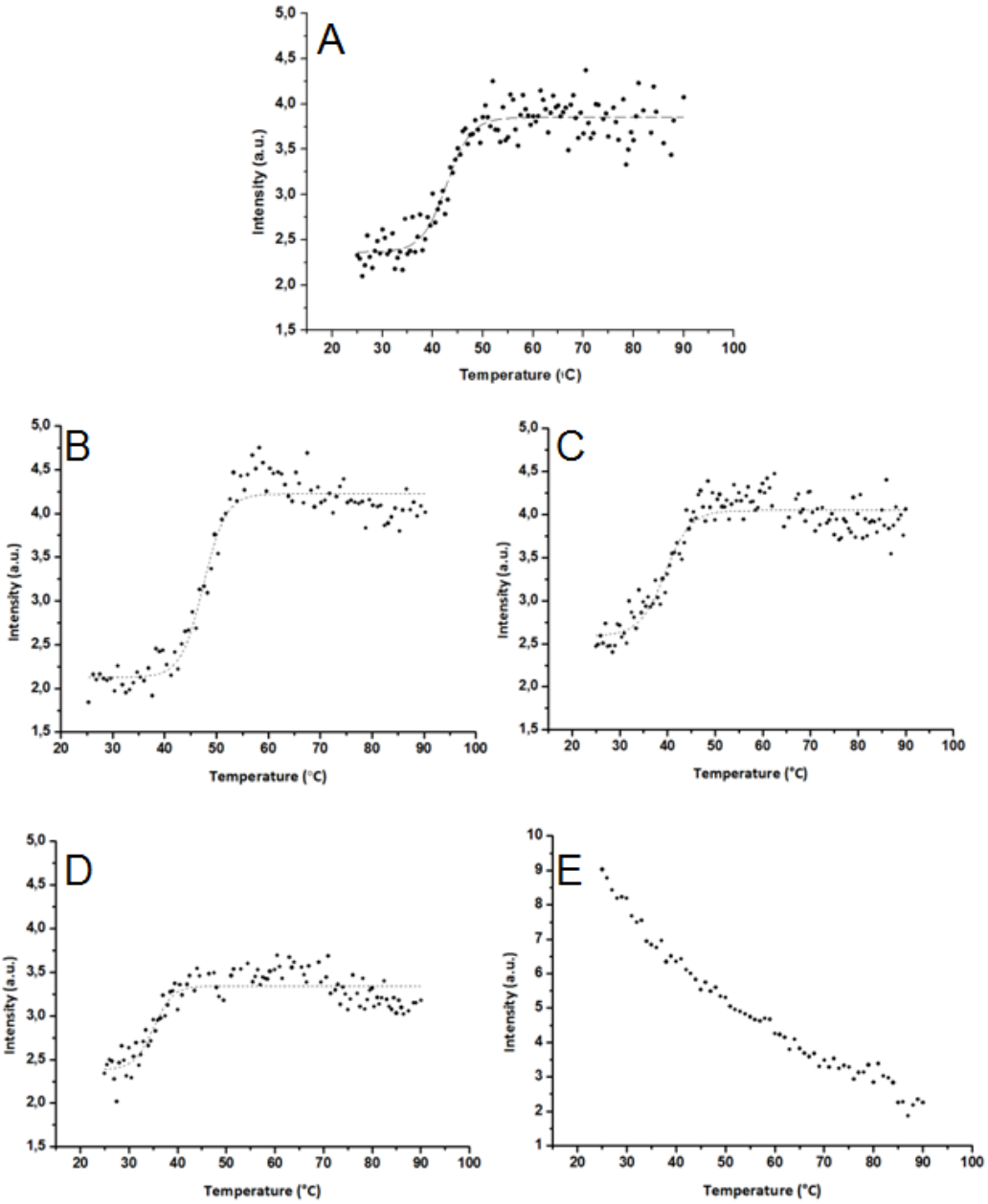

Figure 3. 8 - Thermal denaturation curves of the purified NDH-2_Sa proteins. In black dots is represented the fluorescence emission intensity at 530 nm (excitation at 450 nm) in function of the temperature, between 25 and 90 ºC, to each purified NDH-2_Sa mutant (6 µM). In dashed lines is represented the correspondent sigmoid fit. A – WT; B – E172A; C – E172Q; D – E172S; E – E172D.

In Figure 3.8 we can observe that NDH-2_Sa, E172A, E172Q and E172S have a similar denaturation pattern, with an approximate sigmoid behaviour, starting at lower emission intensities, increasing as the temperature rises. A closer quantitative analysis was performed, determining the Melting Temperature (MT) of each of the studied proteins. The MT can be interpreted as the temperature at which 50 % of the protein's population is considered denaturated, and the other half is still in an approximately folded conformation, this is mathematically represented by the inflexion point in the sigmoid fit. The inflexion point of the sigmoid curve for the studied proteins occurred at ~ 45 ºC for NDH-2_Sa, E172A and E172Q; and 35 ºC for E172S, meaning that the proteins have similar structural stabilities. In panel "E" of the same figure is represented the denaturation profile of the E172D. In this case the denaturation pattern is completely different, starting in high emission intensities, and decreasing linearly as the temperature rises. In this case no inflexion point can be calculated. The obtained result suggests, yet again, that a different structure profile is observed in the case of E172D.

The proteins' secondary structure was studied by Circular Dichroism (CD). Far UV CD spectroscopy allows to study a protein's secondary structure content (% α-helix, β-sheet and random coil), so it was considered a good approach to assess if this feature was maintained in the studied NDH-2_Sa mutants while comparing them with the wild type. The introduction of a mutation could possibly disrupt the stereochemical and electrostatic equilibrium related with the mutated side chain which could be reflected in a conformational change that could spread through the protein, and so the study of the secondary structure may be used as an indirect measurement for the impact of the mutation in the overall protein structure.

CD spectra were measured between 200 and 260 nm. Far UV CD signals at 208 and 222 nm can give us information about the α-helix content as described by Greenfield & Fasman (*64*). The obtained CD spectra for all the studied NDH-2_Sa are shown below in Figure 3.9.

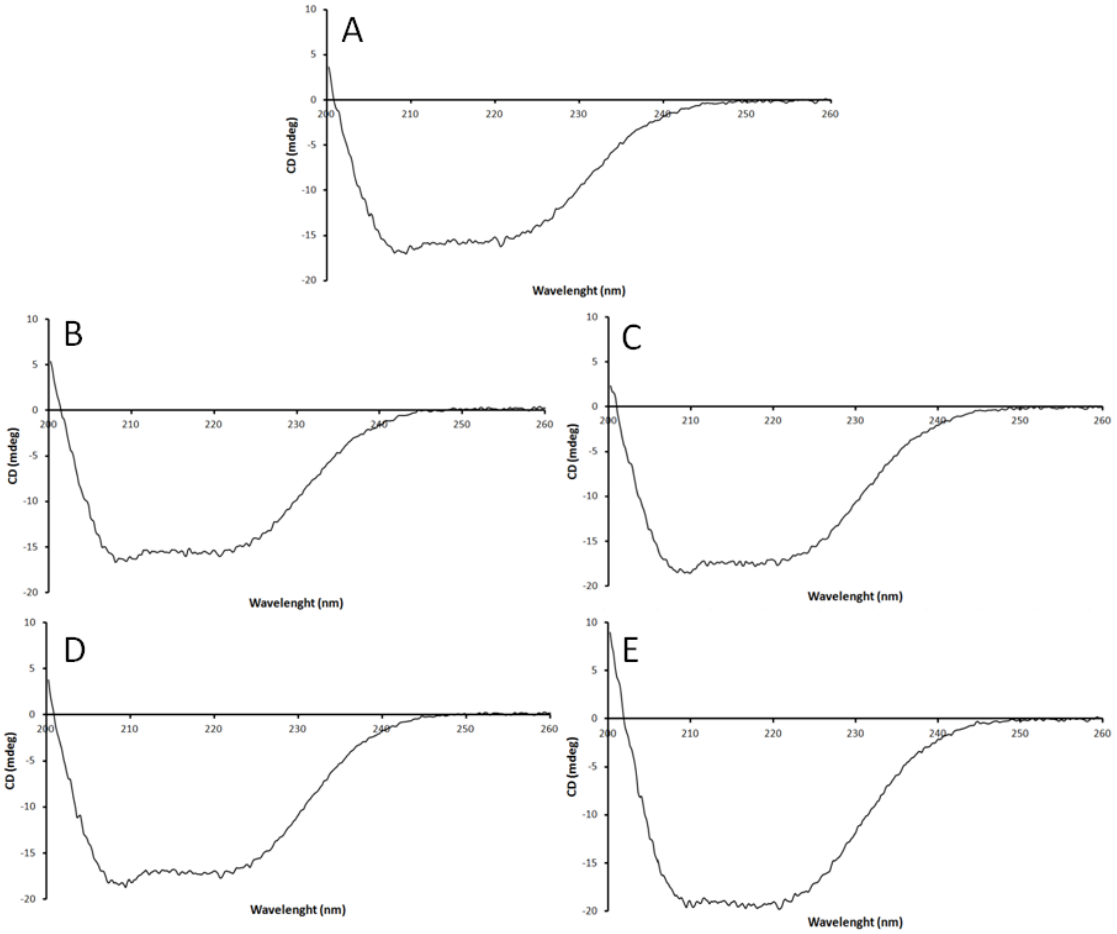

Figure 3. 9 - Far UV CD spectra of the purified NDH-2_Sa wild type and mutants. A – WT; B – E172A; C – E172Q; D – E172S; E – E172D. CD spectra were measured between 200 and 260 nm, 25 ºC using 5 µM NDH-2.

At first glance, the spectra are similar in terms of shape, but we can observe some variations in the intensities at 200 and 208 nm (especially in the case of E172D – Figure 3.9, panel E). A quantitative analysis was performed analysing the CD signal intensities at 208 and 222 nm and the ratio between them. The calculated ratio does not give information about the % of each secondary structure feature, but allows us to make a relative comparison, postulating that if the ratio is maintained so are the relative percentages of the helices, sheets and loops.

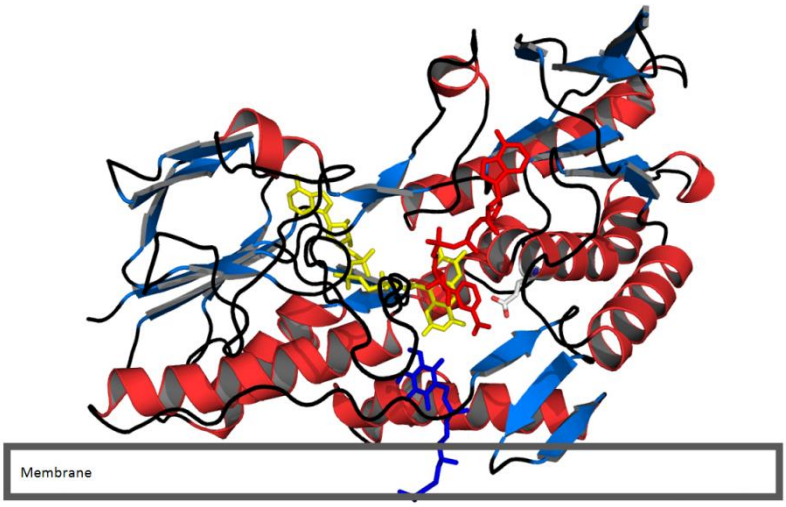

Figure 3. 10 - Cartoon showing the NDH-2_Sa WT structure (PDB 4XDB) colored by its different secondary structure features. In blue are represented the β-sheets, in red are the α-helices and in black is the random coil. In stick is highlighted the position of E172. The position of the cofactors is proposed based with a superimposition of the *S. aureus* structure with the PDB from *S. cerevisiae* NDH-2 (PDB 4G6H).

Using the structural model constructed based in the wild type's X-ray structure, we predicted the fraction of each secondary structure feature content simply by registering the number of amino acid residues belonging to α-helices, β-sheets and loops and dividing it by the total number of amino acid residues in the protein's sequence. The relative percentages calculated were 36, 24 and 40 % for α-helix, β-sheet and loop respectively. Above in Figure 3.10 is shown a cartoon of NDH-2_Sa wild type coloured by the different secondary structure features. The ratios obtained between CD signals at 208 and 222 nm are summarized in the table below.

Table 3. 4 - Purified NDH-2_Sa R $^{208}/_{222}$ and relative percentages. The values were obtained from the CD spectra.

	R $^{208}/_{222}$	**%**
WT	1.1019873	100.0
E172A	1.0826219	98.2
E172Q	1.0596214	96.2
E172S	1.0635349	96.5
E172D	0.9674462	87.8

What can be observed in the table above is that E172D is the mutant that appears to be more affected in its secondary structure content, comparing with the wild type (with a R $^{208}/_{222}$ variation of ~12 %). The remaining mutants seem to be closer related between them, and with the wild type, since the variation in their R $^{208}/_{222}$ is only ~3 %.

FAD's reduction potential

The formal reduction potential from the FAD cofactor was determined by cyclic voltammetry to the NDH-2_Sa wild type and mutants. From the obtained voltamograms, exemplified in Figure 3.11 below, the potential value was calculated as described in section 2 "Materials and Methods". The obtained results are summarized in the Table 3.5.

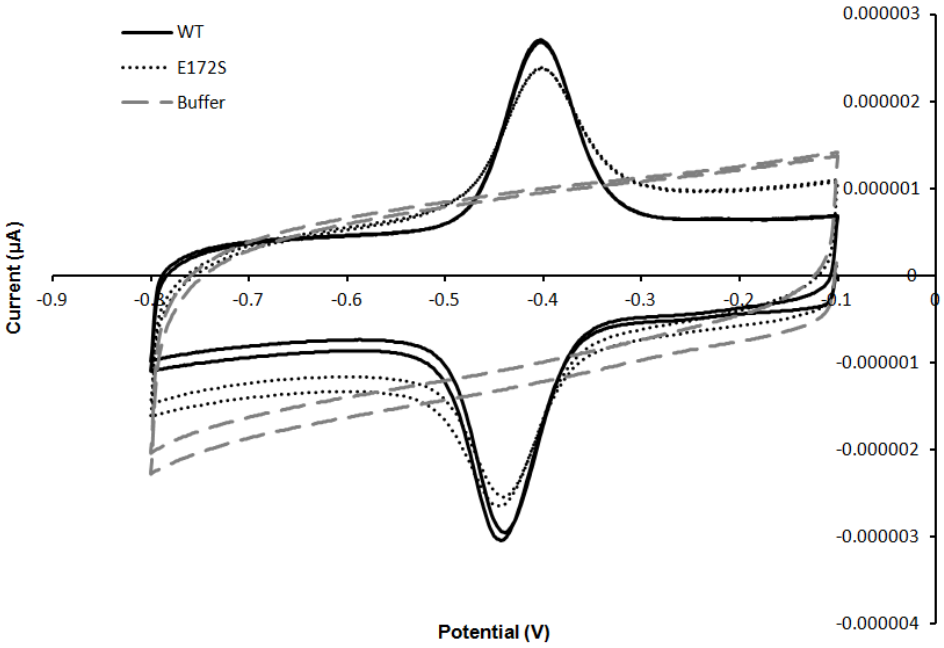

Figure 3. 11 - Example voltammogram from WT and E172S obtained with a scan rate at 50 mV/s. In bold black line is represented the voltammogram from NDH-2_Sa WT; in dashed black line is represented the voltammogram from E172S; in blue dashed line is represented the buffer control. The observed electric current picks occur for every studied NDH-2_Sa at approximately -0.45 V.

Table 3. 5 - Calculated formal reduction potentials for the free oxidized FAD and studied NDH-2_Sa.

Sample	WT	E172A	E172D	E172S	E172Q	FAD
E^0 (mV)	-217 ± 20	-220 ± 20	-218 ± 20	-217 ± 20	-205 ± 20	-226 ± 20

The free oxidized FAD molecule has a determined formal reduction potential of -220 mV (*65*). The obtained result (-226 mV) shows that these readings have a margin of error of several mV. The experience itself has been described as having a margin of error of approximately 20 mV. In the case of this study such a margin would not interfere with the reliability of the results, since if a change in the reduction potential was in fact the cause of the electron transfer rate decrease, such change should be noticeable even with this error margin. For example, in a study by *Tosha et al* (*66*), an electron transfer rate decrease of ~15 % was caused by a shift in the heme's iron potential of approximately 70 mV. In our case, if a change in the reduction potential was to be observed (considering that a decrease of ~80 % was observed), it should be

noticeable even in these situation. Analyzing the obtained results, we observe that between wild type and mutants, the reduction potential varies a maximum of 15 mV (between the highest, E172A, and the lowest, E172Q, calculated values), which is considered to be within the experimental error Even the E172D (which had no detectable specific activity) has a reduction potential comparable with the WT. We can safely state that no significant change in the FAD's reduction potential was detected.

UV-Visible spectroscopy

The obtained UV-Visible spectra for the four purified mutants and wild type were similar between them (Figures 3.12 to 3.16), and they all presented a characteristic flavin spectrum. The performed UV-Visible spectroscopic study consisted in observing the changes in the absorption spectra of the proteins induced by reduction with the substrate electron donor (NADH), and observe if the changes were reversible when the protein was re-oxidized by its other substrate (the quinone – electron acceptor). A two enzyme system was used to guarantee the absence of O_2 traces during the UV-Visible spectroscopy studies, since O_2 is able to function as an alternative electron acceptor. This O_2 "scavenging system" fuels in glucose (also added during the assays) and turns molecular oxygen in water in a two step pathway as shown in Supplementary figure 6.5.

In Figures 3.12 to 3.16 (panel A) are represented the UV-Visible spectra of the samples containing NDH-2_Sa, E172A, E172Q, E172S and E172D respectively. The obtained spectra show an expected flavin protein absorbance spectrum with absorbance picks at 450, 375 (exclusively from the flavin – Supplementary figure 6.1) and 280 nm (mainly from the aromatic amino acid side chains but also from the FAD cofactor).

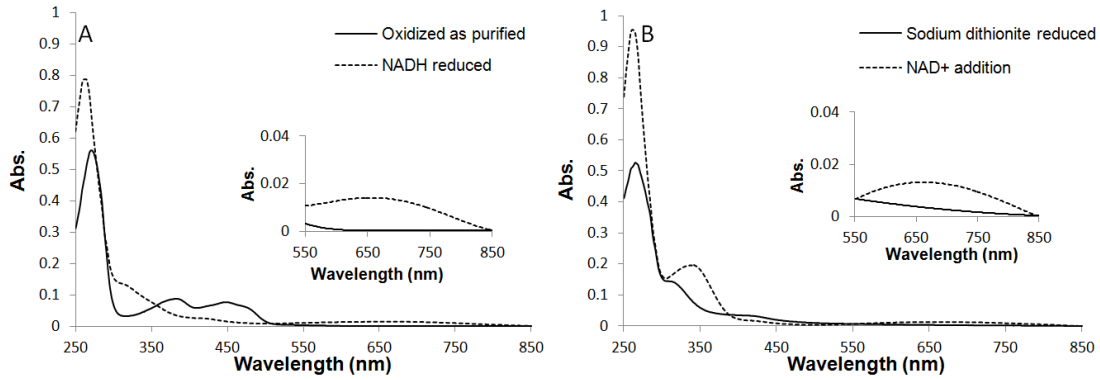

Figure 3. 12 - UV-Visible absorbance spectra of the NDH-2_Sa WT. A – In black filled lines is represented the oxidized protein spectrum, in dashes lines is the NADH reduced protein spectrum; B – In black filled lines is represented the dithionite reduced protein spectrum, in dashes lines is the same spectrum after NAD^+ addition. [NDH-2] = 6 µM. Adapted from (*43*).

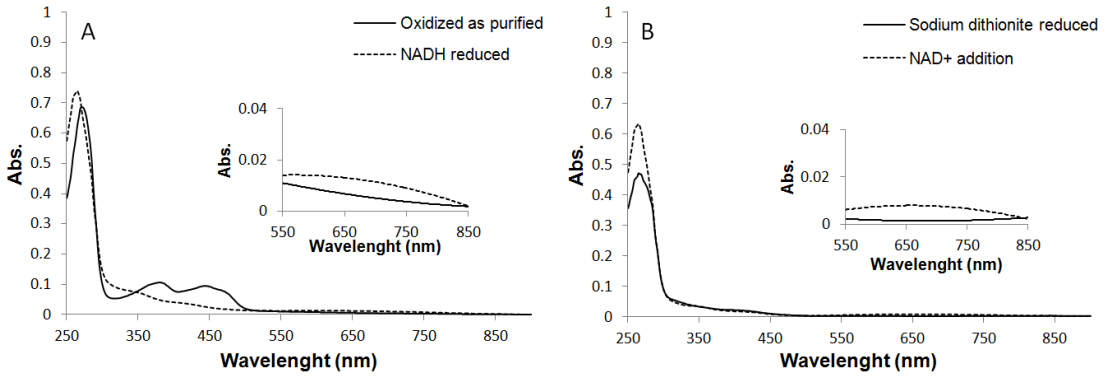

Figure 3. 13 - UV-Visible absorbance spectra of the E172A NDH-2_Sa. A – In black filled lines is represented the oxidized protein spectrum, in dashes lines is the NADH reduced protein spectrum; B – In black filled lines is represented the dithionite reduced protein spectrum, in dashes lines is the same spectrum after NAD^+ addition. [NDH-2] = 6 µM; [NADH] = 12 µM; [NAD^+] = 12 µM.

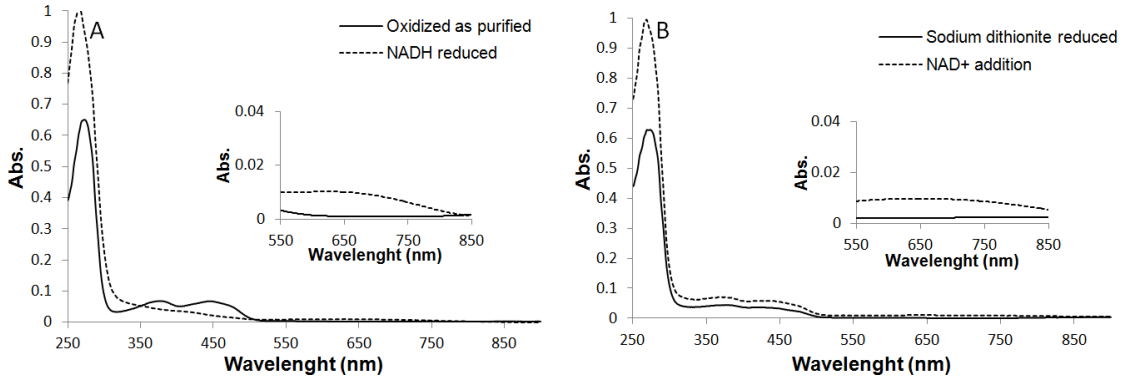

Figure 3. 14 - UV-Visible absorbance spectra of the E172Q NDH-2_Sa. A – In black filled lines is represented the oxidized protein spectrum, in dashes lines is the NADH reduced protein spectrum; B – In black filled lines is represented the dithionite reduced protein spectrum, in dashes lines is the same spectrum after NAD^+ addition. [NDH-2] = 6 µM; [NADH] = 12 µM; [NAD^+] = 12 µM.

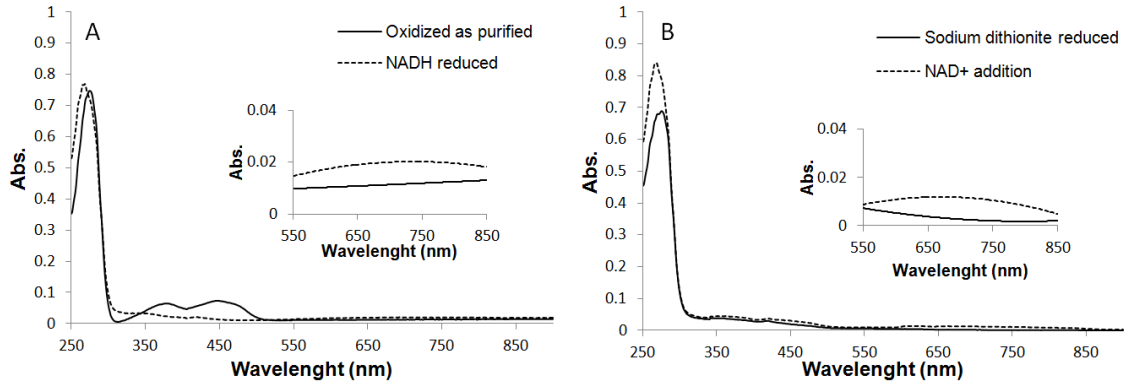

Figure 3. 15 - UV-Visible absorbance spectra of the E172S NDH-2_Sa. A – In black filled lines is represented the oxidized protein spectrum, in dashes lines is the NADH reduced protein spectrum; B – In black filled lines is represented the dithionite reduced protein spectrum, in dashes lines is the same spectrum after NAD^+ addition. [NDH-2] = 6 µM; [NADH] = 12 µM; [NAD^+] = 12 µM.

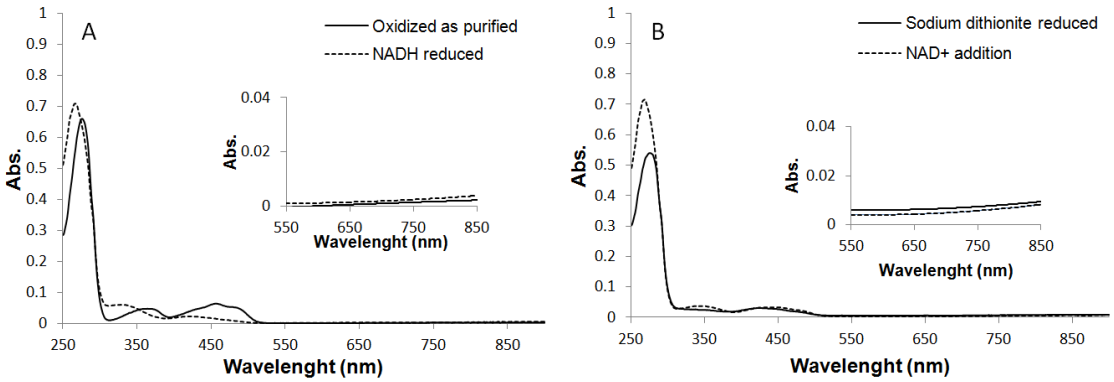

Figure 3. 16 - UV-Visible absorbance spectra of the E172D NDH-2_Sa. A – In black filled lines is represented the oxidized protein spectrum, in dashes lines is the NADH reduced protein spectrum; B – In black filled lines is represented the dithionite reduced protein spectrum, in dashes lines is the same spectrum after NAD^+ addition. [NDH-2] = 6 µM; [NADH] = 18 µM; [NAD^+] = 30 µM.

Represented with a black filled line in panels "A" from figures 3.12 to 3.16, are the spectra correspondent to the oxidized protein. After reduction with NADH (black dashed line, still in panels A) we could observe the disappearance of the absorption bands at 450 and 375 nm in all cases, a typical behaviour of flavoproteins (*67-68*). This reaction also leads to an increase in the absorbance around 670 nm, thus forming a very broad absorption band in this region. This absorption band was observed in all the proteins except E172D (Figure 3.16 panel A). The appearance of this band at 670 nm has been described as a consequence of the formation of a charge transfer complex. Charge transfer complexes are formed when two molecules share part of their electronic charge, in a π- π interaction established between the isoalloxazine ring of FAD and the nicotinamide ring of NADH.

After the addition of NADH, the re-oxidation of the proteins was tested, by adding an analog of the electron acceptor (DMN) in equal amounts to the NADH used to reduce the protein. All the purified NDH-2 had a similar behavior, returning to the oxidized state, allowing to confirm that the proteins were purified in a redox active state.

In order to confirm that the charge transfer complex is due to the presence of NAD^+ bound to the reduced enzyme another set of spectroscopic assays were performed. First the protein was reduced with sodium dithionite and then adding NAD^+ to the mixture (Figures 3.12 to 3.16 – panels B). After reduction with dithionite (black filled lines in panels B) we do not observe the absorbance bands at 450 and 375 nm and no absorbance changes can be observed in the 670 nm region. This result confirms that the 375 and 450 nm changes are directly dependent on the reduction state of the flavin. The increase in the absorbance on the 670 nm region was only observed after the addition of NAD^+, proving that this band is formed thanks to the presence of NAD^+ bound to the protein, which is in agreement to what has been previously described in general to a charge transfer effect, and more specifically in the NDH-2_Sa wild type (*43*).

E172D was the only protein in which changes in the 670 nm region were not observed, even after addition of NAD^+ (Figure 3.16 – panel B). While this assay alone is not enough to draw a definite conclusion, it strongly suggests that the binding of NAD^+ was somehow affected with the introduction of this mutation.

3.1.5 Final structural considerations

The overall structural profile of the NDH-2_Sa wild type and mutants was studied. Based in the "structure vs function" paradigm, testing if the mutant proteins' structure was maintained, when comparing with the wild type, was considered to be the first step if we aimed to study the functional implications of this E172 mutation.

The structure of the mutants was studied at the quaternary, tertiary and secondary level. The size exclusion chromatography and Native-PAGE studies revealed that E172A, E172Q, and E172S maintained the dimeric conformation as the wild type protein, while E172D seemed to form trimers. The tertiary structure studies (FAD fluorescence emission measurements), showed that the E172A and E172Q maintained the same structural stability as the wild type; E172S despite apparently being slightly less stable maintained a relatively similar denaturation pattern; and E172D showed significant structural differences, having a completely different denaturation pattern that we cannot explain with the available data.

Comparing both methodologies, the mutant that had the most different denaturation profile was also the only one that did not present a typical dimer conformation. The remaining three mutants could be considered as overall structurally similar proteins, with slight variations possibly caused by the mutation. It was to confirm if these differences reflected in a different secondary structure profile that the CD studies were performed. Ideally the CD data could give us information about the % of each secondary structure feature, but since the apparatus limited the range of the data we could record, the conclusions taken from the results were also limited. Nevertheless, and once again, the E172D was the mutant that showed more differences between the five studied proteins. The other four proteins (WT and three mutants) showed a relatively similar secondary structure profile. We cannot exclude definitively that the differences observed for E172D were not caused by the presence of some contaminants that we could not separate during the purification protocol (also consider that E172D has the highest $R^{280}/_{450}$ among the NDH-2_Sa mutants).

Cyclic Voltammetry studies showed that there was no change in the reduction potential of FAD, suggesting that E172 has no direct role in the modulation of the cofactor's potential.

The performed UV-Visible spectroscopy studies showed similar oxidized spectra for every purified mutant (which corroborates the flavin content and purity of the samples). Reduction with NADH lead to the disappearance of the absorption bands at 450 and 375 nm in

all cases, with concomitant increase in the absorbance at 670 nm region (for every mutant except E172D). The absorbance in this region was proved to be caused by the formation of a charge transfer complex between FAD and NAD^+. If E172D does not suffer any changes in this region after reduction with NADH this suggests that the binding of this substrate was affected, further corroborating the obtained results for the CD and stability studies.

Together the results suggested that E172D was somehow affected in its structure, resulting in a change of its oligomerization state, tertiary structure stability, secondary structure profile and substrate orientation/binding. The remaining mutants, despite having slight variations comparing with the wild type, were considered to be similar in their structural conformation.

Glutamate has a carboxylic acid as its side chain functional group. This acidic amino acid residue not only has the ability to form hydrogen bonds, it also has the ability to deprotonate, becoming negatively charged. By mutating this residue, the stereochemical and electrostatic equilibrium of this region could be affected, reflecting in a conformational change that could spread through the protein, possibly explaining why some slight structural differences were observed.

Table 3. 6 – Summary of the structural studies results for the purified NDH-2_Sa.

NDH-2_Sa	Observable CT complex	$R^{280}/_{450}$	% Flavin	Oligommerization state	Melting temperture (ºC)
WT	Yes	6.4	69.2	Dimer	45
E172A	Yes	6.3	70.1	Dimer	45
E172Q	Yes	6.1	72.7	Dimer	45
E172S	Yes	6.1	73.4	Dimer	35
E172D	No	7	63.4	Dimer/Trimer	-

3.1.6 Functional analysis of NDH-2 from *Staphylococcus aureus*

Protein functional analysis aimed at studying if the mutations affected the enzymatic reaction catalyzed by the NDH-2 (transfer of electrons from NADH to the quinone); and if they did, explore possible causes that could explain that mutation influence. The enzymatic reaction was studied by steady state and fast kinetics.

Steady state kinetics

The NADH:quinone oxidoreductase activity was measured for all the purified NDH-2_Sa (both mutants and wild type). The reaction was followed spectroscopically, at 340 nm, by measuring the substrate consumption (NADH). This was possible since NADH has a different UV-Visible spectrum than its oxidized form (NAD^+), as shown in Supplementary figure 6.3. Two independent experimental curves were performed for each of the studied proteins, one where [NADH] was kept constant while varying [DMN], and the second where [DMN] was constant with the [NADH] being the variable. Each curve was repeated three times and the measured V_0 were plotted vs the substrate concentration. The Michaelis-Menten kinetic model was used in order to obtain a fitting curve to the data. Since this kind of study has already been performed here in

the lab (*43*) to the wild type NDH-2_Sa, the WT data shown is referent to those studies. The obtained curves for the purified NDH-2_Sa mutants are shown below in Figure 3.17 to 3.19. No curves are presented for E172D NDH-2_Sa, since no activity was detected for all the tested conditions.

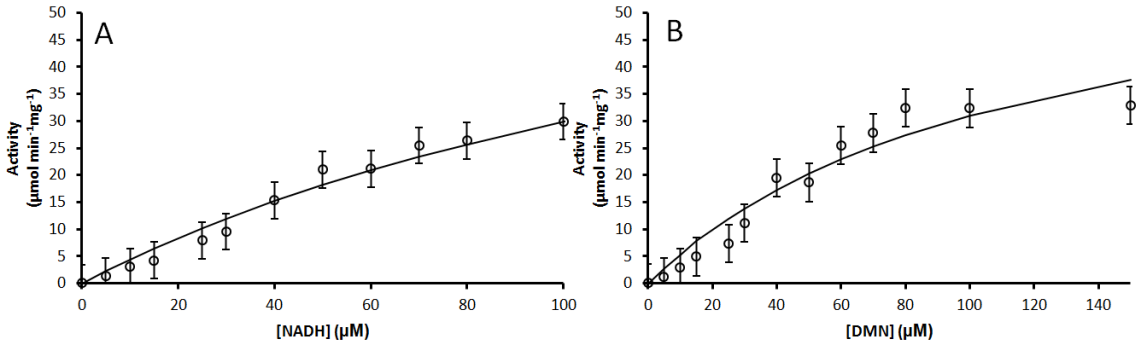

Figure 3. 17 - Steady state kinetic curves from E172A NDH-2_Sa at 500 nM. A – Measured V_0 vs [NADH] at 150 µM DMN; B – Measured V_0 vs [DMN] at 100 µM NADH. The curves in black filled lines represent the fit obtained with the Michaelis-Menten equation. Specific activity was measured by following the decrease in the 340 nm absorbance (NADH consumption).

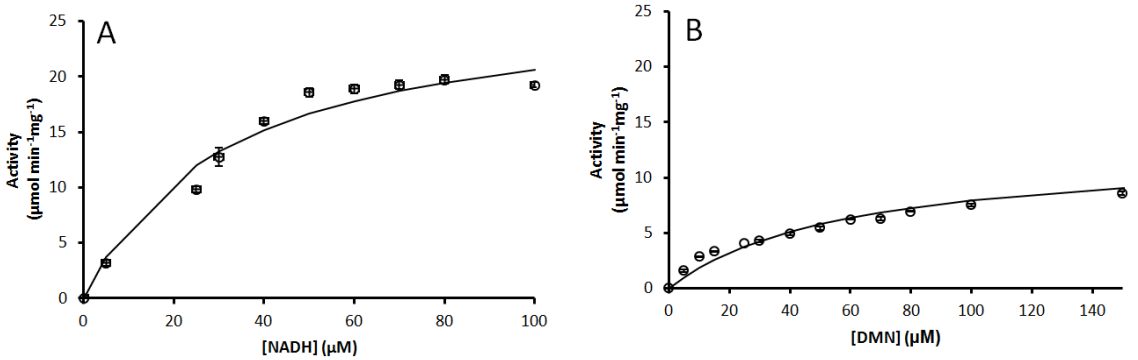

Figure 3. 18 - Steady state kinetic curves from E172Q NDH-2_Sa at 500 nM. A – Measured V_0 vs [NADH] at 150 µM DMN; B – Measured V_0 vs [DMN] at 100 µM NADH. The curves in black filled lines represent the fit obtained with the Michaelis-Menten equation. Specific activity was measured by following the decrease in the 340 nm absorbance (NADH consumption).

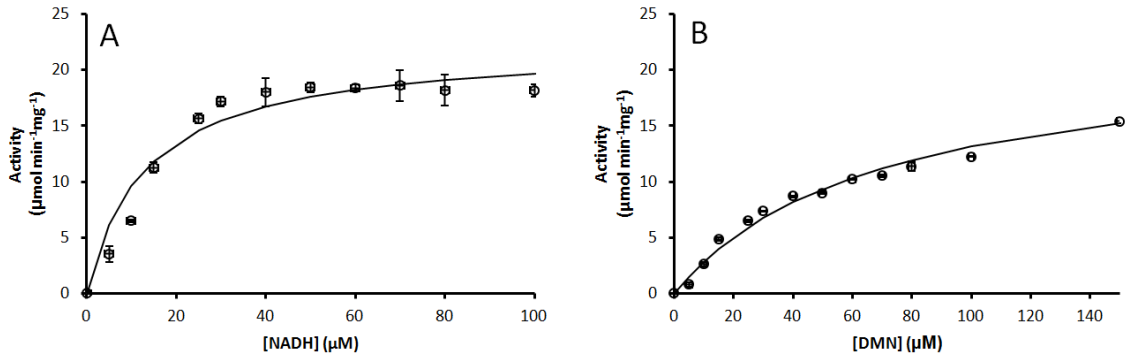

Figure 3. 19 - Steady state kinetic curves from E172S NDH-2_Sa at 500 nM. A – Measured V_0 vs [NADH] at 150 µM DMN; B – Measured V_0 vs [DMN] at 100 µM NADH. The curves in black filled lines represent the fit obtained with the Michaelis-Menten equation. Specific activity was measured by following the decrease in the 340 nm absorbance (NADH consumption).

Visual analysis of the plots shows a poor fit using the curves obtained with the Michaelis-Menten kinetic model. In some cases the data seems to describe a slight sigmoid behaviour, and the measured V_0 values tend to decrease in the higher concentrations (possibly suggesting substrate inhibition). The Michaelis-Menten model equation was first used in order to be able to directly compare the results with the WT data. Comparing the resulting calculated V_{max} and K_M with the observable plots, we conclude that no relevant correspondence could be made. In the case of E172A for example, 181.44 µM and 24.96 $\mu mol_{NADH}/min/mg_{protein}$ were the obtained results for K_M and V_{max} respectively for NADH, while the experimental data showed values of approximately 40 µM and 30 $\mu mol_{NADH}/min/mg_{protein}$. This discrepancy suggests that the activity profile of the mutated enzymes cannot be described by the Michaelis-Menten kinetic model. So we opted to make a visual interpretation of the kinetic data in order to obtain more reliable kinetic parameters, maintaining the fitting curves obtained from the Michaelis-Menten model equation as visual guidelines.

Analysing directly the experimental results, the V_{max} was the value corresponding to the highest measured V_0. As explained above a K_M parameter has no meaning in the case of the mutated NDH-2_Sa. The estimated results for V_{max} are summarized in the table below.

Table 3. 7 - Estimated V_{max} values obtained from visual interpretation of the experimental curves, for the different NDH-2_Sa.

	Vmax ($\mu mol_{NADH}/min/mg_{protein}$)	
	NADH	DMN
WT*	175.9 ± 0.6	132.7 ± 6.6
E172A	30 ± 2.5	30 ± 2.5
E172S	18 ± 2.5	15 ± 2.5
E172Q	20 ± 2.5	10 ± 2.5

*Adapted from (*43*)

The obtained results show a clear decrease in the V_{max} of the mutants while comparing to the previously published data for the wild type. V_{max} dropped, being 8 to 20 % (analyzing both NADH and DMN V_{max}) of the V_{max} observed for the wild type. This result suggests a critical role of the Glutamate 172 in the enzymatic mechanism. Despite varying slightly, the results for the three mutants are not different enough between them to infer any specific mutation effects. The studied mutations seemed to affect equally the overall rate of the reaction.

Flavins are known to be able to reduce molecular oxygen (justifying the need of working in anaerobic conditions), and so to try to understand if the studied mutations had the same impact in the unspecific reaction with oxygen as they did in the NADH:quinone oxidoreductase activity we measured the NADH consumption in aerobic conditions. We performed kinetic measurements in the presence or absence of the quinone acceptor, and compared the results with the anaerobic activities. The calculated specific activities are summarized in the table below.

Table 3. 8 - Aerobic and Anaerobic NADH dehydrogenase activities for the purified NDH-2_Sa mutants and wild type. The presented values from the anaerobic activities were taken from the steady state kinetic titrations with NADH. NADH dehydrogenase activities were measured by following the decrease of the absorbance at 340 nm, corresponding to the consumption of NADH.

	NADH:quinone oxidoreductase (anaerobic conditions) ($\mu mol_{NADH}/min/mg_{protein}$)	**NADH:O_2 oxidoreductase** ($\mu mol_{NADH}/min/mg_{protein}$)	**NADH:quinone oxidoreductase** (aerobic conditions) ($\mu mol_{NADH}/min/mg_{protein}$)
WT	175.90 ± 0.60*	13.52 ± 1.87	421.79 ± 13.60
E172A	30 ± 2.5	0.27 ± 0.05	12.09 ± 0.37
E172S	18 ± 2.5	1.35 ± 0.07	28.07 ± 2.61
E172Q	20 ± 2.5	0.37 ± 0.07	13.92 ± 3.28

*Adapted from (*43*)

The values corresponding to the NADH:quinone oxidoreductase activities in anaerobic conditions result from the ones obtained in the previously discussed assays, and are shown above in Table 3.7. The first observation that can be made while analyzing the obtained results is that the rate of the reaction while using O_2 as the electron acceptor is approximately 5 % (8 % in the wild type) of that in which quinone is used. Since the enzyme is specifically optimized to transfer electrons to physiological analogs of this substrate, a higher activity with the quinone is expected.

The second observation is that the mutations affected the NADH:O_2 oxidoreductase activity. Calculating the relative percentages (mutants' activities vs the wild type) we observe that the rate of the reaction is more affected in the O_2 reduction than in the quinone reduction (2 % vs 10 %). If the difference in these decreases is significant, it is hard to say since the reliability of these results is limited (mainly due to the fact that we are measuring really low activities), but for sure we can state that the mutations affected both reactions, and so the Glutamate 172 role in the enzyme's mechanism has to be common to both these reactions (NADH:quinone oxidoreductase and NADH:O_2 oxidoreductase).

Another important observation is that when we compare the NADH:quinone oxidoreductase activity both in the presence and absence of oxygen, the first one is twice as fast as the second one, in the case of the wild type. Since the protein has a higher activity with the quinone, it will preferentially reduce this substrate. Additionally O_2 (that has a reduction potential of +810 mV) will contribute to further increase the driving force of the reaction in the direction of the quinone reduction, which is reflected by the increase in the electron transfer. This sequence of events can be described as shown in Figure 3.20 below. In the case of NDH-2_Sa mutants there is no evidence for such an increase. This may be explained by the fact that the quinone reduction is so slow that the increase in the quinone availability, induced by the presence of O_2, has no noticeable effect in the reaction rate.

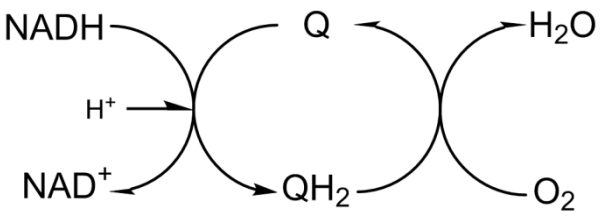

Figure 3. 20 - Diagram illustrating the proposed mechanism of the quinol regeneration by O_2. Molecular oxygen works as a final electron acceptor, since it has a higher reduction potential, increasing the driving force of the quinone reduction (and concomitant FAD oxidation) reaction.

As part of the kinetic characterizations of the purified NDH-2, the inhibitory effect of HQNO on the NADH:quinone oxidoreductase activity of the three NDH-2_Sa mutants was tested. This quinone analog inhibits this specific activity regardless of the type of quinone being reduced (*43*). A titration of the specific activities increasing the concentration of HQNO was performed and the obtained curves are shown in Figure 3.21. From the titration curves it was possible to determine the inhibition constant (K_I), summarized in Table 3.9 bellow.

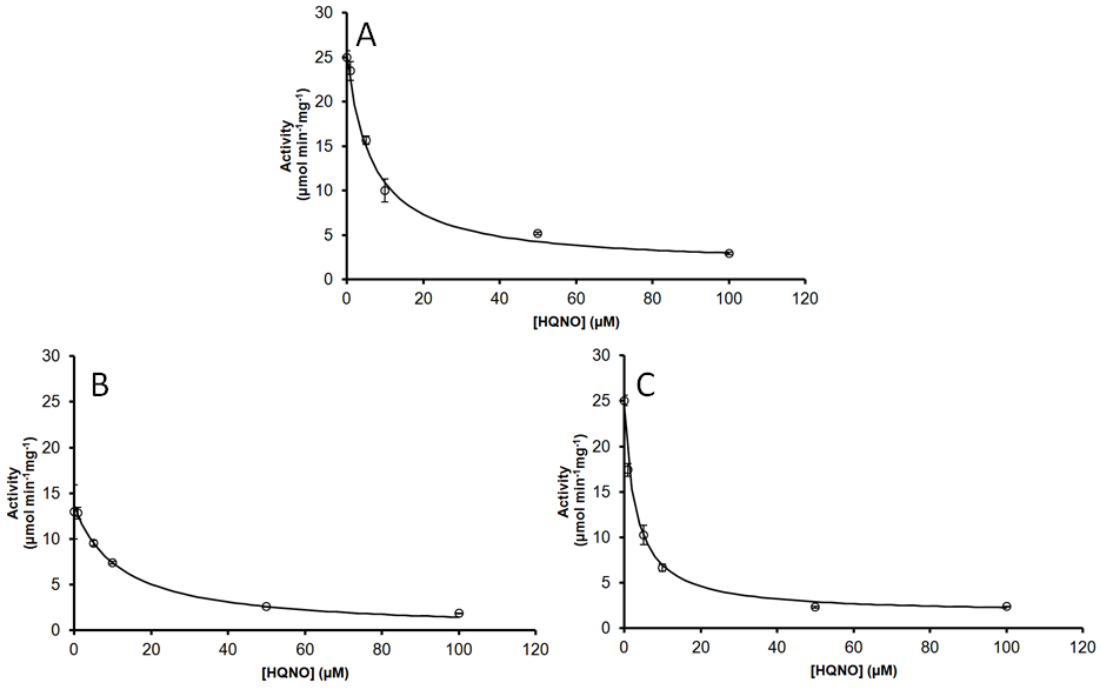

Figure 3. 21 - NADH:DMN oxidoreductase activity inhibition curves with HQNO. A – E172A; B – E172Q; C – E172S. Measured V_0 vs [HQNO] at 100 µM NADH and 150 µM DMN.

Table 3. 9 - Calculated K_I values for the NADH:quinone oxidoreductase activity by HQNO, for the three NDH-2_Sa mutants.

	K_I HQNO (μM)
WT*	6.8 ± 0.4
E172A	6.5 ± 1.3
E172Q	11.8 ± 3.0
E172S	3.1 ± 1.1

*Adapted from (*43*)

The obtained results show a constant of inhibition in the same order of magnitude between the three NDH-2_Sa mutants (varying between 3 and 12 μM). This means that the inhibition effect was the same, indicating that the inhibitory effect of HQNO is achieved independently of Glutamate 172.

Fast kinetics

Steady state kinetics allowed studying the overall NDH-2 catalyzed reaction while following substrate consumption. In these fast kinetics experiments we followed the spectroscopic changes that occurred in the protein itself, and in timescales orders of magnitude below. Since we could follow the changes in specific wavelengths, happening almost every millisecond, it was possible to differentiate both reduction and oxidation half reactions.

Based in the UV-Visible spectroscopy studies, the wavelengths at which the induced spectral changes were most evident had already been identified, justifying why 450 and 670 nm are the chosen wavelengths to monitor the flavin's reduction/oxidation and charge transfer complex formation respectively. The main goal of these experiments was to separately measure the rates of flavin's reduction and oxidation and to study the charge transfer formation; for the different NDH-2_Sa mutants.

Fast kinetics studies were also performed in anaerobic conditions, at pH7 and with potassium phosphate buffer, the only major difference, when comparing with the steady state kinetics conditions, was the temperature. As it was referred in the "Materials and Methods" section, temperature had to be lower than the optimum reaction temperature (35 ºC) in order to guarantee that the electron transfer could be measured. As in steady state kinetics, no observable reaction was detected in the case of E172D, and so, no curves are presented for this mutant. Since the same assays had already been performed in the hosting laboratory for the WT protein (*43*), the calculated rates debated are the ones obtained previously. The obtained curves from both half reactions for 450 and 670 nm, for the three NDH-2_Sa mutants are shown bellow in Figures 3.22, 3.23 and 3.24.

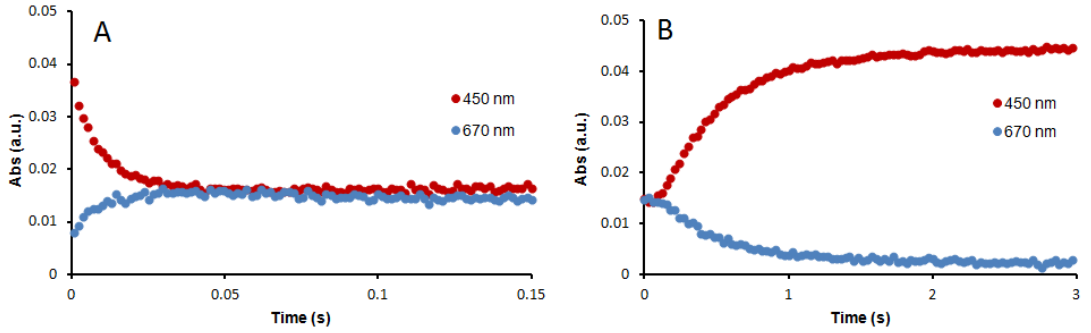

Figure 3. 22 - Reduction and oxidation half reaction curves from E172A at 5 µM (after mixing). A – Reduction half reaction curves (450 nm in red and 670 nm in blue); B – Oxidation half reaction curves (450 nm in red and 670 nm in blue).

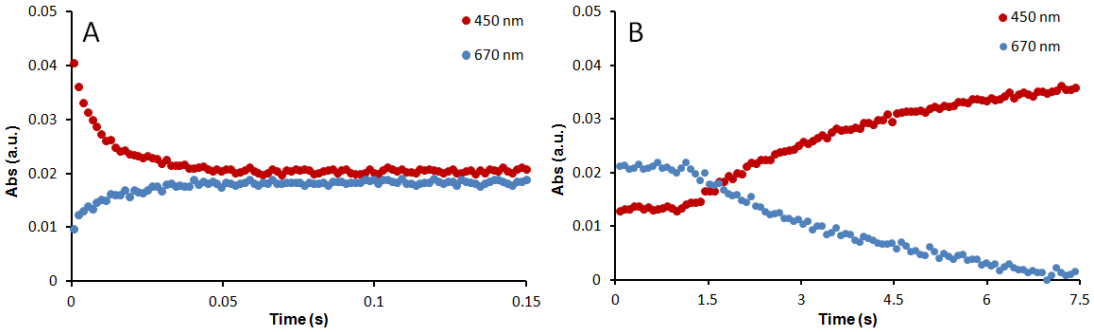

Figure 3. 23 - Reduction and oxidation half reaction curves from E172Q at 5 µM (after mixing). A – Reduction half reaction curves (450 nm in red and 670 nm in blue); B – Oxidation half reaction curves (450 nm in red and 670 nm in blue).

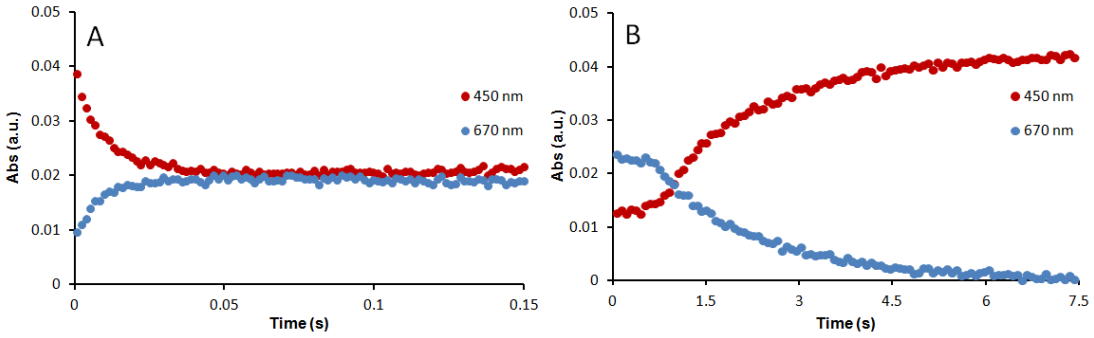

Figure 3. 24 - Reduction and oxidation half reaction curves from E172S at 5 µM (after mixing). A – Reduction half reaction curves (450 nm in red and 670 nm in blue); B – Oxidation half reaction curves (450 nm in red and 670 nm in blue).

The reduction half reactions (panels A) were measured by mixing NADH with oxidized protein in a 1 to 1 ratio. Addition of NADH leads to a decrease in the 450 nm absorbance (red dots), during the first ~0.025 s. Concomitantly with this reduction event, was the increase in the absorbance at 670 nm (blue dots), which was already interpreted as the charge transfer complex formation, between NAD^+ and the isoalloxazine ring from FAD. After the first ~0.05 s, both absorbance intensities are constant since the reduction state of the protein is maintained

and do not return to its starting point (oxidized flavin spectrum) for as long as the spectra are measured.

This last observation strongly suggests that the overall mechanism of the protein is a ternary complex mechanism instead of a ping-pong mechanism proposed by *Iwata et al* (*24*). This possible mechanism defends that NADH is released from the protein before DMN binds to its binding site (the number of binding sites do not support or disprove any of the theories, a ping-pong mechanism can occur with either one or more binding sites). By showing that NADH stays in a bound state to the protein until the flavin is reoxidyzed, we reject the ping-pong mechanism hypothesis and support the ternary complex mechanism hypothesis.

The oxidation half reactions (panels B) were measured similarly, by mixing the oxidized protein with both its substrates in a ratio that guaranteed at least one turnover cycle (1:2:3 – protein:NADH:quinone). As in the reductions half reaction the measured wavelengths were 450 and 670 nm. The reduction event does not seem to be detected (in panels B), since it occurs in the first 0.05 s, making it impossible to be observe with the chosen time scale. Inversely to the reduction event, in this case the absorbance at 450 nm (red dots) increases as the electrons leave the flavin and are transferred to the quinone. Regarding the 670 nm absorbance (blue dots), it also has the inverse behavior as before, being a “mirror reflection” of the 450 nm absorbance. Reduction and oxidation half reaction rates were calculated fitting an exponential curve to the data. The obtained rate constants’ values from both half reactions to each mutant are summarized below in Table 3.10.

Table 3. 10 - Calculated reduction and oxidation half reaction rates of the purified NDH-2_Sa mutants. The rates were calculated based in the variations of the absorbance at 450 nm.

	Reduction Half Reaction (s^{-1})	**Oxidation Half Reaction** (s^{-1})
WT*	180 ± 30	5 ± 0.5
E172A	115 ± 16	0.98 ± 0.21
E172Q	108 ± 12	0.13 ± 0.03
E172S	104.0 ± 0.3	0.319 ± 0.001

*Adapted from (*43*)

When we first analyze the wild type rate constants we conclude that the oxidation half reaction is approximately 30 times slower than the reduction half reaction, and so it can be considered the limiting step of the enzyme’s mechanism. This was one of the main conclusions taken from the previously performed fast kinetics studies (*43*). When we look to the mutants, the same observation can be made, reduction of the flavin is faster than the oxidation step, but the

relative differences between both half reactions are not the same, while comparing the same protein. Instead of 30 times faster, the reduction half reaction is approximately 100, 350 and 800 times quicker than the oxidation step for E172A, E172S and E172Q respectively.

We can also compare directly the NDH-2_Sa mutants' rate constants with the ones obtained to the wild type. From this comparison we can observe that the reduction rates drop to approximately 64, 57 and 60 % from the wild type (to E172A, E172S and E172Q respectively), and the oxidation rates decline to approximately 20, 6 and 3 % (to E172A, E172S and E172Q respectively). From this analysis we can state that the mutation in the Glutamate 172 affected both the reductive and oxidative half reactions, but did it in different extents, having affected with higher impact the FAD oxidation step. Results also corroborate the conclusion taken from previous studies, that the limiting step is the second half reaction of the electron transfer mechanism. When comparing the results between mutants, no relevant variations can be considered, despite the observed differences.

Protein-Substrate interaction

In order to study the binding of the substrates to the mutated proteins, fluorescence quenching studies were performed. These fluorescence studies measure the decrease of the fluorescence intensities of the tryptophan residues as a function of a substrate concentration. The quenching agents, were in this case, the substrates, and by binding to the proteins binding site, they induce conformational changes in the protein that may be reflected as a change in the tryptophan surrounding environment. It is by measuring the changes in the fluorescence, caused by the conformational changes that some extrapolations can be made.

Two independent sets of titrations were performed, one for DMN and the second for NADH. The effect of HQNO in the binding of each substrate was also tested. Below in Figure 3.25 are represented the obtained curves for the titrations with DMN and NADH for each mutant, both in the presence and absence of HQNO. Similar studies had already been performed for the wild type protein (*43*), so despite the curves not being shown, the values are later presented to support the discussion.

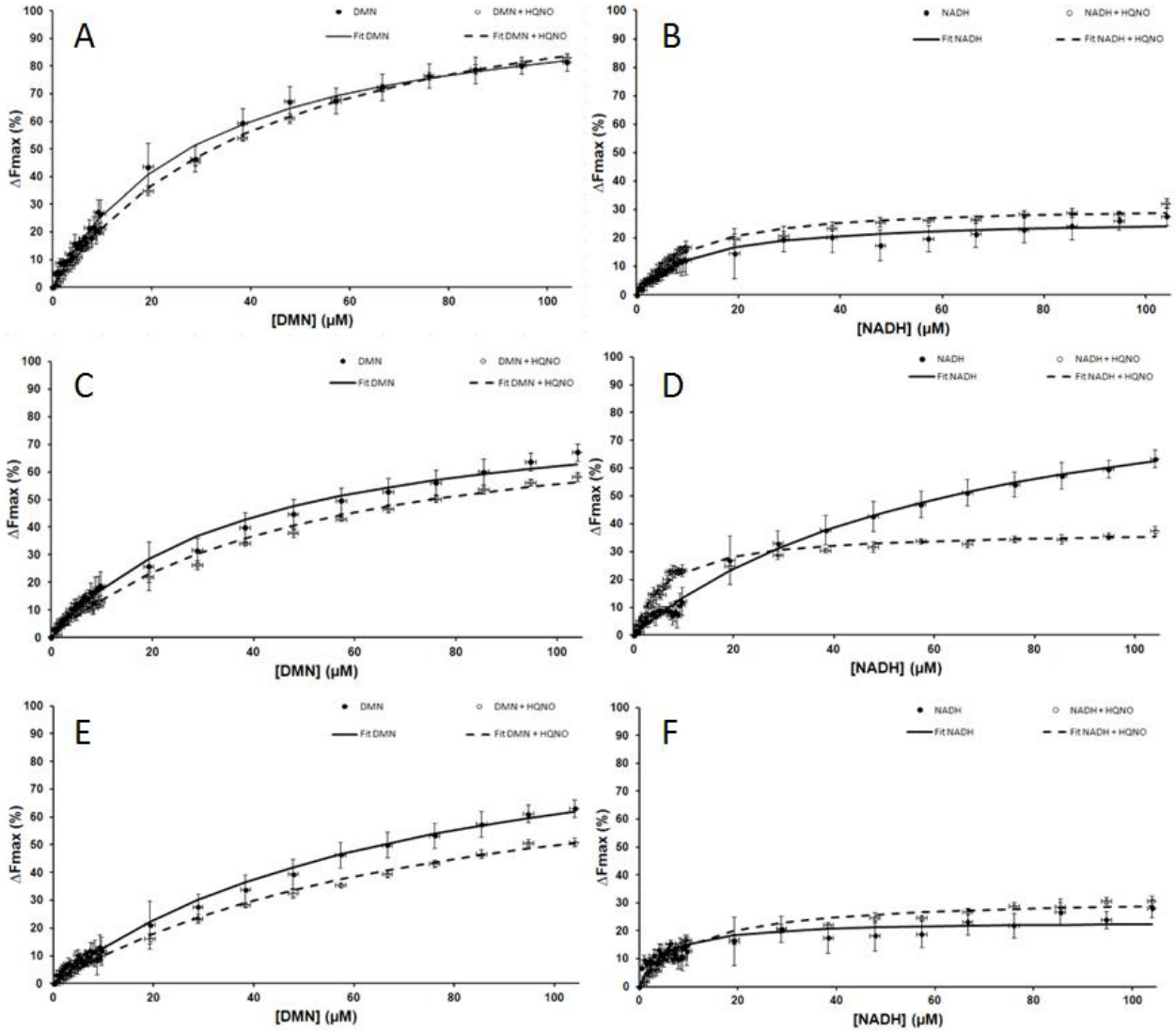

Figure 3. 25 - Protein-substrate interaction curves, representing the % Fluorescence intensity quenching plotted vs substrate concentration for the three studied NDH-2_Sa mutants (2 μM). A – E172A ΔF_{max}% vs [DMN]; B - E172A ΔF_{max}% vs [NADH]; C - E172Q ΔF_{max}% vs [DMN]; D - E172Q ΔF_{max}% vs [NADH]; E - E172S ΔF_{max}% vs [DMN]; F - E172S ΔF_{max}% vs [NADH]. In black filled lines is represented the fit for the HQNO free titrations, in black dashed lines is represented the fit for the curves in the presence of HQNO.

From the experimental data, the fitting curves were calculated using the Monot-Wyman-Changeux (MWC) model equation (*62*) (for dimeric enzymes) shown in the "Materials and Methods" section. This model considers proteins as an oligomer of protomers and each protomer as able to exist in either a tense or a relaxed state in which the relaxed state has a higher affinity to the ligand. The equation proposed by this model allows to consider an allosteric effect, as it was done previously for the wild type NDH-2_Sa titration with DMN and HQNO, but in this case none of the curves seemed to present a sigmoid behavior corresponding to an allosteric effect. All the curves were generated using "L=0" in the MWC equation, corresponding to "no cooperativity" curve. From the fitting curves, the dissociation constants (K_D) of each substrate were calculated. The obtained results for the K_D and maximum

fluorescence quenching, for every NDH-2_Sa mutant (except E172D), are summarized in the Table 3.11.

Table 3. 11 - Calculated K_D and %ΔFmax for both NADH and DMN, for the different NDH-2_Sa WT and mutants in the presence and absence of HQNO.

	DMN		DMN + HQNO		NADH		NADH + HQNO	
	K_D	**%ΔFmax**	**K_D**	**%ΔFmax**	**K_D**	**%ΔFmax**	**K_D**	**%ΔFmax**
WT*	16.3	90	35	80	11.4	45	10	45
E172A	31 ± 4	81 ± 8	45 ± 3	83 ± 3	12 ± 1	28 ± 2	10 ± 1	32 ± 5
E172Q	39 ± 2	67 ± 10	51 ± 6	58 ± 2	-	-	7 ± 2	37 ± 1
E172S	71 ± 16	63 ± 9	79 ± 10	51 ± 10	5 ± 3	28 ± 1	11 ± 2	31 ± 2

*Adapted from (*43*)

The first observation to make is that both by visual analysis of the plots and by comparison of the calculated values, the data corresponding to the NADH titration, of the E172Q, appears to be significantly different from all the others, and so we considered it as non valid for discussion.

The first set of data is referent to the HQNO free titrations. When comparing the obtained dissociation constants of the NDH-2_Sa mutants with the previously determined wild type values, two main observations are suitable to be discussed. The calculated K_D for DMN in the mutants is at least twice the obtained value for the wild type (four times in the case of E172S), but in the case of NADH they seem to be similar (ignoring the suspect E172Q NADH titration). These results suggest that the overall affinity of DMN to the different mutants is lower than to the wild type, but the affinity to the NADH is kept relatively unaltered. If a dissociation constant is higher, it means that the propensity of the ligand to dissociate of the protein is also higher, or in other words it tends to be weakly bound to the protein, meaning a lower affinity. Comparing the DMN K_D's between mutants, E172A and E172Q seem to have similar results, but E172S appears to have a lower affinity (higher K_D). This last observation is to be taken carefully since the E172S K_D to DMN is also the value with higher error.

When analyzing the %ΔFmax results we observe that for DMN they appear to have dropped when comparing with the wild type result. This suggests that as its affinity, the DMN's maximum effect in the protein appears to have decreased. Regarding the NADH %ΔFmax, the calculated values also seem to have decreased (if, again, we ignore the obtained result to E172Q), showing that the actual allosteric effect of a substrate in the protein is not directly dependent of the substrate's affinity. In this specific case the mutations don't seem to affect the NADH affinity, but the same cannot be said about the maximum effect that NADH has in the protein, where it seems to have been decreased.

The second set of data is referent to the titrations with HQNO. In the previously performed studies for the wild type protein (*43*) (Supplementary figure 6.6) the HQNO was shown to have an allosteric effect in the DMN binding but not in the NADH. This resulted lead

the authors to propose that not only the DMN and NADH bound in different locations (conclusion that could be confirmed by the X-ray crystallography results), but that HQNO had an allosteric effect in the binding site of DMN.

In the results obtained for the mutant NDH-2_Sa the same results could not be observed in the DMN case. HQNO did not show an allosteric effect in the DMN binding, but it seemed to decrease slightly the DMN's affinity. This result is not easy to explain since too many variables have to be taken in consideration. Maybe the simplest hypothesis is that the effect of the HQNO could be explained by a competition between both ligands. Considering that in the WT the HQNO and the DMN share partially the same binding pocket. In this case the cooperativity was lost (no sigmoid behavior observed), since only one ligand binds at a time (and some of the bound ligand being HQNO and not DMN, hence the observed K_D is partially the one from HQNO instead of the DMN K_D). This change could be induced by a reduced accessibility for the binding site, created by the mutation and overall rearrangement of the protein, making impossible for DMN and HQNO to bind simultaneously, creating a competition effect between them. In the case of NADH, the HQNO didn't seem to have any effect, both in the K_D and in the %ΔFmax, as previously reported to the wild type.

As in the activity assays, the results obtained for the different mutants do not seem to be different and consistent enough, to allow a further discussion about the different effect of each mutation. We can only conclude that the mutation in Glutamate 172 had in fact an effect in the DMN's affinity and %ΔFmax.

3.1.7 Final functional considerations

Functional studies aimed at studying if the reaction catalyzed by NDH-2 was affected by the introduction of the mutations in E172. The overall reaction rate and both half-reactions were studied by steady state kinetics and fast kinetics respectively. Together these two approaches showed that the V_{max} dropped to values ranging from 8 to 20 %, reflex of both half reactions having been significantly affected (~60 % in the reduction half reaction, and ~90 % in the oxidation half reaction case). These results show the critical role of E172 to the overall mechanism of the NDH-2, and suggest that, directly or indirectly, this amino acid residue is involved in both half reactions of the enzyme. Comparing the measured rates for both half reactions we can also state that the second half reaction (FAD oxidation and concomitant quinone reduction) is the limiting step of the enzymatic mechanism (reaction rate 100-800 times slower in the studied mutants), as it has been proposed before (*43*).

Furthermore these studies aimed at exploring some of the possible reasons why the reaction had been affected. Considering that FAD reduction as an electron flow dependent event, we first hypothesized that the FAD reduction potential could be indirectly modulated by

the E172, and by mutating this amino acid residue, the reduction potential of the mutants could be altered, leading to a decrease in the electron transfer rate (which would be measured as the half reaction rate constants). However as described before in the Structural analysis section, our cyclic Voltammetry studies showed was that the reduction potential of the proteins was maintained (~ -220 mV) despite of the mutations, suggesting that the overall driving force of the electron flow had been kept.

FAD reduction leads to the formation of its protonated form $FADH_2$, which is formed by transferring two electrons and two protons. The electrons flow from NADH to FAD, by a mechanism that is still unknown: NADH can reduce FAD one electron at a time (with formation of a semi-quinone intermediary state) or it can transfer two electrons and one proton in a single event by hydride transfer. In our fast kinetics data we do not observe any semi-quinone state during the FAD reduction. And so we consider the hydride transfer to be the most likely mechanistic option to happen, as it was described to other flavoproteins (*69*). Either way, FAD needs to receive its second proton to achieve the full reduced state. If we observe a change in the rate constant of the first half reaction, and we have data that suggest that the electron flux was not affected (reduction potential was maintained), we can propose that this decrease in the reaction rate happened because the proton availability was affected. This hypothesis is furthermore corroborated by analyzing the NDH-2_Sa models based on the X-Ray crystallography studies. Figure 3.26 below shows the relative position of two other Glutamate residues besides E172.

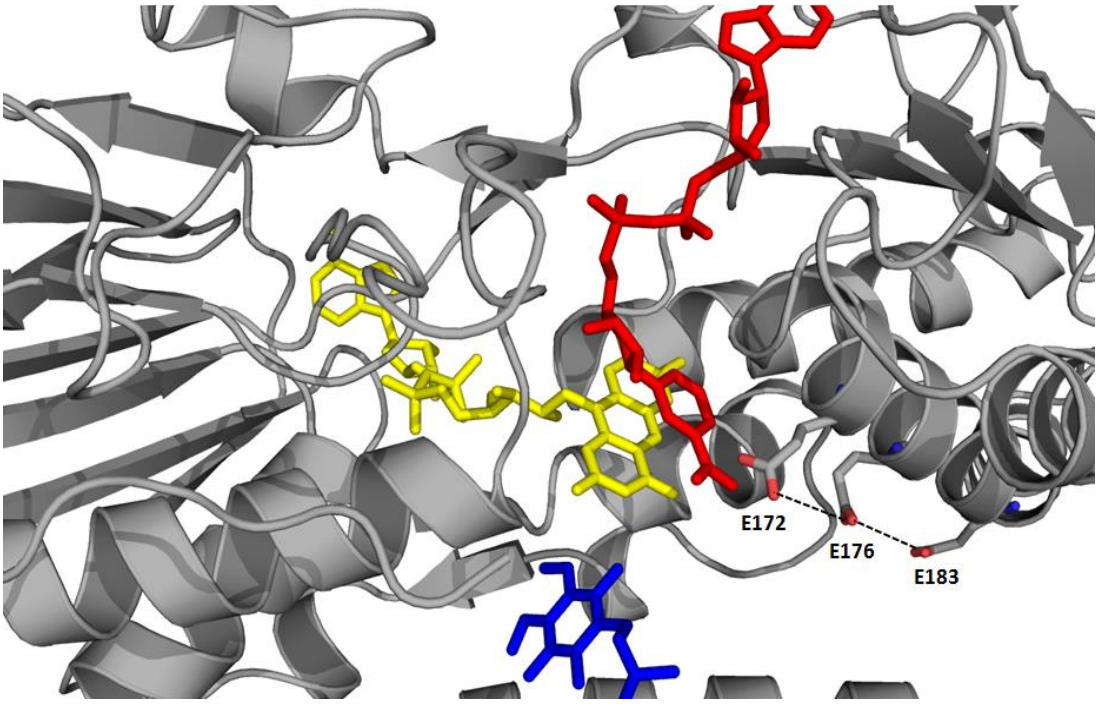

Figure 3. 26 - Cartoon representing NDH-2_Sa WT structure (PDB 4XDB) showing the E172 localization and relative position to FAD (yellow), NADH (red) and quinone (blue), highlighted in sticks. The position of the substrates is proposed based with a superimposition of the *S. aureus* structure with the PDB from *S. cerevisiae* NDH-2 (PDB 4G6H). The structural positions of E176 and E183 are also highlighted in sticks. The dashed black line serves as a visual guideline to the observable Glutamate line.

By analysing the presented figure we can observe an oriented line of three Glutamate residues, connecting the NADH binding pocket to the surface of the protein. Considering that the Glutamate side chain is a carboxylic acid, it has the ability of deprotonating, serving as a possible proton donor. Based in the chemical characteristics of the Glutamate side chain, and in the observation of this Glutamate channel, we hypothesize that E172 may be the terminal residue of a proton channel that can serve as the proton delivering system to the FAD. By mutating this residue to either an Alanine (E172A), a Glutamine (E172Q) or a Serine (E172S) we are introducing a mutation that allegedly alters the proton network, limiting proton availability to the reaction, thus resulting in severe activity losses. This hypothesis would explain why the V_{max} was severely affected, why the mutation affected both NADH:quinone and NADH:O_2 oxidoreductase activities (both acceptors need protons to be reduced); and why the decrease in the rate of the reaction was detected in both half reactions (since the two steps involve protonation related reactions). Nevertheless, alone this hypothesis does not explain why the second half reaction was more affected than the first one.

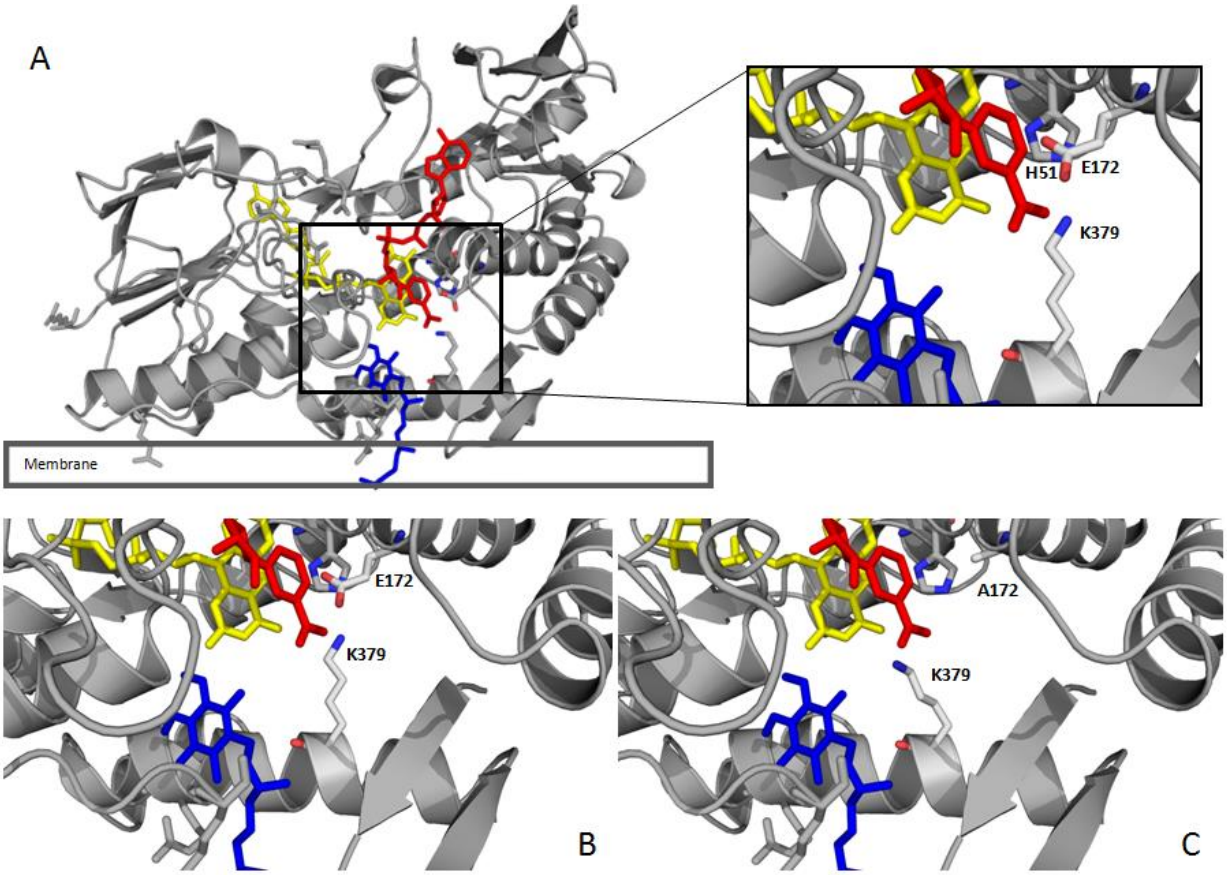

Figure 3. 27 - Cartoon representing NDH-2_Sa WT structure (PDB 4XDB) showing the E172, K379 and H51 localization and relative position to FAD (yellow), NADH (red) and quinone (blue), highlighted in sticks. A – NDH-2_Sa structure cartoon with a zoom in the E172 and proposed quinone binding location, showing in sticks the two amino acid residues with a positive side chain that are close enough to interact directly with E172; B – Zoomed image of the structural NDH-2_Sa WT model showing the proposed position of K379 relative to the quinone; C - Zoomed image of the structural NDH-2_Sa WT model showing the proposed position of K379 relative to the quinone after mutating E172 to an Alanine residue. The position of the substrates is proposed based with a superimposition of the *S. aureus* structure with the PDB from *S. cerevisiae* NDH-2 (PDB 4G6H).

The binding of the substrates was also studied, since it could affect the overall rate of the reaction mechanism. Protein-substrate interaction was studied by fluorescence quenching measurements and allowed us to determine dissociation constants for the binding of both substrates. What this set of results shows is an increase in the K_D of the electron acceptor (DMN) and the conservation of this parameter for the NADH. These results suggest that the overall affinity of DMN to the different mutants is lower than to the wild type, but the affinity to the NADH is kept unaltered. A possible explanation for the observed DMN affinity decrease is illustrated in Figure 3.27. In panel B of this figure is highlighted in sticks the relative position of the two closest positive amino acid residues (Lisine 379 and Histidine 51). Since Glutamate has a side chain that may be negatively charged while deprotonated, it can establish electrostatic interactions with those amino acid residues, affecting the conformation of their respective side chains by attracting them. If we consider the E172A mutant for example (panel C) the negative charge of E172 is not present, no longer orienting the position of K379. This amino acid residue could possibly rearrange its side chain position possibly interfering with the quinone binding pocket, which could lead to a decrease in the DMN affinity. This hypothesis is corroborated by the protein-substrate interaction studies (DMN's affinity decrease) and by the fast kinetics studies, where the second half reaction was shown to be more affected by the mutations, since the FAD oxidation half reaction would be affected by two different events (with the same origin): proton availability and quinone affinity decrease.

3.2 Type II NADH:quinone oxidoreductase from *Vibrio cholerae*

3.2.1 Protein expression and purification

We attempted to express and purify the type II NADH:quinone oxidoreductase from *Vibrio cholerae* for the first time. The first results of protein expression were negative. The levels of expression appeared to be null and after applying the purification protocols for the first time, no protein could be obtained. We later identified the problem as *E. coli* cells having been domesticated (gaining new resistances to antibiotics used in the laboratory), leading to incorrect interpretation of data since the very beginning. The supposedly transformed cells would be selected by antibiotic resistances introduced by the transformed plasmid (Kanamycin resistance), but considering that the non transformed cells had that same resistances *a priori*, an efficient selection of the cells of interest was not achieved. New cells were obtained, made competent and transformed, and new expression tests were performed (varying different conditions such as: growth extension; cell density (OD_{600}) at the time of induction; type of expression cells; and temperature). This time, a set of positive expression conditions was identified.

We were able to induce NDH-2_Vc expression in *E. coli* Rosetta cells, by adding 1 mM IPTG to the growing cells media (with 100 μg/mL kanamycin (Roth) and 34 μg/mL chloramphenicol (Roth)) when cells reached a cell density corresponding to an OD_{600} of 0.6 similarly to the case of cells expressing NDH-2_Sa (*43*). Protein expression was confirmed both by SDS-PAGE (Figure 3.28) and visually by the change in the cells' color from a "yellowish brown" to a "muddy green".

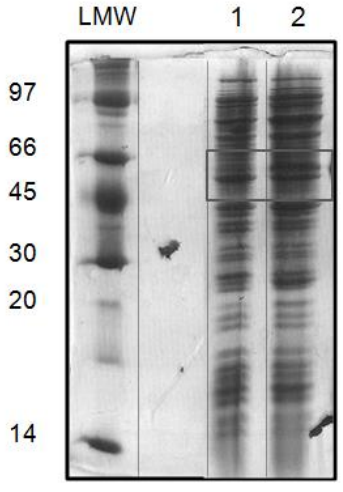

Figure 3. 28 - SDS-PAG exemplifying the NDH-2_Vc expression *E. coli* Rosetta. SDS-PAGE: Stacking Gel – 4 % acrilamide; Resolving Gel – 15 % acrilamide; Molecular mass of NDH-2_Vc: ~ 47 KDa. Wells: 1 – LMW markers; 2 – E. coli Rosetta growth before induction with IPTG; 3 - E. coli Rosetta growth after four hours of induction with IPTG.

After confirming the expression of the protein, enough cell material was obtained from 4 L growths and the same protocol as for the purification of NDH-2_Sa was applied. As described in “Materials and Methods”, and starting from approximately 100 g of cells, protein was purified using sequentially an ionic exchange chromatography column (Q-Sepharose High Performance) and a size exclusion chromatography column (Gel filtration S-200), with pH 7. Preliminary results from SDS-PAGE, UV-Visible spectroscopy, Dynamic Light Scattering (DLS) and S-200 elution volume, indicated that the obtained protein sample was not pure and oligomerized. The UV-Visible spectrum of the sample (Figure 3.29), specifically the absorption pick at 410 nm, suggested that the main contaminant was a cytochrome that appeared to have associated with the NDH-2 during the purification process.

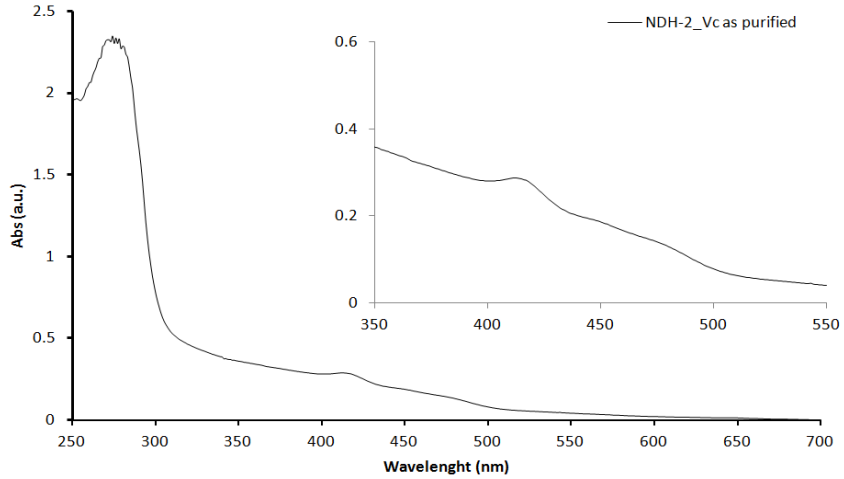

Figure 3. 29 - UV-Visible spectrum of NDH-2_Vc from the second purification. The UV-Visible spectrum reveals an extra absorption pick at ~410 nm (left of the 450 nm flavin pick), thus supporting the idea that a cytochrome was contaminating the sample.

Reduction of the referred sample with sodium dithionite lead to the appearance of characteristic absorption picks at approximately 425 and 560 nm, suggesting that the cytochrome was a type “b”, possibly *E. coli*’s cytochrome b562 (WP_001232252). Using Expasy’s PI/MW computation tool (http://web.expasy.org/compute_pi/) the theoretical isoelectric point (IP) to both NDH-2_Vc and Cytochrome b562 were estimated in 9.3 and 6.7 respectively.

Considering that a protein has different protonation profiles depending on the pH of the surrounding environment (mostly protonated in pHs lower than its IP), we decided to modify the conditions of the purification in order to try to change the general electrostatic profile of both NDH-2_Vc and Cytochrome b562; and by doing that, prevent their co-purification. New cells were grown and a new purification was performed. This time a set of three parallel conditions was tested.

A control condition was performed (pH 7, similar to the previous purification for comparison. In parallel, purifications with buffers at pH 6 and 8 were performed (changed buffers included the ones used prior to chromatography column injections).

The obtained protein fractions were studied spectroscopically, electrophoretically and injected in an analytical S-200 column to conclude about their oligomerization state. Samples from pH 6 and 7 purifications, were still not pure, were still oligomerized and had the associated cytochrome (in the case of pH 7 this was the expected result). In the case of the pH 8 purification, the protein was still oligomerized (and so the pH didn't appeared to have any effect in the protein aggregation) but despite not being pure, there was no cytochrome present in the sample.

This result was a considerable improvement in the overall purification process because cytochromes are redox active proteins, and so, the presence of such a contaminant would limit the information that we could conclude from the different studies that could be performed. The dissociation of cytochrome probably resulted from a change in its surface electrostatic profile caused by the different pH that was now considerably higher than its IP.

Based in these results a new purification was performed at pH8 and room temperature. With this pH condition we expected that the cytochrome was still absent from the purified sample and by doing the whole purification procedure at room temperature we were aimed to avoid the protein aggregation. Similarly to the previous purifications, protein membrane extraction was achieved by increasing the ionic strength (2 M NaCl) of the buffer where the disrupted cells were in. Protein was confirmed to leave the membrane fraction spectroscopically and visually, with the soluble fraction turning into a yellowish liquid.

The initial fraction was injected in an ionic exchange chromatography (Q-Sepharose HP) column and eluted with the same NaCl gradient as the NDH-2_Sa purification (0 to 1 M). The obtained chromatogram was similar to the one shown in Figure 3.4 to the purification of E172A NDH-2_Sa. The fractions containing NDH-2 were identified using UV-Visible spectroscopy. In this case, the protein eluted at around 25 % B (comparing to the ~35 % shown in the Figure 3.4), corresponding to 250 mM NaCl, meaning it interacts less strongly with the resin. This behaviour may be a reflect of a different surface electrostatic profile, which is supported by the different oligomerization state when compared with the NDH-2_Sa, at similar conditions (*70*). The fractions containing NDH-2 were separated by their $R^{280}/_{450}$ concentrated and further purified in a size exclusion chromatography.

The resulting chromatogram was similar to the one presented in Figure 3.5, but the main pick corresponding to the NDH-2 elution occurred at the column "dead volume" (instead of the 380 mL presented in the previously referred figure), indicating a higher molecular mass of the sample. The fractions containing NDH-2 were identified using UV-Visible spectroscopy, separated according to their $R^{280}/_{450}$ and until further analysis they were stored at 25 ºC. Despite still having some contaminants and still being oligomerized, the sample was now suitable to be studied within some limitations.

3.2.2 UV-Visible spectroscopy and protein purity

The NDH-2_Vc sample was first analyzed using SDS-PAGE (Figure 3.30 below) to infer its purity. We can detect an intense/thick band at around 66 KDa which probably corresponds to the protein of interest (molecular mass of 47 KDa), but is in fact slightly over its molecular mass. NDH-2_Vc appears to have a similar behaviour in the SDS-PAG as a membrane protein (which sometimes do not run in their appropriate molecular mass). This may have happened because NDH-2_Vc may have retained some lipidic content during the purification protocol which could be facilitated by the fact that the protein appears to be oligomerized. We also observe that the protein is not 100 % pure, since there are other bands, as intense as the first one, contaminating the sample.

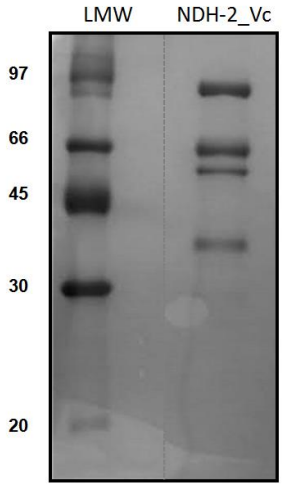

Figure 3. 30 - SDS-PAG of NDH-2_Vc preparation, after size exclusion chromatography. SDS-PAGE: Stacking Gel – 4 % acrilamide; Resolving Gel – 15 % acrilamide; Molecular mass of NDH-2_Vc: ~ 47 KDa.

This result was corroborated by the UV-Visible spectroscopy studies. The UV-Visible spectrum of the sample containing NDH-2_Vc, is shown in Figure 3.31 below. It resembles the spectrum obtained for the NDH-2_Sa. In addition to a higher $R^{280}/_{450}$, ~10.9, (confirming the result obtained from the SDS-PAGE analysis), the absorbance picks at 450 and 375 nm are not so distinct. Also, the absorbance at the 600 to 800 nm region is not close to zero. In this case the absorbance decreases from the 450 nm band and only reaches the zero at around 800 nm (observation compatible with light dispersion possibly due to its oligomerization state). After NADH addition the absorbance between 350 and 500 nm drops to half, but no changes were observedin the 670 nm region. This does not necessarily mean that the charge transfer complex was not formed, but it is simply undetectable due to the light dispersion. It is also noticeable that a pick at 340 nm appears. This is due to the fact that NADH absorbs in this region, and the fact that a higher amount of NADH was required to reduce the protein.

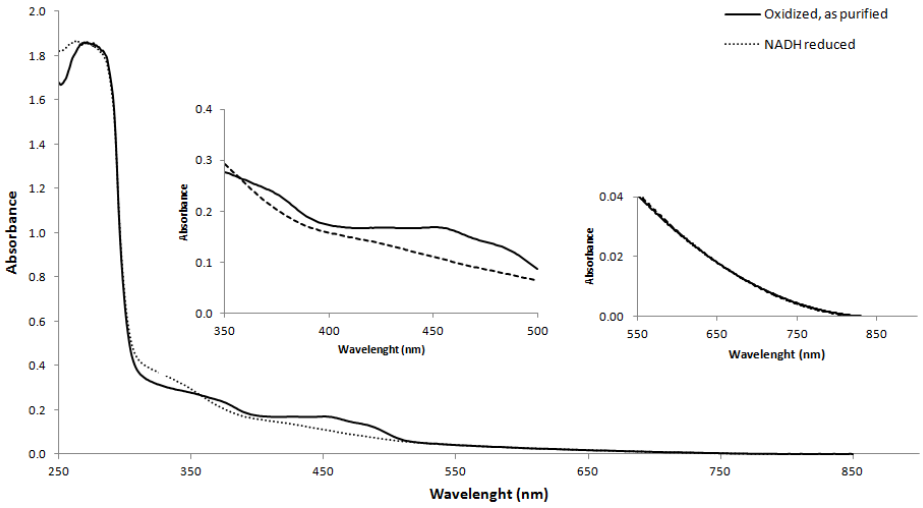

Figure 3. 31 - Purified NDH-2_Vc UV-Visible absorbance spectrum. In black filled lines is represented the spectrum of the oxidized protein; in dashed lines is represented the NADH reduced protein spectrum.

Applying the same methodology that was previously described to the NDH-2_Sa, the protein purity was also analysed based in the predicted $R^{280}/_{450}$. Based in the number of Trp, Tyr and Cys residues in the NDH-2_Vc sequence, and in the contribution of the FAD cofactor to each of these wavelengths, we can calculate the theoretical $R^{280}/_{450}$ to the protein. Considering both ε values (NDH-2_Vc: ε280 = 35.534 $mM^{-1}cm^{-1}$; ε450 = 11.300 $mM^{-1}cm^{-1}$), the $R^{280}/_{450}$ to the NDH-2_Vc was estimated to be of about 5.0. Considering that the fraction that had the lowest $R^{280}/_{450}$ ratio had a corresponding value of 10.9, the sample can be considered as not pure, thus confirming the results observed in the SDS-PAG.

3.2.3 Protein concentration and flavin content

Using the same ε values reported in the previous section, the concentrations based in the absorbencies at 280 and 450 nm can be calculated, and by comparing both values %Flavin can be estimated. As shown in Table 3.12, only approximately one third of the protein (28.9 %) has its cofactor. This result would be extremely negative when it comes to the viability of the sample to further studies, if it wasn't for the fact that the protein is not pure. The fact that there are other proteins in the sample (as suggested by the SDS-PAG and UV-Visible spectroscopy data), means that the absorbance at 280 nm is not entirely from the protein of interest, and so the real value would be lower (hence a better/lower $R^{280}/_{450}$ value). A lower value in the 280 nm absorbance would also mean a different flavin content. So we can safely say that the 28.9 % calculated value is overestimated, and without knowing the contribution of the "other proteins" in the sample (and based only in the data obtained in the scope of this thesis), it is not possible to conclude about the real % Flavin. All that we can conclude is that in the "worst case scenario", only one third of the protein has its cofactor, but this number is probably much higher.

Table 3. 12 - NDH-2_Vc concentration calculated by both the 280 and 450 nm absorbance intensities, and calculated %Flavin.

	[Protein] $_{280\ nm}$ (μM)	**[Protein] $_{450\ nm}$** (μM)	**%Flavin**
NDH-2_Vc	5.17	1.50	29.0

3.2.4 Structural analysis of NDH-2 from *Vibrio cholerae*

As it was described earlier, besides the purity of the sample, another problematic observation was the fact that the protein appeared to be oligomerized throughout the different purifications. As to NDH-2_Sa, the oligomerization state of the studied proteins was determined using two different approaches.

The first approach was injecting the sample in an analytical size exclusion chromatography. The same calibration curve was used in both NDH-2_Sa and NDH-2_Vc, and the methodology used for both proteins was the same with one exception, in the NDH-2_Vc two injections were done separately. One injection was done at 12 ºC, as the NDH-2_Sa, and so the same calibration curve was used; and a second injection was performed, but this time at room temperature (to maintain the purification protocol temperature), in order to check if any differences occurred in the oligomerization state, by changing the sample's condition at this point. The table below shows the obtained value for the injection at 12 ºC.

Table 3. 13 – Purified NDH-2_Vc elution volume in a Size exclusion chromatography column.

	Elution Volume (mL)	**Calculated MW (KDa)**
NDH-2_Vc	8.0	-

The registered elution value was ~8 mL, which corresponds approximately to the "dead volume" of the analytical chromatography column. Since no molecular mass can be calculated based in the registered volume, we cannot determine the oligomerization state of the protein. Nevertheless we can safely state that the protein has a considerably higher molecular mass than the last protein used in the calibration curve (440 KDa), clearly suggesting that the protein is in fact oligomerized. In the second injection, performed at room temperature, no significant differences were observed, indicating that the oligomerization state of the protein was maintained in the 12-25 ºC temperature range.

The oligomerization state of the protein was also evaluated by Native-PAGE (Figure 3.32 below). In the presented gel are observable some bands that could also be observed in the NDH-2_Sa samples. But the most interesting observation is the highlighted band, which is clearly at a higher molecular mass than 669 KDa (the last marker), and is the most intense band in the gel. This band was not observable in the NDH-2_Sa samples (that were shown to be in a non oligomerized state), which, combined with the size exclusion chromatography result, strongly suggests that the protein is in an oligomerized state.

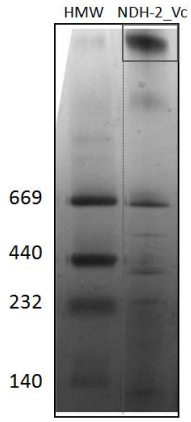

Figure 3. 32 - Native PAG with of NDH-2_Vc preparation, after size exclusion chromatography. Native PAGE 3-12 % polyacrylamide gradient gel. Molecular mass of NDH-2_Vc monomer: ~ 47 KDa.

The fact that the obtained NDH-2_Vc sample was oligomerized, not pure and had an unknown % Flavin, made it unviable for most of the studies that were performed for NDH-2_Sa. Some basic studies could still be performed, but the next step was trying to desegregate the protein and by doing so, maybe enhance its purity to a point where the sample was suitable to more advanced and more complex biochemical studies.

Several attempts to disaggregate the protein were done using different methodologies. The first one as described was to change the temperature at which the purification protocol was performed, and as it was also described it did not have any effect. This was the only strategy that was applied during a whole purification procedure, with the remaining attempts having been applied in already “purified” protein samples.

As it was mentioned in the “Protein expression and purification” subsection the pH of the buffer has an effect in the contaminants content of the sample, making possible to “remove” a cytochrome that did separate from the NDH-2_Vc at pH7. Based in the same rational (different pH’s could lead to different superficial electrostatic profiles) we varied the pH of the NDH-2_Vc sample ranging from 6-8 (keeping the same buffer), but only after size exclusion chromatography analysis. No change had been observed. Another approach that was taken, both separately and together with the pH variation was the ionic strength from the buffer. Higher salt concentrations in the sample could stabilize possible ionic interactions between protein

monomers, in a rational similar to the one that occurs in the ionic exchange chromatography. The ionic strength of the buffer was varied in concentrations ranging from 50 to 2000 mM NaCl, but again no observable change was registered.

The third variable that was tested in order to try to desagregate the NDH-2_Vc sample was the presence of detergent. It is a well established procedure, to include detergent in the buffers used in transmembrane protein purifications (*71*). This is due to the fact that this type of proteins have regions that are specifically adapted in interacting with the membrane, and by adding detergent, these compounds mimic the membrane environment, possibly stabilizing the protein and avoiding its aggregation or precipitation. In this case *n*-Dodecyl-β-D-maltopyranoside (DDM) was used. This detergent has a critical micelle concentration of 0.17 mM (*72*), and so the concentrations tested ranged from 0.03 to 0.09 mM. After addition of the detergent to the 100 mM phosphate buffer pH 7.0, 250 mM NaCl; the sample was left in the cold chamber (~ 4 ºC) with agitation during approximately 48 hours. A similar analysis of the sample, to the ones described before, lead us to conclude that this detergent condition had no effect in the oligomerization state of the protein.

The last attempt to disaggregate the NDH-2_Vc sample was done by changing the protein's buffer itself. Buffer exchange was achieved using an ultra filtration approach. Sequenced centrifugations were performed in a "centricon" with a molecular mass cutoff lower than the proteins monomer mass, allowing the buffer to pass through the membrane and not the protein. The new buffer was added sequentially in order to slowly substitute the previous one. The tested buffer was potassium phosphate 50 mM, pH 8, NaCl 1 M, glycerol 10%. This buffer tried to simulate a high ionic strength condition, coupled with a slightly basic pH (that was shown to influence the electrostatic superficial profile of the sample components) and a low glycerol concentration that has been show to stabilize the proteins, avoiding their aggregation (*73*). As in the previous approaches, this seemed to have no effect in the protein's oligomerization state.

What this set of experiences seemed to suggest is that in order to achieve proteins disaggregation, the tested conditions must be applied during the whole purification procedure. Since there is a limited time during this thesis, no further structural tests could be performed, but testing protein disaggregation during the purification protocol, and not after, seems like the next approach to be taken. It is also noteworthy that different conditions from the ones we tested could lead to protein disaggregation, conditions that are out of the ranges we tested, or conditions that consider totally different approaches that we did not considered (ultra sound treatments or different buffers for example).

3.2.5 Functional analysis of NDH-2 from *Vibrio cholerae*

Despite the NDH-2_Vc sample not being in conditions that are allow correct interpretation of data in the majority of the functional studies, for the sake of this thesis, the specific NADH:quinone oxidoreductase activities were measured for the first time in this protein, using two different quinone acceptors. Since preliminary results showed low activities, steady state curves weren't performed, and only the activities in substrate excess conditions were measured. Table 3.14, shows the obtained specific activity results from the measured V_0 in 100 µM NADH and 150 µM DDB (ubiquinone) and DMN (menaquinone), performed in anaerobic conditions.

Table 3. 14 - NADH:quinone oxidoreductase activities from NDH-2_Vc for different quinones analogs.

	NADH:DDB oxidoreductase ($\mu mol_{NADH}/min/mg_{protein}$)	**NADH:DMN oxidoreductase** ($\mu mol_{NADH}/min/mg_{protein}$)
NDH-2_Vc	1.38 ± 0.06	0.27 ± 0.05

Two main observations can be made about the results shown in Table 3.14. The first one is that comparing the specific activity measured with DMN, the NDH-2_Vc activity is only ~1 % from the one measured to NDH-2_Sa WT. Despite the fact that the activity to DMN may be in fact lower in the NDH-2_Vc case, this result is not comparable to the NDH-2_Sa WT one, since the first protein is in an oligomerized state, and so, substrate accessibility related differences have to be considered (substrate may not be able to reach the majority of the binding sites, since they may be blocked by other protein monomers). The NADH:DMN oxidoreductase activity for NDH-2_Vc is only comparable to the NADH:DDB oxidoreductase activity from the same protein, which leads us the second observation. We can state that the activity measured with DDB is higher than the one measured with DMN, and we can speculate that this happens because NDH-2_Vc is optimized to reduce this kind of quinone (Suplemantary figure 6.2), since ubiquinone is the physiological quinone detected in *Vibrio cholerae*. In terms of its absolute value, this result is not relevant, but nevertheless it confirms what has been previously reported (*43*): proteins have different activities with different quinone acceptors, and they seem to be optimized to reduce the fisiological quinone from the organism they belong.

In this work we report for the first time kinetic studies with NDH-2_Vc which was also purified for the first time. These preliminary results open new perspectives for future studies with this protein that are currently in progress in the hosting laboratory.

4. Conclusions

We aimed at investigating the catalytic mechanism of type II NADH:quinone oxidoreductases. For this we investigated two NDH-2 from two different organisms, aiming to recognize functional determinants that regulate the enzymatic mechanism as well as the different structural features that establish substrate selectivity.

NDH-2 from *Vibrio cholerae* was expressed and partially purified. Nevertheless we were able to perform preliminary UV-Visible spectroscopic analysis showing that the NDH-2_Vc had a characteristic flavin spectrum and was redox active. We measured its NADH:quinone oxidoreductase activity with two different acceptors (DDB and DMN), proving that **NDH-2 from *Vibrio cholerae* has a higher activity to its physiological quinone, ubiquinone.**

In the study of NDH-2 from *Staphylococcus aureus* we took advantage of a mutagenic approach, mutating selected key amino acid residues. In this work we examined the role of E172. This residue is present in 96 % of all NDH-2 and is located at the NADH binding site. We produced mutants which were successfully expressed and purified. All the proteins were active and structurally similar to the wild type, with the exception of E172D.

Steady state kinetics indicated that the **mutations in E172 severely affect the V_{max} of the reaction,** fast kinetics studies showed that **both half reaction rates were slower in the mutated proteins, being the FAD oxidation the half reaction that was more affected**. From the cyclic voltammetry studies, we observed that the reduction potential of FAD is the same in all the mutants, suggesting that **E172 does not take part in the modeling of the reduction potential of FAD**. Studying protein-substrate interactions, by following fluorescence of the tryptophan residues, we observe that **mutation of E172 leads to a decrease of affinity to the quinone**, having no observable impact in the NADH's affinity. By analyzing the constructed structural models we were able to detect a possib le proton channel in which E172 is included, and to suggest that E172 mediated by K379 may interacts with the quinone binding.

Based on our observations, we propose that **E172 is a crucial amino acid residue for the catalytic mechanism in NDH-2_Sa, working as the gate of a proton channel that allows the protonation of the substrates and the FAD cofactor.**

The work here presented on the study of two NDH-2, opens new perspectives for future studies in this area. The optimization of NDH-2_Vc purification, the study of the electrons and protons transfer mechanisms, or the parallel study of NDH-2 from different organisms (enabling to compare the obtained results with the ones here reported for NDH-2 from *V. cholerae* and *S. aureus*; and possibly infer about the actual metabolic role of these proteins and the different substrate binding specificity determinants) are just some examples of possible approaches to take in the future or questions that are still open to debate. With this work we directly contributed to the advance of the state of the art on NDH-2 and on the catalytic mechanisms of NADH and quinone oxido reduction.

5. References

1. Nelson, M. C. a. D. L. (2005) *Lehninger Principles of Biochemistry*.
2. Gennis, R. B., and Stewart, V. (1996) Respiration, in *Escherichia coli and Salmonella typhimurium: Cellular and Molecular Biology* (others, F. C. N. a., Ed.) 2nd ed., American Society for Microbiology.
3. Lane, N., and Martin, W. (2010) The energetics of genome complexity, *Nature 467*, 929-934.
4. (2004) Respiration in Archaea and Bacteria - Diversity of Prokaryotic Respiratory Systems, in *Advances in Photosyntesis and Respiaration* (Zannoni, D., Ed.), Springer.
5. Pereira, M. M., Bandeiras, T. M., Fernandes, A. S., Lemos, R. S., Melo, A. M., and Teixeira, M. (2004) Respiratory chains from aerobic thermophilic prokaryotes, *J Bioenerg Biomembr 36*, 93-105.
6. Nichols, S. J. F. a. D. G. (2002) *Bioenergetics 3*.
7. Sazanov, L. A. (2014) The mechanism of coupling between electron transfer and proton translocation in respiratory complex I, *J Bioenerg Biomembr 46*, 247-253.
8. Zickermann, V., Wirth, C., Nasiri, H., Siegmund, K., Schwalbe, H., Hunte, C., and Brandt, U. (2015) Structural biology. Mechanistic insight from the crystal structure of mitochondrial complex I, *Science 347*, 44-49.
9. Kramer, D. M., Nitschke, W., and Cooley, J. W. (2009) The Cytochrome bc1 and Related bc Complexes: The Rieske/Cytochrome b Complex as the Functional Core of a Central Electron/Proton Transfer Complex, in *The purple Phototrophic Bacteria* (C.N. Hunter, e. a., Editors, Ed.), pp 451-473, Springer Science ans Buiseness Media B.V.
10. Mitchell, P. (1975) Protonmotive redox mechanism of the cytochrome b-c1 complex in the respiratory chain: protonmotive ubiquinone cycle, *FEBS Lett 56*, 1-6.
11. (1998) Crystal Structure and Reaction Mechanism of Bovine Heart Cytochrome c Oxidase, in *Oxygen Homeostasis and Its Dynamics*, pp 13-23, Springer.
12. Saraste, M. (1999) Oxidative phosphorylation at the fin de siecle, *Science 283*, 1488-1493.
13. Kerscher, S., Dröse, S., Zickermann, V., and Brandt, U. (2007) The Three Families of Respiratory NADH Dehydrogenases, in *Bioenergetics* (Schäfer, G., and Penefsky, H. S., Eds.), pp 185-222, Springer Berlin Heidelberg.
14. Rasmusson, A. G., Soole, K. L., and Elthon, T. E. (2004) Alternative NAD(P)H dehydrogenases of plant mitochondria, *Annu Rev Plant Biol 55*, 23-39.
15. Melo, A. M., Duarte, M., Moller, I. M., Prokisch, H., Dolan, P. L., Pinto, L., Nelson, M. A., and Videira, A. (2001) The external calcium-dependent NADPH dehydrogenase from Neurospora crassa mitochondria, *J Biol Chem 276*, 3947-3951.
16. Fang, J., and Beattie, D. S. (2003) External alternative NADH dehydrogenase of Saccharomyces cerevisiae: a potential source of superoxide, *Free Radic Biol Med 34*, 478-488.
17. Heikal, A., Nakatani, Y., Dunn, E., Weimar, M. R., Day, C. L., Baker, E. N., Lott, J. S., Sazanov, L. A., and Cook, G. M. (2014) Structure of the bacterial type II NADH dehydrogenase: a monotopic membrane protein with an essential role in energy generation, *Molecular Microbiology 91*, 950-964.
18. Bjorklof, K., Zickermann, V., and Finel, M. (2000) Purification of the 45 kDa, membrane bound NADH dehydrogenase of Escherichia coli (NDH-2) and analysis of its interaction with ubiquinone analogues, *Febs Letters 467*, 105-110.
19. Liu, J., Krulwich, T. A., and Hicks, D. B. (2008) Purification of two putative type IINADH dehydrogenases with different substrate specificities from alkaliphilic Bacillus pseudofirmus OF4, *Biochimica Et Biophysica Acta-Bioenergetics 1777*, 453-461.

20. Anemuller, S. (1998) Studies of the Electron Transport Chain of the Euryarcheon Halobacterium salinarum: Indications for a Type II NADH Dehydrogenase and a Complex III Analog, *Journal of Bioenergetics and Biomembranes 30*.
21. Kerscher, S. J. (2000) Diversity and origin of alternative NADH : ubiquinone oxidoreductases, *Biochimica Et Biophysica Acta-Bioenergetics 1459*, 274-283.
22. Ojha, S., Meng, E. C., and Babbitt, P. C. (2007) Evolution of function in the "two dinucleotide binding domains'" flavoproteins, *Plos Computational Biology 3*, 1268-1280.
23. Argyrou, A., and Blanchard, J. S. (2004) Flavoprotein disulfide reductases: Advances in chemistry and function, *Progress in Nucleic Acid Research and Molecular Biology, Vol 78 78*, 89-142.
24. Iwata, M., Lee, Y., Yamashita, T., Yagi, T., Iwata, S., Cameron, A. D., and Maher, M. J. (2012) The structure of the yeast NADH dehydrogenase (Ndi1) reveals overlapping binding sites for water- and lipid-soluble substrates, *Proceedings of the National Academy of Sciences of the United States of America 109*, 15247-15252.
25. Yang, Y., Yamashita, T., Nakamaru-Ogiso, E., Hashimoto, T., Murai, M., Igarashi, J., Miyoshi, H., Mori, N., Matsuno-Yagi, A., Yagi, T., and Kosaka, H. (2011) Reaction mechanism of single subunit NADH-ubiquinone oxidoreductase (Ndi1) from Saccharomyces cerevisiae: evidence for a ternary complex mechanism, *J Biol Chem 286*, 9287-9297.
26. Mogi, T., Matsushita, K., Murase, Y., Kawahara, K., Miyoshi, H., Ui, H., Shiomi, K., Omura, S., and Kita, K. (2009) Identification of new inhibitors for alternative NADH dehydrogenase (NDH-II), *Fems Microbiology Letters 291*, 157-161.
27. Eschemann, A., Galkin, A., Oettmeier, W., Brandt, U., and Kerscher, S. (2005) HDQ (1-hydroxy-2-dodecyl-4(1H)quinolone), a high affinity inhibitor for mitochondrial alternative NADH dehydrogenase, *Journal of Biological Chemistry 280*, 3138-3142.
28. Warman, A. J., Rito, T. S., Fisher, N. E., Moss, D. M., Berry, N. G., O'Neill, P. M., Ward, S. A., and Biagini, G. A. (2013) Antitubercular pharmacodynamics of phenothiazines, *Journal of Antimicrobial Chemotherapy 68*, 869-880.
29. Vilcheze, C., Weisbrod, T. R., Chen, B., Kremer, L., Hazbon, M. H., Wang, F., Alland, D., Sacchettini, J. C., and Jacobs, W. R. (2005) Altered NADH/NAD(+) ratio mediates coresistance to isoniazid and ethionamide in mycobacteria, *Antimicrobial Agents and Chemotherapy 49*, 708-720.
30. Weinstein, E. A., Yano, T., Li, L. S., Avarbock, D., Avarbock, A., Helm, D., McColm, A. A., Duncan, K., Lonsdale, J. T., and Rubin, H. (2005) Inhibitors of type IINADH :-menaquinone oxidoreductase represent a class of antitubercular drugs, *Proceedings of the National Academy of Sciences of the United States of America 102*, 4548-4553.
31. Yano, T., Li, L. S., Weinstein, E., Teh, J. S., and Rubin, H. (2006) Steady-state kinetics and inhibitory action of antitubercular phenothiazines on Mycobacterium tuberculosis type-II NADH-menaquinone oxidoreductase (NDH-2), *Journal of Biological Chemistry 281*, 11456-11463.
32. Biagini, G. A., Viriyavejakul, P., O'Neill, P. M., Bray, P. G., and Ward, S. A. (2006) Functional characterization and target validation of alternative complex I of Plasmodium falciparum mitochondria, *Antimicrobial Agents and Chemotherapy 50*, 1841-1851.
33. Madigan, M. T. (2006) Brock Biology of Microorganisms, *Pearson-Prentice Hall*.
34. Bowersox, J. (1999) Experimental Staph Vaccine Broadly Protective in Animal Studies, National Institute of Allergy and Infectious Diseases.
35. Chambers, H. F. (2001) The changing epidemiology of Staphylococcus aureus?, *Emerging Infectious Diseases 7*, 178-182.
36. Dulon, M., Haamann, F., Peters, C., Schablon, A., and Nienhaus, A. (2011) MRSA prevalence in european healthcare settings: a review, *Bmc Infectious Diseases 11*.

37. Drago, L., De Vecchi, E., Nicola, L., and Gismondo, M. R. (2007) In vitro evaluation of antibiotics' combinations for empirical therapy of suspected methicillin resistant Staphylococcus aureus severe respiratory infections, *Bmc Infectious Diseases 7*.
38. Cosgrove, S. E., Sakoulas, G., Perencevich, E. N., Schwaber, M. J., Karchmer, A. W., and Carmeli, Y. (2003) Comparison of mortality associated with methicillin-resistant and methicillin-susceptible Staphylococcus aureus bacteremia: A meta-analysis, *Clinical Infectious Diseases 36*, 53-59.
39. Cosgrove, S. E., Qi, Y. L., Kaye, K. S., Harbarth, S., Karchmer, A. W., and Carmeli, Y. (2005) The impact of methicillin-resistance in Staphylococcus aureus bacteremia on patient outcomes: Mortality, length of stay, and hospital charges, *Infection Control and Hospital Epidemiology 26*, 166-174.
40. Taber, H. W., and Morrison, M. (1964) Electron transport in Staphylococci: Properties of a particle preparation from exponential phase Staphylococcus aureus, *Arch Biochem Biophys*, 367- 379.
41. Collins, M. D., and Jones, D. (1981) Distribution of Isoprenoid Quinone Structural Types in Bacteria and Their Taxonomic Implications, *Microbiological Reviews 45*, 316-354.
42. Schurig-Briccio, L. A., Yano, T., Rubin, H., and Gennis, R. B. (2014) Characterization of the type 2 NADH:menaquinone oxidoreductases from Staphylococcus aureus and the bactericidal action of phenothiazines, *Biochimica Et Biophysica Acta-Bioenergetics 1837*, 954-963.
43. Sena, F. V., Batista, A. P., Catarino, T., Brito, J. A., Archer, M., Viertler, M., Madl, T., Cabrita, E. J., and Pereira, M. M. (2015) Type-II NADH:quinone oxidoreductase from Staphylococcus aureus has two distinct binding sites and is rate limited by quinone reduction, *Mol Microbiol*.
44. Sena, F. V., and Rosário, A. L. (2015) Expression, purification, crystallization and preliminary X-ray diffraction analysis of a type II NADH:quinone oxidoreductase from the human pathogen Staphylococcus aureus, *Acta Crystallographica Section F 71*.
45. Faruque, S. M., Albert, M. J., and Mekalanos, J. J. (1998) Epidemiology, genetics, and ecology of toxigenic Vibrio cholerae, *Microbiol Mol Biol Rev 62*, 1301-1314.
46. Leibovici-Weissman, Y., Neuberger A., Bitterman R., Sinclair D., Salam M.A., Paul M. (2014) Antimicrobial drugs for treating cholera, *The Cochrane Library*
47. WHO. (2014) Cholera, 2013, *Weekly epidemiological record*, 345-356.
48. Kan, B., Habibi, H., Schmid, M., Liang, W., Wang, R., Wang, D., and Jungblut, P. R. (2004) Proteome comparison of Vibrio cholerae cultured in aerobic and anaerobic conditions, *Proteomics 4*, 3061-3067.
49. Xu, Q., Dziejman, M., Mekalanos, J. J. (2003) Determination of the transcriptome of Vibrio cholerae during intraintestinal growth and midexponential phase in vitro, *Proc Natl Acad Sci U S A 100*, 1286-1291.
50. Barquera, B., Hellwig, P., Zhou, W., Morgan, J. E., Hase, C. C., Gosink, K. K., Nilges, M., Bruesehoff, P. J., Roth, A., Lancaster, C. R., and Gennis, R. B. (2002) Purification and characterization of the recombinant Na(+)-translocating NADH:quinone oxidoreductase from Vibrio cholerae, *Biochemistry 41*, 3781-3789.
51. Steuber, J., Vohl, G., Casutt, M. S., Vorburger, T., Diederichs, K., and Fritz, G. (2014) Structure of the V. cholerae Na+-pumping NADH:quinone oxidoreductase, *Nature 516*, 62-U379.
52. Altschul, S. F., Gish, W., Miller, W., Myers, E. W., and Lipman, D. J. (1990) Basic local alignment search tool, *J Mol Biol 215*, 403-410.
53. Kelley, L. A., and Sternberg, M. J. E. (2009) Protein structure prediction on the Web: a case study using the Phyre server, *Nature Protocols 4*, 363-371.
54. DeLano, W. L. (2002) The PyMOL Molecular Graphics System, DeLano Scientific, San Carlos, CA, USA.

55. Froger, A., and Hall, J. E. (2007) Transformation of plasmid DNA into E. coli using the heat shock method, *J Vis Exp*, 253.
56. Kruber, O. (1929) Über das 2.3-Dimethyl-naphthalin im Steinkohlenteer.
57. Kelly, S. M., Jess, T. J., and Price, N. C. (2005) How to study proteins by circular dichroism, *Biochim Biophys Acta 1751*, 119-139.
58. Mabbott, G. A. (1983) An Introduction to Cyclic Voltammetry, *Journal of Chemical Education 60*, 697-702.
59. Kissinger, P. T., and Heineman, W. R. (1983) Cyclic Voltammetry, *Journal of Chemical Education 60*, 702-706.
60. (2006) Quenching of Fluorescence, in *Principles of Fluorescence Spectroscopy* (Lakowicz, J. R., Ed.), pp pp 277-330, Springer US.
61. Eftink, M. R., and Ghiron, C. A. (1981) Fluorescence Quenching Studies with Proteins, *Analytical Biochemistry 114*, 199-227.
62. Changeux, J. P. (1964) Allosteric Interactions Interpreted in Terms of Quaternary Structure, *Brookhaven Symp Biol 17*, 232-249.
63. Kanehisa, M., and Goto, S. (2000) KEGG: kyoto encyclopedia of genes and genomes, *Nucleic Acids Res 28*, 27-30.
64. Greenfield, N., and Fasman, G. D. (1969) Computed circular dichroism spectra for the evaluation of protein conformation, *Biochemistry 8*, 4108-4116.
65. Edwards, A. M. (2014) *Flavins and Flavoproteins*, Vol. 1146, Springer Science, New York.
66. Tosha, T., Yoshioka, S., Hori, H., Takahashi, S., Ishimori, K., and Morishima, I. (2002) Molecular mechanism of the electron transfer reaction in cytochrome P450(cam)--putidaredoxin: roles of glutamine 360 at the heme proximal site, *Biochemistry 41*, 13883-13893.
67. Morrison, E., Kantz, A., Gassner, G. T., and Sazinsky, M. H. (2013) Structure and mechanism of styrene monooxygenase reductase: new insight into the FAD-transfer reaction, *Biochemistry 52*, 6063-6075.
68. Lin, T. Y., Werther, T., Jeoung, J. H., and Dobbek, H. (2012) Suppression of electron transfer to dioxygen by charge transfer and electron transfer complexes in the FAD-dependent reductase component of toluene dioxygenase, *J Biol Chem 287*, 38338-38346.
69. Miller, R. T., and Hinck, A. P. (2001) Characterization of hydride transfer to flavin adenine dinucleotide in neuronal nitric oxide synthase reductase domain: geometric relationship between the nicotinamide and isoalloxazine rings, *Arch Biochem Biophys 395*, 129-135.
70. Rosario, A. L., Sena, F. V., Batista, A. P., Oliveira, T. F., Athayde, D., Pereira, M. M., Brito, J. A., and Archer, M. (2015) Expression, purification, crystallization and preliminary X-ray diffraction analysis of a type II NADH:quinone oxidoreductase from the human pathogen Staphylococcus aureus, *Acta Crystallogr F Struct Biol Commun 71*, 477-482.
71. Fernandes, A. S., Pereira, M. M., and Teixeira, M. (2002) Purification and characterization of the complex I from the respiratory chain of Rhodothermus marinus, *J Bioenerg Biomembr 34*, 413-421.
72. VanAken, T., Foxall-VanAken, S., Castleman, S., and Ferguson-Miller, S. (1986) Alkyl glycoside detergents: synthesis and applications to the study of membrane proteins, *Methods Enzymol 125*, 27-35.
73. Vagenende, V., Yap, M. G., and Trout, B. L. (2009) Mechanisms of protein stabilization and prevention of protein aggregation by glycerol, *Biochemistry 48*, 11084-11096.
74. Ghisla, S., and Edmondson, D. E. (2001) Flavin Coenzymes.

6. Supplements

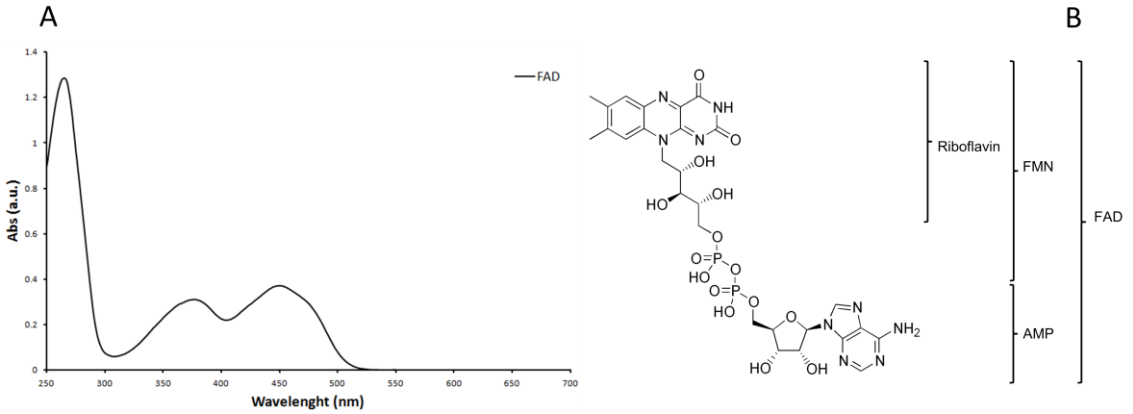

Supplementary figure 6. 1 - Flavin structure and UV-Vis spectrum. A – Free oxidized FAD UV-Visible spectrum. FAD has an absorbance pick at 280 nm as well as the two characteristic bands at approximately 375 and 450 nm. B – FAD molecular structure adapted from (*74*).

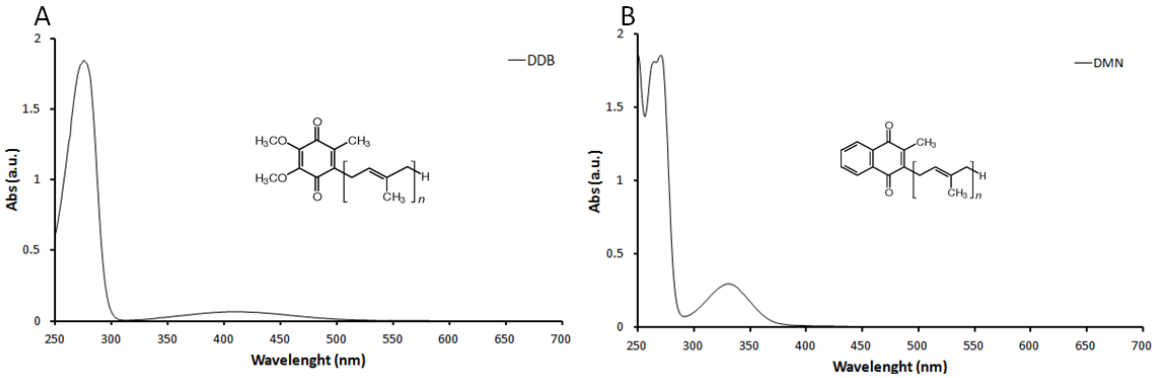

Supplementary figure 6. 2 – Quinones chemical structure and UV-Visible spectra. A – Ubiquinone analog (DDB) structure and UV-Visible spectrum; B – Menaquinone analog (DMN) structure and UV-Visible spectrum.

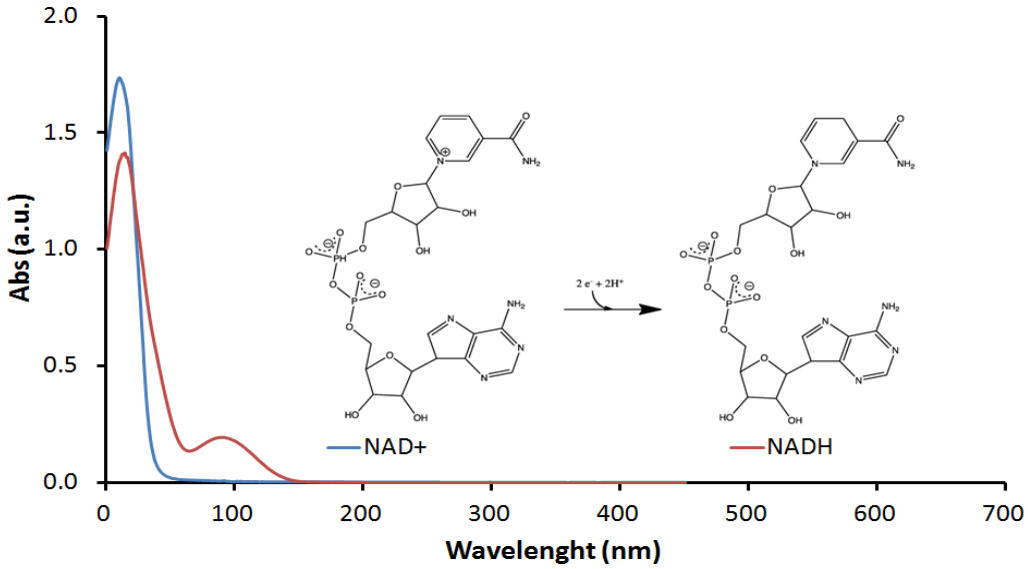

Supplementary figure 6. 3 - Flavin structure and UV-Vis spectrum. In blue is represented the UV-Visible spectrum from NAD+ and in red is represented the one from NADH. Spectra were collected in the lab, and the structures were adapted from: [https://en.wikipedia.org/wiki/NADH:ubiquinone_reductase_(H%2B-translocating)].

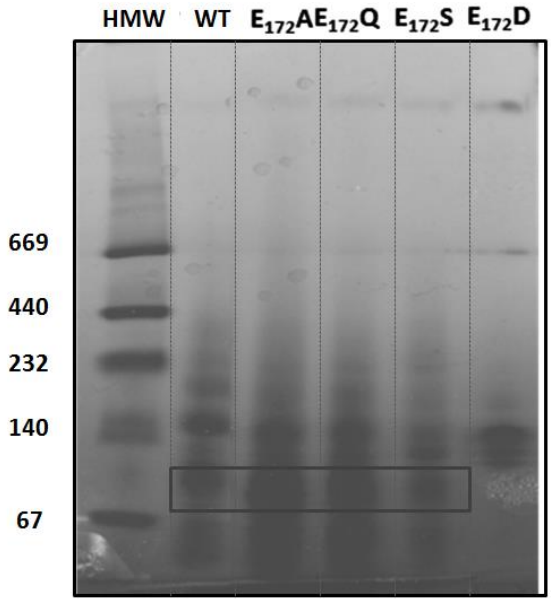

Supplementary figure 6. 4 - Native PAG with purified NDH-2_Sa and its mutants. Native PAGE 3-12 % polyacrylamide gradient gel. ; Molecular mass of NDH-2_Sa monomer: ~ 44Kda. Wells: 1 - HMW markers; 2 – NDH-2_Sa; 3 – E172A; 4 – E172Q; 5 – E172S; 6 – E172D.

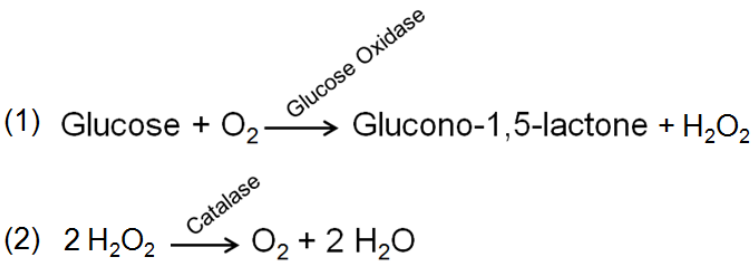

Supplementary figure 6. 5 - Scavenging System reactions. (1) - Glucose oxidase consumes glucose and oxygen to form oxygen peroxide; (2) – Catalase consumes de formed oxygen peroxide to form water.

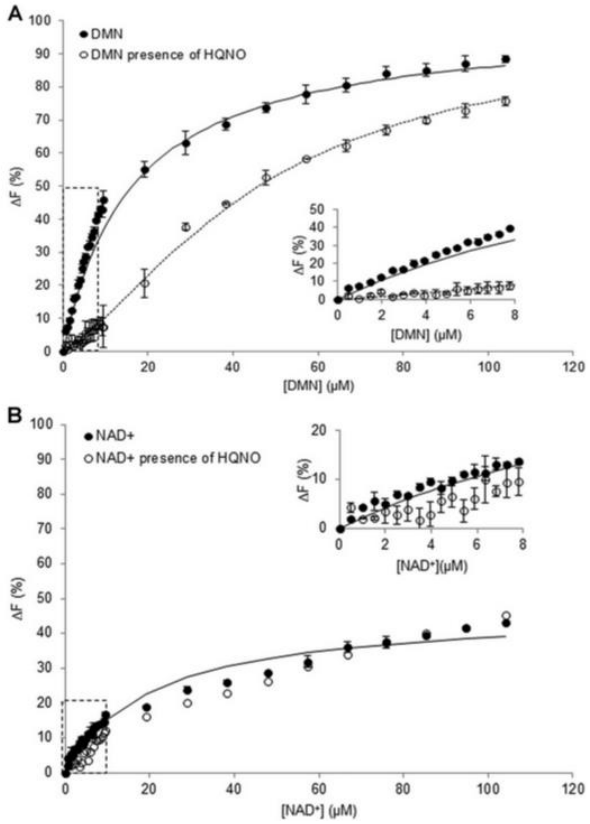

Supplementary figure 6. 6 – NDH-2_Sa WT fluorescence spectroscopy studies. Change in the fluorescence emission at 330 nm with emission at 280 nm. A – titration with increasing concentrations of DMN, in the presence (empty dots) and absence (filled dots) HQNO; B – titration with increasing concentrations of NAD^+, in the presence (empty dots) and absence (filled dots) HQNO. Adapted from (*43*).